

Genetic regulation of photoperiod-dependent flowering time in barley (*Hordeum vulgare* L.)

Inaugural-Dissertation

zur Erlangung des Doktorgrades
der Mathematisch-Naturwissenschaftlichen Fakultät
der Heinrich-Heine-Universität Düsseldorf

vorgelegt von

Gesa Helmsorig
aus Bielefeld

Düsseldorf, November 2023

aus dem Institut für Pflanzengenetik
der Heinrich-Heine-Universität Düsseldorf

Gedruckt mit der Genehmigung der
Mathematisch-Naturwissenschaftlichen Fakultät der
Heinrich-Heine-Universität Düsseldorf

Berichtersteller:

1. Prof. Dr. Maria von Korff Schmising

2. Prof. Dr. Rüdiger Simon

Tag der mündlichen Prüfung: 07.02.2024

Eidesstattliche Versicherung

Ich, Frau Gesa Helmsorig, versichere an Eides statt, dass die vorliegende Dissertation von mir selbstständig und ohne unzulässige fremde Hilfe unter Beachtung der "Grundsätze zur Sicherung guter wissenschaftlicher Praxis an der Heinrich-Heine-Universität Düsseldorf" erstellt worden ist.

Des Weiteren versichere ich, dass ich diese Dissertation nur in diesem und keinem anderen Promotionsverfahren eingereicht habe und dass diesem Promotionsverfahren kein gescheitertes Promotionsverfahren vorausgegangen ist.

Düsseldorf, der 29. November 2023

Unterschrift

Table of Contents

Summary	1
Zusammenfassung	3
Introduction	7
Aims and Approaches	9
References	10
1 <i>early maturity 7</i> promotes early flowering by controlling the light input into the circadian clock in barley	13
Abstract	15
Introduction	15
Results	16
<i>eam7</i> accelerates reproductive development in long-day and short-day conditions	16
The expression pattern of circadian clock genes is altered in <i>eam7</i> plants under SD	19
Biparental mapping identifies <i>LIGHT-REGULATED WD 1 (LWD1)</i> as a candidate gene for <i>eam7</i>	20
CRISPR-generated mutants confirm <i>LWD1</i> as the gene underlying the <i>eam7</i> locus	23
Natural variation of <i>LWD1</i>	24
Discussion	25
<i>LWD1</i> is a candidate for the <i>eam7</i> locus	25
<i>EAM7</i> is important for photoperiod sensing in barley	26
Materials and Methods	27
References	30
Supplemental Data	33
2 <i>FLOWERING LOCUS T1</i> is a pleiotropic regulator of reproductive development, plant architecture, and source-sink relations in barley	49
Abstract	51
Introduction	53
Results	57
<i>FT1</i> affects plant architecture and accelerates flowering under long days	57
<i>FT1</i> accelerates the vegetative and reproductive development and increases fertility on whole-plant and single-spike level	58
<i>FT1</i> strongly affects the expression of genes involved in carbon metabolism and stress response in the leaf	61
<i>FT1</i> regulates chromatin accessibility and meristem maintenance in the developing MSA	64
Discussion	67
<i>FT1</i> has a pleiotropic effect on plant development	67
<i>FT1</i> changes the expression of genes involved in stress response and source-sink relationships	68
Materials and Methods	71
References	76
Figures	84
Supplemental Data	90
Acknowledgements	107

Summary

Time to flower is critical for the successful propagation of a plant and to optimize crop yield. Several internal and external factors, including photoperiod, regulate flowering. Photoperiodic flowering is well-studied in model organisms such as *Arabidopsis* (*Arabidopsis thaliana*), and key flowering time regulators are conserved across angiosperm species. However, the functions of these floral regulators and molecular networks have diverged between angiosperm lineages and species. In the cereal crop barley (*Hordeum vulgare* L.), the central flowering time regulator in response to long photoperiods is *PHOTOPERIOD 1* (*Ppd-H1*), ortholog of the pseudo-response regulator genes of the circadian clock in *Arabidopsis*. *Ppd-H1* induces the expression of *FLOWERING LOCUS T1* (*FT1*), the barley ortholog of *Arabidopsis* florigen *FT*, which in *Arabidopsis* moves from leaf to shoot apex to induce the formation of flowers. In contrast to *Arabidopsis*, the barley genome holds several *FT*-like genes, of which only some have been characterized so far, and the exact role of *FT1* remains poorly understood. In this work, I aimed to identify and characterize an upstream regulator of *Ppd-H1* and *FT1* and detect downstream molecular and phenotypic effects in the developing shoot and inflorescence meristems. For this, I identified and functionally characterized the gene underlying the *early maturity 7* (*eam7*) locus, which confers photoperiod-independent early flowering in barley. In addition, I dissected the function of *FT1* in controlling reproductive timing, and shoot and inflorescence meristem development and linked this to molecular networks in the leaf, stem and inflorescence.

In the first part of this dissertation, I identified the gene underlying the *eam7* locus. Barley is a facultative long-day plant; photoperiods above 12 hours strongly induce flowering, whereas those below 12 hours of light delay flowering. Plants carrying the *eam7* locus are early flowering under non-inductive short-day conditions. Phenotypic characterization of *eam7* plants showed that *eam7* interacts with *Ppd-H1* to regulate photoperiodic flowering, inflorescence development, and plant fertility. I generated a biparental mapping population segregating for *Ppd-H1* and *eam7* to map the position of the *eam7* locus on the short arm of chromosome 6H. Target gene sequencing revealed a 34 base pair deletion in the coding sequence of *LIGHT-REGULATED WD 1* (*LWD1*), homologous to a gene involved in the light entrainment of the circadian clock in *Arabidopsis*, to co-segregate with the early flowering phenotype of *eam7* under short days. With CRISPR-Cas9, I generated *lwd1* mutants to confirm the early flowering phenotype of homozygous mutants under short-day conditions. Subsequent complementation crosses confirmed *LWD1* as a promising candidate gene to underlie *eam7*. Gene expression studies showed that changes in the *LWD1* coding sequence caused the de-repression of *Ppd-H1* at night and consequent upregulation of *FT1* under short

days. Furthermore, mutations in *lwd1* caused altered diurnal expression patterns of phytochromes and clock genes, indicating that *LWD1* controls the photoperiod response by modifying the light entrainment of the clock and clock gene expression.

In the second part of this thesis, I characterized *FLOWERING LOCUS T1 (FT1)*, which is one of several *FT*-like genes in barley. *FT1* is suggested to be the central inducer of flowering in barley as allelic variation at *Ppd-H1* correlates with altered *FT1* expression levels and consequent timing of flowering under long days. I aimed to understand how and to what extent *FT1* affects flowering, plant development, and architecture, whether the photoperiodic response conveyed by *Ppd-H1* is transmitted exclusively through *FT1*, and to identify gene regulatory networks downstream of *FT1*. Phenotyping CRISPR-Cas9-generated *ft1* knock-out mutants revealed that *FT1* strongly promotes flowering in barley but is not essential for the formation and development of inflorescences. Allelic variation at *Ppd-H1* did not affect flowering time in *ft1* mutants, indicating that *Ppd-H1* regulates reproductive development exclusively via *FT1*. The *ft1* mutant plants were characterized by a strong delay in the transition from vegetative to reproductive development and in the subsequent floral development, and tillered and flowered over many months. These results showed that *FT1* affects the timing, synchrony, and duration of flowering. Through the microscopic dissection of the main shoot apex, I could show that *ft1* mutants are characterized by increased spikelet meristems induced on the inflorescence. However, floret fertility decreased, resulting in an overall strong reduction in grain number per spike. *FT1* impacts the balance of vegetative to reproductive tissue, as *ft1* plants produced more side shoots but significantly fewer grains than parental wild-type plants. I used transcriptomic analyses to decipher the genetic network regulated by *FT1*. This revealed that *FT1* affects numerous developmental genes in the shoot apex, possibly causative for the observed changes in meristem determinacy and, consequently, differences in longevity and duration of flowering. In addition, the expression of photosynthesis components and elements of the carbohydrate metabolism were altered, indicating that source-sink relationships are regulated through *FT1*. The expression patterns of genes involved in stress response were upregulated in the leaf and shoot apex, possibly due to an imbalance of source-sink relationships in the *ft1* mutants.

In summary, I identified a novel regulator of photoperiodic flowering in barley, *LWD1*, and provided new insights into the role of *FT1* in the complex network of flowering time regulation. This expands our knowledge of the molecular and genetic regulation of flowering time and can help us adapt our crops to increasingly challenging environmental conditions.

Zusammenfassung

Der Blühzeitpunkt ist entscheidend für die erfolgreiche Reproduktion einer Pflanze und um den Ertrag von Nutzpflanzen zu optimieren. Mehrere interne und externe Faktoren, darunter die Photoperiode, regulieren die Blüte. Die photoperiodische Blüte ist in Modellorganismen wie *Arabidopsis thaliana* gut erforscht, und wichtige Regulatoren des Blühzeitpunkts sind innerhalb der Angiospermen konserviert. Die Funktionen dieser Blütenregulatoren und molekularen Netzwerke haben sich jedoch zwischen verschiedenen Angiospermen auseinanderentwickelt. In der Getreideart Gerste (*Hordeum vulgare* L.) ist *PHOTOPERIOD 1* (*Ppd-H1*), ein Ortholog der *pseudo-response regulator* Gene der circadianen Uhr in Arabidopsis, der zentrale Blühzeitregulator in langen Photoperioden. *Ppd-H1* induziert die Expression von *FLOWERING LOCUS T1* (*FT1*), dem Gerstenortholog des Florigens *FT*, welches in Arabidopsis vom Blatt zur Sprossspitze wandert, um die Bildung von Blüten zu induzieren. Im Gegensatz zu Arabidopsis enthält das Gerstengenom mehrere *FT*-ähnliche Gene, von denen bisher nur einige wenige charakterisiert wurden, und die genaue Rolle von *FT1* ist weiterhin unklar. Das Ziel dieser Arbeit war es daher, einen vorgeschalteten Regulator von *Ppd-H1* und *FT1* zu identifizieren und charakterisieren und nachgelagerte molekulare und phänotypische Effekte in den sich entwickelnden Spross- und Blütenstandsmeristemen zu identifizieren. Zu diesem Zweck habe ich das Gen, welches dem *early maturity 7* (*eam7*) Locus unterliegt und in Gerste eine photoperiodisch unabhängige frühe Blüte bewirkt, identifiziert und funktionell charakterisiert. Darüber hinaus habe ich die Funktion von *FT1* in der Regulation des Reproduktionszeitpunkts und der Entwicklung von Spross- und Blütenstandsmeristemen untersucht und diese mit molekularen Netzwerken in Blatt, Stängel und Blütenstand verknüpft.

Im ersten Teil dieser Dissertation habe ich das Gen identifiziert, welches dem *eam7*-Locus unterliegt. Gerste ist eine fakultative Langtagpflanze; Photoperioden von mehr als 12 Stunden induzieren die Blüte daher stark, während solche von weniger als 12 Stunden Licht die Blüte verzögern. Pflanzen, welche den *eam7*-Locus tragen, blühen früh unter nicht-induzierenden Kurztagsbedingungen. Die phänotypische Charakterisierung von *eam7*-Pflanzen zeigte, dass *eam7* mit *Ppd-H1* interagiert um die photoperiodische Blüte, die Entwicklung der Blütenstände und die Fertilität der Pflanzen zu regulieren. Mithilfe einer biparentalen Kartierungspopulation, welche für *Ppd-H1* und *eam7* segregiert, konnte ich die Position des *eam7*-Locus auf dem kurzen Arm von Chromosom 6H kartieren. Die Sequenzierung von Kandidatengenen ergab, dass eine Deletion von 34 Basenpaaren in der kodierenden Sequenz von *LIGHT-REGULATED WD 1* (*LWD1*) mit dem frühen Blühphänotyp von *eam7* im Kurztag kosegregiert. *LWD1* ist homolog zu einem Gen in Arabidopsis, welches an der Synchronisation der zirkadianen Uhr durch Licht beteiligt ist. Mithilfe von CRISPR-Cas9 habe ich *lwd1*-

Mutanten erzeugt, um den Phänotyp der frühen Blüte homozygoter Mutanten unter Kurztagsbedingungen zu bestätigen. Anschließende Komplementationskreuzungen bestätigten *LWD1* als vielversprechendes Kandidatengen für *eam7*. Genexpressionsstudien zeigten, dass Veränderungen in der kodierenden Sequenz von *LWD1* die Unterdrückung der Expression von *Ppd-H1* in der Nacht aufheben und somit die Hochregulierung von *FT1* unter Kurztagsbedingungen bewirkten. Darüber hinaus führten Mutationen in *lwd1* zu veränderten Expressionsmustern von Phytochromen und Genen der zirkadianen Uhr im Tagesverlauf, was darauf hindeutet, dass *LWD1* die photoperiodische Antwort steuert, indem es die Synchronisation der zirkadianen Uhr durch Licht und die Expression von Uhrengenen modifiziert.

Im zweiten Teil dieser Arbeit habe ich *FLOWERING LOCUS T1 (FT1)*, eines von mehreren *FT*-ähnlichen Genen in Gerste, charakterisiert. Es wird angenommen, dass *FT1* der zentrale Regulator der Blüte in Gerste ist, da allelische Variation in *Ppd-H1* mit veränderten *FT1*-Expressionsniveaus und demzufolge dem Zeitpunkt der Blüte im Langtag korreliert. Mein Ziel war es zu verstehen, wie und in welchem Ausmaß *FT1* die Blüte und die Entwicklung und Architektur der Pflanze beeinflusst, ob die von *Ppd-H1* vermittelte photoperiodische Antwort ausschließlich durch *FT1* übermittelt wird, und ich wollte genregulatorische Netzwerke identifizieren, welche *FT1* nachgeschaltet sind. Die Phänotypisierung von CRISPR-Cas9-erzeugten *ft1*-Knockout-Mutanten ergab, dass *FT1* die Blüte in Gerste stark fördert, aber nicht wesentlich für die Bildung und Entwicklung von Blütenständen ist. Allelische Variation in *Ppd-H1* hatte keinen Einfluss auf die Blütezeit in *ft1*-Mutanten, was darauf hindeutet, dass *Ppd-H1* die reproduktive Entwicklung ausschließlich über *FT1* reguliert. Die *ft1*-Mutanten zeichneten sich durch eine starke Verzögerung beim Übergang von der vegetativen zur reproduktiven Entwicklung sowie der anschließenden Blütenentwicklung aus und produzierten Seitentriebe und Blüten über viele Monate. Diese Ergebnisse zeigten, dass *FT1* den Zeitpunkt, die Synchronität und die Dauer der Blüte beeinflusst. Durch die mikroskopische Sektion der Hauptsprossspitze konnte ich zeigen, dass *ft1*-Mutanten durch eine erhöhte Anzahl an Ährchenmeristemen am Blütenstand gekennzeichnet sind. Allerdings war die Anzahl der sich daraus entwickelnden Blüten verringert, was zu einer insgesamt stark reduzierten Kornzahl pro Ähre führte. *FT1* wirkt sich auf das Gleichgewicht von vegetativem und reproduktivem Gewebe aus, da *ft1*-Pflanzen mehr Seitentriebe, aber deutlich weniger Körner als elterliche Wildtyp-Pflanzen produzieren. Mithilfe von Transkriptionsanalysen habe ich das von *FT1* regulierte genetische Netzwerk entschlüsselt. Dabei zeigte sich, dass *FT1* zahlreiche Entwicklungsgene in der Sprossspitze beeinflusst, was möglicherweise die Ursache für die beobachteten Veränderungen in der Determination von Meristemen und folglich für die Unterschiede in der Langlebigkeit und Dauer der Blüte ist. Darüber hinaus wurde die Expression von Komponenten des Photosyntheseapparates und Elementen des

Kohlenhydratstoffwechsels verändert, was darauf hindeutet, dass die *Source-Sink*-Interaktion durch *FT1* reguliert werden. Die Expressionsmuster von Genen, welche an Stressreaktionen beteiligt sind, wurden im Blatt und in der Sprossspitze hochreguliert, was möglicherweise auf ein Ungleichgewicht der *Source-Sink*-Interaktion in den *ft1*-Mutanten zurückzuführen ist.

Zusammenfassend habe ich einen neuen Regulator der photoperiodischen Blüte in Gerste, *LWD1*, identifiziert und neue Einblicke in die Rolle von *FT1* in dem komplexen Netzwerk der Blütezeitregulierung geschaffen. Dies erweitert unser Wissen über die molekulare und genetische Regulierung des Blühzeitpunktes und kann uns helfen, unsere Nutzpflanzen an immer anspruchsvollere Umweltbedingungen anzupassen.

Introduction

The development of modern high-yielding crop varieties in the 1960s is often referred to as the “Green Revolution,” and advances in breeding have more than doubled crop production since then (Khush, 2001). Nonetheless, agriculture will face enormous challenges in the future since the demand for higher-yielding crops will not subside as the world population grows continuously and changing diets require higher amounts of fodder crops (Godfray et al., 2010). Yield increase is suggested as the most sustainable option to meet these demands, and estimates are that a 100-110% increase in food production is required by 2050 (Godfray et al., 2010; Tilman et al., 2011). To complicate efforts, yields have stalled due to rising temperatures and declining rainfall, and recent models predict that climatic changes resulting from global warming will decrease global crop production significantly in the near future (Hochman et al., 2017; Hasegawa et al., 2022). Major food-producing regions will experience changing climate profiles and, therefore, altered requirements for crop cultivation. Consequently, strategies to breed high-yielding crops that withstand increasingly extreme weather conditions are required to accomplish food security in the future. This can be achieved by breeding plants more resilient to episodes of heat, drought, and high rainfall or by changing the timing of flowering and crop maturation to most likely circumvent these events.

Flowering is a central process in the life cycle of a plant. To flower in the most favorable conditions is essential for successful propagation and secures high yield in crops, as suboptimal conditions such as low or high temperatures can damage floral organs and, thus, reduce fertility (Frederiks et al., 2015; Ejaz and von Korff, 2017). Photoperiod, ambient temperature, and vernalization are essential environmental cues to ensure flowering at the correct time of the year as they change with seasons (Andrés and Coupland, 2012). The photoperiodic response varies across plant species; long-day plants induce flowering in day lengths above 12 hours, whereas short-day plants require less than 12 hours of light per day (Garner and Allard, 1920).

The facultative long-day plant barley (*Hordeum vulgare*) is the fourth most abundantly grown cereal crop and is unique in its adaptability to different environments (FAO, 2021). Barley is cultivated across a wide range of latitudes, and depending on their flowering habit, varieties are divided into two growth types: winter and spring. Winter varieties are sown during autumn and require a prolonged period of cold, called vernalization, to flower, preventing premature transition to reproductive development during the cold winter months. In contrast, spring cultivars are sown in spring and do not require vernalization. Instead, long days promote flowering. The photoperiodic response is a strong selection trait, as, depending on the environment, early or delayed flowering in response to inductive long days can improve plant performance (Fernández-Calleja et al., 2021).

The main photoperiod response gene in barley, *PHOTOPERIOD 1 (Ppd-H1)*, is a crucial component of the adaptation to different climatic regions. The emergence of a long-day insensitive *Ppd-H1* allele allowed the expansion of barley cultivation from the fertile crescent to higher latitudes (Turner et al., 2005; Jones et al., 2008). Allelic variation at *Ppd-H1* is correlated with different expression levels of *FLOWERING LOCUS T1 (FT1)*, a central inducer of flowering in barley (Turner et al., 2005; Faure et al., 2007). Studies in *Arabidopsis* have shown that the *FT1* ortholog, *FT*, acts as a mobile signal to transfer the information of sufficient day length from the leaves to the shoot apical meristem (SAM), which is surrounded by several leaf layers and, therefore, shielded from light (Kardailsky et al., 1999; Corbesier et al., 2007). In the SAM, FT interacts with other proteins to induce the formation of reproductive organs and, thus, flowering (Abe et al., 2005; Li and Dubcovsky, 2008).

Flowering time and photoperiod responsiveness have been a target of barley breeding for decades. Plants optimized for short growing seasons, as *early maturity (eam)* mutants, have been used in Scandinavian breeding programs since the 1960s (Lundqvist, 2009). With rapid technological advances and a substantial increase in the availability of genomic resources over the last few years, new opportunities are emerging for plant research. Several genes underlying *eam* loci have been identified; all are part of the photoperiod response, the light perception pathway, or the circadian clock, and all are characterized by changes in gene expression of *FT1* (Faure et al., 2012; Campoli et al., 2013; Pankin et al., 2014). The assembly of high-quality reference genomes has been instrumental in identifying these genes. The first barley reference genome was published in 2012 and has been updated and improved multiple times since (IBSC, 2012; Mascher et al., 2021). Furthermore, the release and subsequent improvement of a reference transcriptome allows more precise predictions of gene expression patterns (Rapazote-Flores et al., 2019; Coulter et al., 2022). In addition, new techniques, most prominently the genome editing tool CRISPR-Cas9, open new possibilities and accelerate the discovery of new targets to improve plant performance.

Aims and Approaches

The overall aim of this work was to deepen the understanding of the genetic and molecular networks acting up- and downstream of *Ppd-H1* and *FT1* by utilizing modern tools of gene editing and improved genetic resources. Two different barley genotypes with opposing effects on flowering time were investigated: An introgression line that carries the *early maturity 7* (*eam7*) locus, enabling plants to flower early in non-inductive photoperiods (short days), and *ft1* mutants generated with the help of CRISPR-Cas9, which were expected to be strongly delayed in their development. The aims can be divided into four main objectives:

1. To characterize plant development in *eam7* and *ft1* mutants, different phenotypic traits related to plant architecture and yield components were scored. The development of the main shoot apex (MSA) was dissected to understand how vegetative and reproductive development is affected by *eam7* or *FT1*. As the effect of *eam7* is highly dependent on photoperiod, this was done under long and short photoperiods for *eam7* plants, whereas phenotyping was performed only under long days for *FT1* mutants.
2. A primary objective was to understand the effect of allelic variation at *Ppd-H1* in *ft1* and *eam7* mutant plants. Allelic variation at *Ppd-H1* is correlated with different *FT1* expression levels. Therefore, *Ppd-H1* controls flowering time through *FT1* (Turner et al., 2005; Digel et al., 2015). However, it is not known whether this regulation is a direct one or through additional factors. Therefore, *ft1* mutants were investigated in the background of both allelic variations of *Ppd-H1* to unravel this genetic interaction. Similarly, genes underlying *eam* loci have been shown to interact with *Ppd-H1* to modify the photoperiodic response (Faure et al., 2012; Campoli et al., 2013; Pankin et al., 2014). To test whether this applies to *eam7* as well, mutant lines in both *Ppd-H1* backgrounds were used for phenotyping and gene expression analysis.
3. To unravel the genetic networks surrounding *eam7* and *FT1*, qRT-PCR was used to test the expression of specific target genes in *eam7* leaves and RNA sequencing to identify new targets of *FT1* in leaves, stems, and shoot apices.
4. Lastly, to identify the gene underlying the *eam7* locus, a biparental mapping population segregating for *eam7* and *Ppd-H1* was utilized, as plants carrying a homozygous *eam7* locus and at least one wild-type *Ppd-H1* allele are early flowering under short-day conditions. CRISPR-Cas9 mutant generation and subsequent allelism testing were used to confirm the obtained candidate gene.

References

- Abe M, Kobayashi Y, Yamamoto S, Daimon Y, Yamaguchi A, Ikeda Y, Ichinoki H, Notaguchi M, Goto K, Araki T** (2005) Fd, a bZIP protein mediating signals from the floral pathway integrator FT at the shoot apex. *Science (New York, N.Y.)*, **309**(5737): 1052–1056.
- Andrés F, Coupland G** (2012) The genetic basis of flowering responses to seasonal cues. *Nature Reviews. Genetics*, **13**(9): 627–639.
- Campoli C, Pankin A, Drosse B, Casao CM, Davis SJ, von Korff M** (2013) *HvLUX1* is a candidate gene underlying the *early maturity 10* locus in barley: Phylogeny, diversity, and interactions with the circadian clock and photoperiodic pathways. *The New Phytologist*, **199**(4): 1045–1059.
- Corbesier L, Vincent C, Jang S, Fornara F, Fan Q, Searle I, Giakountis A, Farrona S, Gissot L, Turnbull C, et al.** (2007) FT protein movement contributes to long-distance signaling in floral induction of *Arabidopsis*. *Science (New York, N.Y.)*, **316**(5827): 1030–1033.
- Coulter M, Entizne JC, Guo W, Bayer M, Wonneberger R, Milne L, Schreiber M, Haaning A, Muehlbauer GJ, McCallum N, et al.** (2022) BaRTv2: A highly resolved barley reference transcriptome for accurate transcript-specific RNA-seq quantification. *The Plant Journal : For Cell and Molecular Biology*, **111**(4): 1183–1202.
- Digel B, Pankin A, von Korff M** (2015) Global Transcriptome Profiling of Developing Leaf and Shoot Apices Reveals Distinct Genetic and Environmental Control of Floral Transition and Inflorescence Development in Barley. *The Plant Cell*, **27**(9): 2318–2334.
- Ejaz M, von Korff M** (2017) The Genetic Control of Reproductive Development under High Ambient Temperature. *Plant Physiology*, **173**(1): 294–306.
- FAO** (2021). FAOSTAT Statistical Databases. Retrieved from <http://www.fao.org/faostat/>
- Faure S, Higgins J, Turner A, Laurie DA** (2007) The *FLOWERING LOCUS T*-like gene family in barley (*Hordeum vulgare*). *Genetics*, **176**(1): 599–609.
- Faure S, Turner AS, Gruszka D, Christodoulou V, Davis SJ, von Korff M, Laurie DA** (2012) Mutation at the circadian clock gene *EARLY MATURITY 8* adapts domesticated barley (*Hordeum vulgare*) to short growing seasons. *Proceedings of the National Academy of Sciences of the United States of America*, **109**(21): 8328–8333.
- Fernández-Calleja M, Casas AM, Igartua E** (2021) Major flowering time genes of barley: Allelic diversity, effects, and comparison with wheat. *Theoretical and Applied Genetics*, **134**(7): 1867–1897.
- Frederiks TM, Christopher JT, Sutherland MW, Borrell AK** (2015) Post-head-emergence frost in wheat and barley: Defining the problem, assessing the damage, and identifying resistance. *Journal of Experimental Botany*, **66**(12): 3487–3498.
- Garner WW, Allard HA** (1920) Effect of the relative length of day and night and other factors of the environment of growth and reproduction in plants. *Monthly Weather Review*, **48**(7): 415.

- Godfray HCJ, Beddington JR, Crute IR, Haddad L, Lawrence D, Muir JF, Pretty J, Robinson S, Thomas SM, Toulmin C** (2010) Food security: The challenge of feeding 9 billion people. *Science*, 327(5967): 812–818.
- Hasegawa T, Wakatsuki H, Ju H, Vyas S, Nelson GC, Farrell A, Deryng D, Meza F, Makowski D** (2022) A global dataset for the projected impacts of climate change on four major crops. *Scientific Data*, 9(1): 58.
- Hochman Z, Gobbett DL, Horan H** (2017) Climate trends account for stalled wheat yields in Australia since 1990. *Global Change Biology*, 23(5): 2071–2081.
- IBSC** (2012) A physical, genetic and functional sequence assembly of the barley genome. *Nature*, 491(7426): 711.
- Jones H, Leigh FJ, Mackay I, Bower MA, Smith LMJ, Charles MP, Jones G, Jones MK, Brown TA, Powell W** (2008) Population-based resequencing reveals that the flowering time adaptation of cultivated barley originated east of the Fertile Crescent. *Molecular Biology and Evolution*, 25(10): 2211–2219.
- Kardailsky I, Shukla VK, Ahn JH, Dagenais N, Christensen SK, Nguyen JT, Chory J, Harrison MJ, Weigel D** (1999) Activation tagging of the floral inducer *FT*. *Science* (New York, N.Y.), 286(5446): 1962–1965.
- Khush GS** (2001) Green revolution: The way forward. *Nature Reviews. Genetics*, 2(10): 815–822.
- Li C, Dubcovsky J** (2008) Wheat FT protein regulates *VRN1* transcription through interactions with FDL2. *The Plant Journal : For Cell and Molecular Biology*, 55(4): 543–554.
- Lundqvist U** (2009) Eighty Years of Scandinavian Barley Mutation Genetics and Breeding. In Q. Y. Shu (Ed.), *Joint FAO/IAEA Programme. Induced plant mutations in the genomics era* (pp. 39–43). Rome: FAO.
- Mascher M, Wicker T, Jenkins J, Plott C, Lux T, Koh CS, Ens J, Gundlach H, Boston LB, Tulpová Z, et al.** (2021) Long-read sequence assembly: A technical evaluation in barley. *The Plant Cell*, 33(6): 1888–1906.
- Pankin A, Campoli C, Dong X, Killian B, Sharma R, Himmelbach A, Saini R, Davis SJ, Stein N, Schneeberger K, et al.** (2014) Mapping-by-sequencing identifies *HvPHYTOCHROME C* as a candidate gene for the *early maturity 5* locus modulating the circadian clock and photoperiodic flowering in barley. *Genetics*, 198(1): 383–396.
- Rapazote-Flores P, Bayer M, Milne L, Mayer C-D, Fuller J, Guo W, Hedley PE, Morris J, Halpin C, Kam J, et al.** (2019) BaRTv1.0: An improved barley reference transcript dataset to determine accurate changes in the barley transcriptome using RNA-seq. *BMC Genomics*, 20(1): 968.
- Tilman D, Balzer C, Hill J, Befort BL** (2011) Global food demand and the sustainable intensification of agriculture. *Proceedings of the National Academy of Sciences of the United States of America*, 108(50): 20260–20264.
- Turner A, Beales J, Faure S, Dunford RP, Laurie DA** (2005) The pseudo-response regulator *Ppd-H1* provides adaptation to photoperiod in barley. *Science* (New York, N.Y.), 310(5750): 1031–1034.

1 *early maturity 7* promotes early flowering by controlling the light input into the circadian clock in barley

The following manuscript was published in *Plant Physiology* in November 2023.

Authors:

Gesa Helmsorig¹, Agatha Walla¹, Thea Rütjes¹, Gabriele Buchmann¹, Rebekka Schüller¹, Götz Hensel^{2,3,4} and Maria von Korff^{1,2}

Affiliations:

¹Institute of Plant Genetics, Heinrich-Heine-Universität Düsseldorf, 40223 Düsseldorf, Germany

²Cluster of Excellence on Plant Sciences "SMART Plants for Tomorrow's Needs", 40223 Düsseldorf, Germany

³Centre for Plant Genome Engineering, Institute of Plant Biochemistry, Heinrich-Heine-Universität Düsseldorf, 40223 Düsseldorf, Germany

⁴Division of Molecular Biology, Centre of the Region Hana for Biotechnological and Agriculture Research, Faculty of Science, Palacký University, Olomouc, Czech

Contributions:

GH and MvK conceived and designed the experiments. GH conducted plant phenotypic analyses, generated BW(*Ppd-H1,eam7*) crosses, designed CAPS markers, cloned CRISPR-Cas9 transformation vectors, did sequence analyses, and analyzed the data. AW performed the haplotype analysis. TR and GH performed qPCR experiments and genotyping of the mapping population. GB and GöH transformed plants and regenerated *lwd1* mutants. RS generated allelic *lwd1* crosses. GH wrote the manuscript with the help of AW and MvK.



early maturity 7 promotes early flowering by controlling the light input into the circadian clock in barley

Gesa Helmsorig ¹, Agatha Walla ¹, Thea Rütjes ¹, Gabriele Buchmann ¹, Rebekka Schüller ¹,
Götz Hensel ^{2,3,4} and Maria von Korff ^{1,2,*}

1 Institute of Plant Genetics, Heinrich-Heine-Universität Düsseldorf, 40223 Düsseldorf, Germany

2 Cluster of Excellence on Plant Sciences “SMART Plants for Tomorrow’s Needs”, 40223 Düsseldorf, Germany

3 Centre for Plant Genome Engineering, Institute of Plant Biochemistry, Heinrich-Heine-Universität Düsseldorf, 40223 Düsseldorf, Germany

4 Division of Molecular Biology, Centre of the Region Hana for Biotechnological and Agriculture Research, Faculty of Science, Palacký University, CZ-779 00 Olomouc, Czech

*Author for correspondence: maria.korff.schmising@hhu.de

The author responsible for distribution of materials integral to the findings presented in this article in accordance with the policy described in the Instructions for Authors (<https://academic.oup.com/plphys/pages/General-Instructions>) is Maria von Korff.

Abstract

Breeding for variation in photoperiod response is crucial to adapt crop plants to various environments. Plants measure changes in day length by the circadian clock, an endogenous timekeeper that allows plants to anticipate changes in diurnal and seasonal light–dark cycles. Here, we describe the *early maturity 7* (*eam7*) locus in barley (*Hordeum vulgare*), which interacts with *PHOTOPERIOD 1* (*Ppd-H1*) to cause early flowering under non-inductive short days. We identify *LIGHT-REGULATED WD 1* (*LWD1*) as a putative candidate to underlie the *eam7* locus in barley as supported by genetic mapping and CRISPR-Cas9-generated *lwd1* mutants. Mutations in *eam7* cause a significant phase advance and a misregulation of core clock and clock output genes under diurnal conditions. Early flowering was linked to an upregulation of *Ppd-H1* during the night and consequent induction of the florigen *FLOWERING LOCUS T1* under short days. We propose that *EAM7* controls photoperiodic flowering in barley by controlling the light input into the clock and diurnal expression patterns of the major photoperiod response gene *Ppd-H1*.

Introduction

Flowering time substantially impacts crop yield and is thus a vital breeding target to produce new varieties better adapted to diverse and changing climatic conditions (Cockram et al. 2007). Climate models predict an increase in global temperatures and extreme weather events. Breeding for early maturing varieties is among the most effective strategies to improve adaptation to short growing seasons with terminal stress such as heat and drought events (Tewolde et al. 2006; He et al. 2022). Identification and characterization of alleles conferring early maturity greatly support these efforts.

The temperate crop barley (*Hordeum vulgare*) is among the most widely grown cereals with superior adaptation to marginal stress-prone agricultural lands (von Korff et al.

2008). Like most temperate cereals, barley is a quantitative long-day (LD) species that accelerates reproductive development with increasing photoperiods. In contrast, short photoperiods delay or even impair floral development (Digel et al. 2015). *PHOTOPERIOD 1* (*Ppd-H1*), orthologous to *PSEUDO-RESPONSE-REGULATOR* (*PRR*) genes in *Arabidopsis* (*Arabidopsis thaliana*), has been identified as the central gene in photoperiodic flowering in barley (Laurie et al. 1995). Natural variation at *Ppd-H1* determines variation in reproductive development under LD. The wild-type *Ppd-H1* allele, prevalent in wild and winter barley, induces rapid floral development in response to LD (Turner et al. 2005; Jones et al. 2008). A single amino acid change in the conserved CCT (CONSTANS, CO-like, and TOC1) domain of *Ppd-H1*

Received June 22, 2023. Accepted September 26, 2023. Advance access publication November 10, 2023

© The Author(s) 2023. Published by Oxford University Press on behalf of American Society of Plant Biologists.

This is an Open Access article distributed under the terms of the Creative Commons Attribution-NonCommercial-NoDerivs licence (<https://creativecommons.org/licenses/by-nc-nd/4.0/>), which permits non-commercial reproduction and distribution of the work, in any medium, provided the original work is not altered or transformed in any way, and that the work is properly cited. For commercial re-use, please contact journals.permissions@oup.com

Open Access

delays flowering. This allele was selected and is prevalent in spring barley varieties in central and northern Europe (Jones et al. 2008). *Ppd-H1* initiates flowering by inducing the expression of *FLOWERING LOCUS T1* (*FT1*) in the leaves (Turner et al. 2005). *FT1* is orthologous to florigen *FT* in Arabidopsis and *Hd3a* in rice (*Oryza sativa*), which move as proteins from the leaf to the shoot apical meristem and induce the transition from vegetative to reproductive growth (Kardailsky et al. 1999; Corbesier et al. 2007; Tamaki et al. 2007). In barley, increased *FT1* expression in the leaf correlates with early flowering and the upregulation of floral inducers such as *MADS*-box genes *VERNALIZATION 1* (*VRN1*), *BARLEY MADS-BOX 3* (*BM3*), and *BM8* in the leaf and meristem (Turner et al. 2005; Digel et al. 2015).

Differences in photoperiod are perceived by photoreceptors, which transmit this information to the circadian clock. The circadian clock is an endogenous timekeeper that allows organisms to anticipate seasonal and daily changes in light–dark rhythms. The core circadian clock is largely conserved across eudicots and monocots (Song et al. 2010). It comprises 3 interlocking, negative feedback loops of transcriptional repressors that are expressed sequentially during a 24-h period and repress previous and subsequent clock components. Transcription factors *CIRCADIAN CLOCK ASSOCIATED 1* (*CCA1*) and *LATE ELONGATED HYPOCOTYL* (*LHY*) are expressed first in the morning, followed by *PRR9*, 7, and 5 during the progressing day, and *PRR1* at dusk. *CCA1/LHY* represses the expression of *PRR* genes, which, in turn, suppress *CCA1/LHY*. During the night, the evening complex (EC) genes *EARLY FLOWERING 3* (*ELF3*), *EARLY FLOWERING 4* (*ELF4*), and *LUX ARRHYTHMO* (*LUX*) are expressed, repressing *PRR* genes and *CCA1/LHY* (Farré et al. 2005; Kikis et al. 2005; Huang et al. 2012; Mizuno et al. 2014). In Arabidopsis, the clock controls the diurnal expression pattern of the central photoperiod response gene *CONSTANS* (*CO*), resulting in *CO* expression peaking at the end of the light period in LD, but in the dark under SD (Suárez-López et al. 2001). The coincidence of *CO* expression with the light period is necessary for protein stabilization and the expression of the florigen *FT* under LD (Suárez-López et al. 2001; Valverde et al. 2004; Sawa et al. 2007; Jang et al. 2008). By contrast, in temperate monocots, the length of the night, rather than the length of the day, is critical for the perception of inductive photoperiods (Pearce et al. 2017; Gao et al. 2019). The length of the night is measured by *PHYTOCHROME B* (*PHYB*) and *PHYTOCHROME C* (*PHYC*), which are necessary for the light activation of *Ppd-H1*, and mutations in either of these genes result in the downregulation of *Ppd-H1* and very late flowering (Chen et al. 2014; Kippes et al. 2020). In addition, *PHYB* and *PHYC* control the light-induced degradation of *ELF3* (Gao et al. 2019; Alvarez et al. 2023). *ELF3*, proposedly together with EC members *LUX1* and *ELF4*, binds to the promoter of *Ppd-H1* during the night to repress its expression (Gao et al. 2019; Andrade et al. 2022; Alvarez et al. 2023).

Mutations conferring photoperiod-independent early flowering, so-called *early maturity* (*eam*) loci, have been

used in Scandinavian breeding programs since the 1960s to enable a geographic range extension of barley cultivation to areas with short growing seasons (Lundqvist 2009). Several genes that underlie *eam* loci have been identified in the last decade: *eam5* was identified as a gain-of-function mutation in *PHYC*, *eam8* as a knock-out mutation in *ELF3*, and *eam10* as a single amino acid exchange in *LUX1* (Faure et al. 2012; Zakhrebekova et al. 2012; Campoli et al. 2013; Pankin et al. 2014). Plants carrying *eam* mutations are characterized by reduced photoperiod sensitivity and accelerated flowering in inductive LD and non-inductive short days (SDs). While clock mutants are characterized by loss of circadian transcriptome oscillations and severely perturbed clock functions (Müller et al. 2016, 2020), they have been instrumental in expanding the cultivation of many crops to new geographic regions with altered annual patterns of temperature and photoperiod (McClung 2021). It is thus interesting to identify new genes and alleles and decipher the molecular networks important for photoperiod response in crops.

Here, we describe the *early maturity 7* (*eam7*) locus, originally identified as a natural mutation in the line Atsel derived from the cultivar Atlas, that causes early flowering under non-inductive SD conditions (Stracke and Börner 1998). We identify *LIGHT-REGULATED WD 1* (*LWD1*) as a putative candidate to underlie the *EAM7* locus in barley as supported by genetic mapping and allelism tests with CRISPR-Cas9-generated *lwd1* mutants. We demonstrate that *eam7* interacts with *Ppd-H1* to promote flowering under non-inductive photoperiods and affects plant architecture, spike development, spike fertility, and grain set. We propose that *EAM7* controls photoperiodic flowering in barley by repressing *Ppd-H1* at night, possibly mediated through *ELF3*. Mutations in *EAM7* cause a significant phase advance and a downregulation of core clock and clock output genes under diurnal conditions. We thus suggest that *EAM7/LWD1* controls photoperiod response by modifying the light entrainment of the clock and clock gene expression.

Results

eam7 accelerates reproductive development under short-day conditions

We investigated the effects of *eam7* and *Ppd-H1* on flowering time under long and short photoperiods. For this purpose, the spring cultivar Bowman (BW) and 3 derived introgression lines were cultivated under controlled conditions under long-day (LD, 16 h light/8 h dark, 20 °C/16 °C) or short-day (SD, 8 h light/16 h dark, 20 °C/16 °C) conditions to score flowering time. BW carries a natural mutation in the CCT domain of *Ppd-H1* that delays flowering time under LD conditions (Turner et al. 2005). The derived introgression line BW(*Ppd-H1*) carries a wild-type *Ppd-H1* allele and is early flowering under LD (Druka et al. 2011). In addition, we used BW(*eam7*), an introgression line with the *eam7.g* mutation that causes early maturity under LD and SD (Stracke and Börner 1998; Druka et al. 2011). We crossed BW(*Ppd-H1*) and

BW(*eam7*) to generate a line with a wild-type *Ppd-H1* allele and the mutation at *eam7*, which we termed BW(*Ppd-H1*, *eam7*).

Under LD, both introgression lines with a wild-type *Ppd-H1* allele, BW(*Ppd-H1*) and BW(*Ppd-H1*, *eam7*), flowered 27 and 26 days after emergence (DAE), respectively, and therefore significantly earlier than BW and BW(*eam7*), which flowered 41 DAE (Fig. 1A). No significant differences in time to flowering were observed between BW and BW(*eam7*) and between BW (*Ppd-H1*) and BW(*Ppd-H1*, *eam7*) under LD. Consequently, *Ppd-H1* but not *eam7* controlled time to flowering under LD. Under SD, BW(*eam7*) flowered 90 DAE and thus significantly earlier than BW and BW(*Ppd-H1*), which flowered on average 98 and 101 DAE, respectively (Fig. 1B). However, 10% of BW and 22% of BW(*Ppd-H1*) plants had not flowered until the experiment was stopped at 125 d. BW(*Ppd-H1*, *eam7*) exhibited the fastest development and flowered 38 DAE and thus 52 d earlier than BW(*eam7*), indicating that *eam7* and *Ppd-H1* interacted to accelerate flowering under SD.

We then analyzed which stages of reproductive development were affected by variation at *EAM7* and *Ppd-H1*. The main shoot apices (MSAs) of plants grown under LD and SD were dissected over development and scored according to the scale by Waddington et al. (1983). The Waddington scale rates the development based on the carpel of the most advanced floret of the spike. MSA development can be categorized into vegetative growth (W1.0 to W2.0), in which leaf primordia are initiated, early reproductive growth (W2.0 to W3.5) with the initiation of spikelet meristems (SM), and late reproductive growth and floral development until anthesis and pollination (W3.5 to W10.0).

Under LD, BW(*Ppd-H1*, *eam7*) transitioned to reproductive growth (W2.0) 6 DAE and thus 2 d earlier than BW(*Ppd-H1*) and BW (*eam7*) and 3 d earlier than BW (Fig. 1D). While BW(*Ppd-H1*, *eam7*) developed faster than BW(*Ppd-H1*) during early reproductive growth, their development synchronized during floral organ growth, and both genotypes reached pollination (W10.0) 34 DAE. In contrast, BW(*eam7*) and BW developed similarly during early reproductive growth but BW(*eam7*) development accelerated after carpel initiation (W4.5), and plants reached pollination 3 d earlier than BW (Fig. 1D). Under SD, the MSA of BW(*Ppd-H1*, *eam7*) transitioned to reproductive growth 9 DAE and thus 11 d earlier compared to the other 3 genotypes (Fig. 1E). BW(*Ppd-H1*, *eam7*) plants displayed a linear reproductive development under SD so that pollination (W10.0) occurred 41 DAE and thus only 7 d later compared to LD (Fig. 1C). By contrast, BW, BW(*Ppd-H1*), and BW(*eam7*) showed a substantial delay in floral development after carpel initiation (W4.5). However, floral development was still faster in BW(*eam7*) compared to BW and BW(*Ppd-H1*), and pollination occurred at 98 DAE, compared to 111 DAE in BW and BW(*Ppd-H1*) (Fig. 1E).

While we cannot exclude the possibility that BW(*Ppd-H1*), BW(*eam7*), and BW(*Ppd-H1*, *eam7*) carry additional variation for photoperiod response in the introgressed regions, our

results suggested that *Ppd-H1* interacted with *eam7* to control photoperiod response. Under LD, *eam7* accelerated spikelet initiation in the background of *Ppd-H1* and floral growth in the background of *Ppd-H1*. Under SD, *eam7* strongly accelerated all stages of reproductive development in the background of the wild-type *Ppd-H1* allele. In contrast, it only accelerated floral organ growth by a few days in the background of the mutated *Ppd-H1* allele.

Next, we investigated the effects of variation at *EAM7* and *Ppd-H1* on inflorescence architecture by scoring the initiation of SM and the number of florets and grains on the main spike. Under LD, BW produced the highest number of florets and grains per main spike, followed by BW(*eam7*), BW(*Ppd-H1*), and BW(*Ppd-H1*, *eam7*) (Supplemental Fig. S2, A to C, E). This result was associated with a longer duration of SM initiation and a higher number of total SM initiated in BW (Supplemental Fig. S1A, Supplemental Table S1). Spike fertility, the number of grains per florets on the spike, was close to 75% for BW, BW(*Ppd-H1*), and BW(*eam7*) in contrast to BW(*Ppd-H1*, *eam7*) with reduced fertility of only 25% (Fig. 2D). The low number of grains per spike in BW(*Ppd-H1*, *eam7*) was thus caused by a reduced number of initiated SM and reduced floret fertility. Under SD, BW(*Ppd-H1*, *eam7*) still initiated significantly less SM compared to the other genotypes, spike fertility, however, was relatively higher in BW(*eam7*) and BW(*Ppd-H1*, *eam7*) compared to BW(*Ppd-H1*) and BW (Fig. 2); Supplemental Fig. S1B, Supplemental Table S1). The effects of *Ppd-H1* and *EAM7* on inflorescence architecture and floret fertility thus differed between photoperiods (Fig. 2, F, G to I).

In addition, we determined the effects of *EAM7* on plant height, tiller number, and number of leaves on the main culm under LD and SD. Under LD, variation in shoot architecture was mainly affected by *Ppd-H1*, as BW(*Ppd-H1*) and BW(*Ppd-H1*, *eam7*) transitioned to reproductive growth earlier and thus produced fewer leaves on the main culm, fewer tillers and grew less tall compared to BW and BW(*eam7*) (Supplemental Fig. S2, A to C). Similarly, under SD, the fast-developing BW(*Ppd-H1*, *eam7*) plants produced significantly fewer leaves and tillers and were characterized by shorter plant height compared to the other 3 genotypes with a slower reproductive development (Supplemental Fig. S2, D to J). We also scored flag leaf size under SD and found that flag leaf length and width were reduced in BW(*Ppd-H1*, *eam7*) and BW(*eam7*) compared to BW and BW(*Ppd-H1*) (Supplemental Fig. S2, K to M).

In conclusion, under LD, *Ppd-H1* had a significant effect on developmental timing, while variation at *EAM7* only had minor effects on floral growth and the timing of pollination. *Ppd-H1* strongly affected the rate and duration of SM initiation and floret and grain number, further modulated by variation at *EAM7*. Under SD conditions, *eam7* in the background of *Ppd-H1* strongly accelerated reproductive development and caused near day-length neutrality and early flowering independent of the photoperiod. *EAM7* interacted

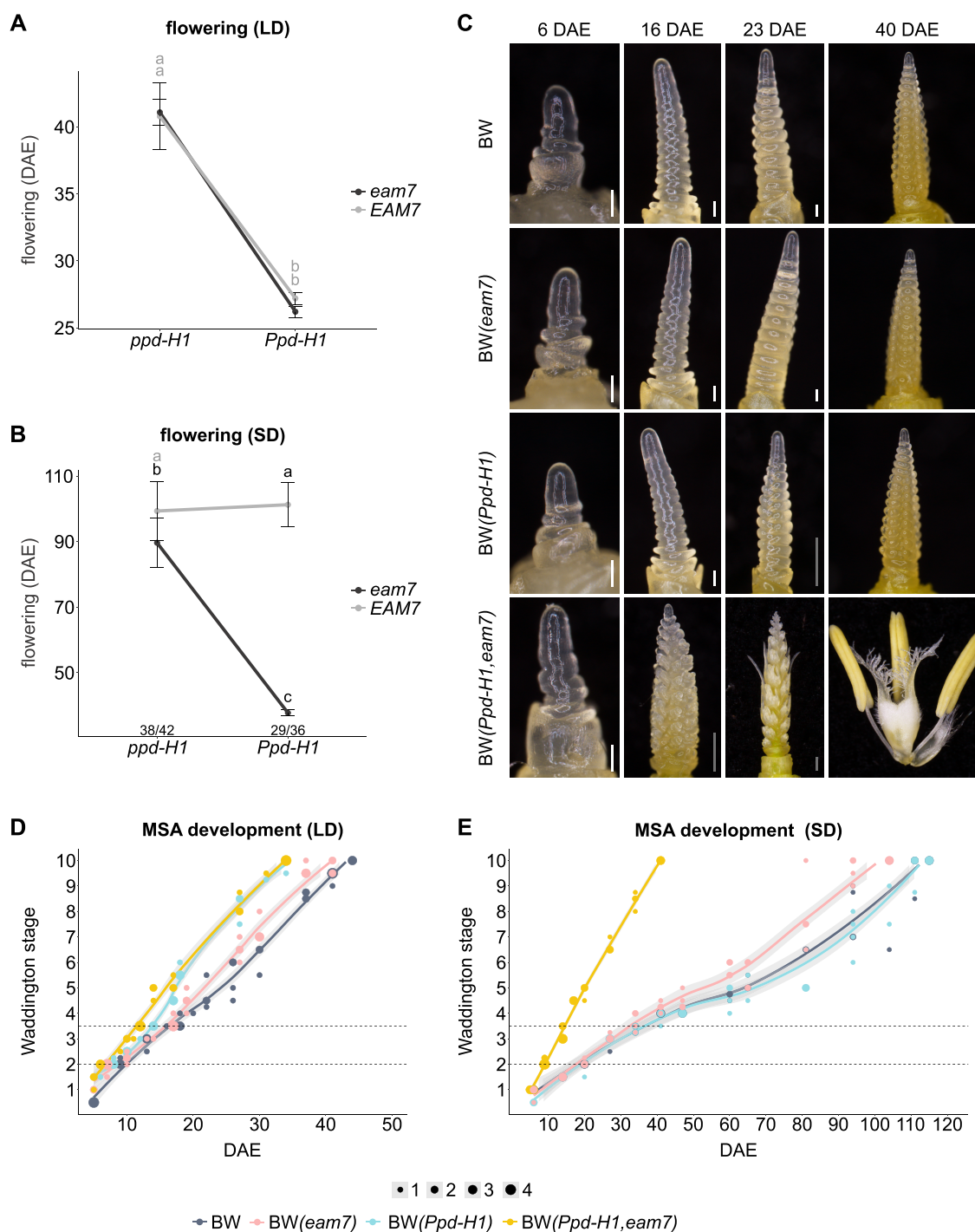


Figure 1. Effects of *eam7* and *Ppd-H1* on plant reproductive development. **A and B** Flowering time of spring cultivar Bowman (BW) and introgression lines BW(*eam7*), BW(*Ppd-H1*), and BW(*Ppd-H1,eam7*) was scored in days after emergence (DAE) under long days (LDs) (**A**) and short days (SDs) (**B**). Genotypes carrying the *EAM7* allele (BW and BW(*Ppd-H1*)) are shown in light gray, and genotypes carrying the *eam7* allele (BW(*eam7*) and BW(*Ppd-H1,eam7*)) in dark gray. Each dot represents the mean of 5 to 42 plants, error bars indicate the standard deviation of the mean. Significance levels were determined by one-way ANOVA and subsequent Tukey's test, $P \leq 0.05$, $n = 5$ to 42 plants. Numbers below the graph in (B) indicate the number of plants that flowered in *EAM7* genotypes BW and BW(*Ppd-H1*) until the end of the experiment (125 DAE) compared to the total number of plants scored. **C**) Inflorescences of BW, BW(*eam7*), BW(*Ppd-H1*), and BW(*Ppd-H1,eam7*) plants grown under short days. The main culm was dissected 6, 16, 23, and 40 DAE. White scale bars indicate 100 μm , and gray scale bars indicate 500 μm . **D and E**) Main shoot apex (MSA) development under long-day (**D**) and short-day (**E**) conditions according to the scale by Waddington et al. (1983) by DAE. Dot sizes indicate the number of plants per data point (1 to 4), and gray areas show a 95% confidence interval of a polynomial regression (Loess smooth line). Horizontal lines indicate the start of spikelet initiation (W2.0) and the start of floral development (W3.5).

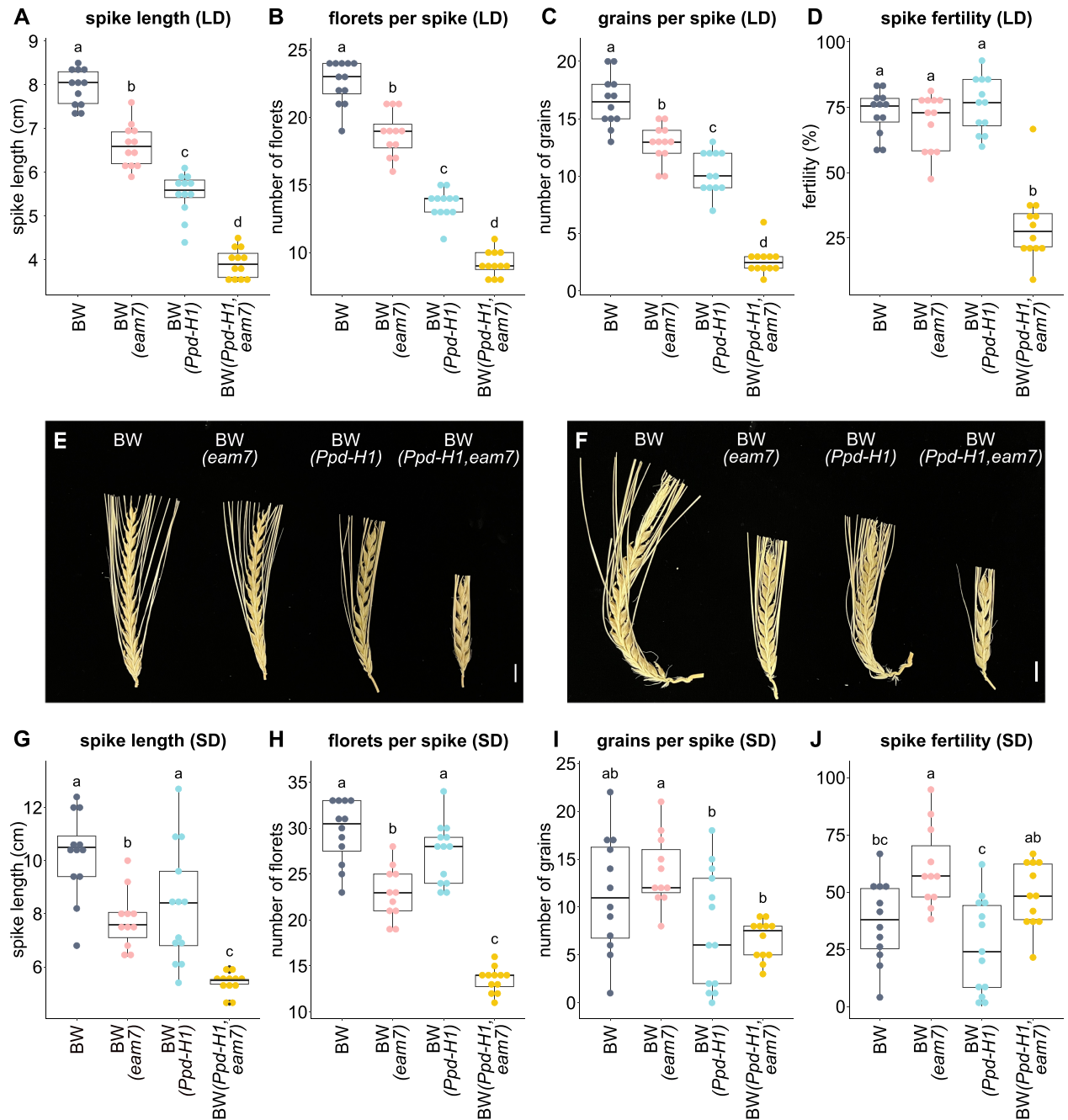


Figure 2. Effect of *eam7* on fertility under LD and SD. Spike length (in cm), floret and grain number on the spike, and spike fertility (in %) were scored on the main culm of plants grown under long days (LDs) (**A to D**) or short days (SDs) (**G to J**). Spike fertility was calculated by dividing the number of grains by the number of florets on the main spike. Boxplots show the median (central line), the upper and lower quartiles (box), the maximum values (whiskers), and individual values (points). Significance levels were determined by one-way ANOVA and subsequent Tukey's test, $P \leq 0.05$, $n = 11$ to 13 plants. **E and F**) Representative images of fully developed spikes from the main culm of plants grown under long days (**E**) or short days (**F**). Scale equals 1 cm.

with *Ppd-H1* to control SM initiation and floret fertility under SD. In the background of a mutated *Ppd-H1* allele, *eam7* did not affect SM initiation but still affected floret and grain number, and spike fertility. Early flowering decreased plant height, the number of leaves and tillers, and flag leaf size under LD and SD.

The expression pattern of circadian clock genes is altered in *eam7* plants under SD

Day-length neutrality and early flowering under SD conditions have been associated with genetic variation in circadian clock genes and phytochromes in cereal crops (Faure et al. 2012; Campoli et al. 2013; Pankin et al. 2014; Müller et al.

2020; Alvarez et al. 2023). We, therefore, tested if the diurnal expression pattern of phytochromes and core clock genes was altered by *eam7*. As the most substantial effects of *eam7* on development were observed under SD, we tested the diurnal expression of phytochromes and core clock genes under SD conditions.

The expression patterns of *PHYB*, *PHYC*, and clock genes were strongly altered in BW(*eam7*) and BW(*Ppd-H1*, *eam7*) compared to BW and BW(*Ppd-H1*) (Fig. 3). At the same time, expression patterns of phytochromes and clock genes did not differ between BW and BW(*Ppd-H1*) and between BW(*eam7*) and BW (*Ppd-H1*, *eam7*), suggesting that *eam7*, but not *Ppd-H1* had a major impact on the diurnal expression patterns. *PHYB/C* and *ELF3* were significantly downregulated at their expression peaks in BW(*eam7*) and BW(*Ppd-H1*, *eam7*) compared to BW and BW(*Ppd-H1*) (Fig. 3, A to C). Furthermore, expression peaks of the evening-expressed clock genes *LUX1*, *PRR59*, *GI*, *PRR1*, and *LHY* were advanced by 2 to 4 h and strongly reduced in BW(*eam7*) and BW(*Ppd-H1*, *eam7*) (Fig. 3, D, G, I to K). The night-time repression of *Ppd-H1*, *PRR73*, *PRR59*, and *PRR95* was released in BW(*eam7*) and BW(*Ppd-H1*, *eam7*), which resulted in high transcript levels in the night and morning (Fig. 3, E to H). This effect was particularly prominent for *Ppd-H1*.

Since *eam7* caused the diurnal misregulation of circadian genes and the central photoperiod response gene *Ppd-H1*, we further tested the expression of central floral activators in the photoperiod response pathway of barley (Campoli et al. 2012). *CO1* expression occurred only during the dark period in BW and BW(*Ppd-H1*) but was advanced by 4 to 6 h and peaked at the end of the light period in BW(*eam7*) and BW(*Ppd-H1*, *eam7*) (Fig. 3L). *CO2* transcripts could not be detected at any time point during the day in any of the genotypes. *FT1*, typically only expressed under LD, showed detectable, but low levels of expression in BW(*Ppd-H1*, *eam7*), while no transcripts could be detected in the other 3 genotypes (Fig. 3M). *FT1* expression under SD was thus controlled by *eam7* together with allelic variation at *Ppd-H1*. The upregulation of *FT1* in BW(*Ppd-H1*, *eam7*) is linked to significantly higher transcript levels of the *MADS*-box gene and floral inducer *VRN1* compared to BW, BW(*eam7*), and BW(*Ppd-H1*) (Fig. 3N).

Because *FT1* was only expressed in BW(*Ppd-H1*, *eam7*), but also BW(*eam7*) flowered earlier under SD, we tested the expression of *FT1* and its homologs *FT2* and *FT3* at later time points during development. We sampled leaf material every 1 to 2 wk between 20 and 60 DAE at ZT9 (1 h after dusk) in BW and the introgression lines and tested *FT1*, *FT2*, *FT3*, and *VRN1* transcript levels. However, we could not detect any *FT1* transcripts during development in BW(*eam7*). We could also not link differences in expression levels in any of the additionally tested genes to the early flowering of BW(*eam7*) under SD compared to BW (Supplemental Fig. S3, A to D).

In conclusion, clock genes and phytochromes displayed marked alterations in diurnal expression patterns. This

suggests that the gene underlying *eam7* is either a component of the circadian clock or is involved in the light-driven entrainment of the barley circadian clock. The *eam7*-controlled misexpression of clock genes, together with functional variation in *Ppd-H1*, were linked to differences in the diurnal expression of *Ppd-H1* and *CO1*, and the upregulation of *FT1* in BW(*Ppd-H1*, *eam7*) under SD conditions.

Biparental mapping identifies *LIGHT-REGULATED WD 1 (LWD1)* as a candidate gene for *eam7*

The recessive *eam7* mutation was mapped to the centromeric region of chromosome 6H5 (Stracke and Börner 1998). For the identification and characterization of *eam7*, the mutant locus *eam7.g* was backcrossed several times to Bowman to generate the introgression lines BW287 (BC₂) and BW288 (BC₃, BW(*eam7*)) (Druka et al. 2011). Both lines are early flowering under SD and were thus proposed to carry the same *eam7.g* mutation (Franckowiak and Lundqvist 2015). Genotyping of BW(*eam7*) (BW288) with the 1,536 SNP array identified an introgression of 151.1 cM (BOPA 2_0886 to BOPA 1_1261) on chromosome 6H as the likely location of the causative *eam7* mutation (Druka et al. 2011). We genotyped BW(*eam7*) with the 50k SNP array to confirm the large introgression on 6H, which could be separated into 2 individual introgressions (Fig. 4A; Supplemental Table S2, Supplemental Data Set 1). The first introgression (6H-1) is spanning 54.75 cM/380.6 Mbp (position 2.2 to 382.8 Mbp, Morex V3, Mascher et al. 2021) and contains 802 polymorphic SNPs compared to the recipient parent BW and 2,329 high-confidence (HC) genes. The second introgression could be excluded as a likely location of the *eam7* locus since it is located on the long arm of chromosome 6 (Supplemental Table S2).

To confirm and narrow down the *eam7* location on 6H, we scored 423 F2 plants from a cross between BW(*eam7*) and BW(*Ppd-H1*) for flowering time under SD and genotyped the population for selected SNPs in the introgressed region on 6H (Supplemental Tables S3 and S4). The population showed a bimodal distribution in flowering time, with 89 plants flowering between 36 and 59 d and thus significantly earlier than the 334 remaining lines, which flowered between 77 and 128 d or did not flower until the end of the experiment. We could confirm that all F2 plants that exhibited early flowering under SD carried a homozygous introgression on 6H and were either homozygous or heterozygous for the wild-type *Ppd-H1* allele on 2H (Supplemental Data Set 2). The observed segregation ratio corresponded to the expected ratio of 13:3 ($\chi^2 = 1.459$, $P = 0.2271$), assuming a recessive *eam7* mutation and a dominant *Ppd-H1* wild-type allele. We could reduce the area of introgression 6H-1 to 2.98 cM/286 Mbp (position 96.64 to 382.8 Mbp) containing 1,084 HC genes (introgression 6H-1-reduced, Fig. 4A; Supplemental Table S2). These included 10 genes homologous to Arabidopsis genes with functions in the circadian clock (Araport 11 annotation, Cheng et al. 2017) (Supplemental Table S5, Supplemental Data Set 3).

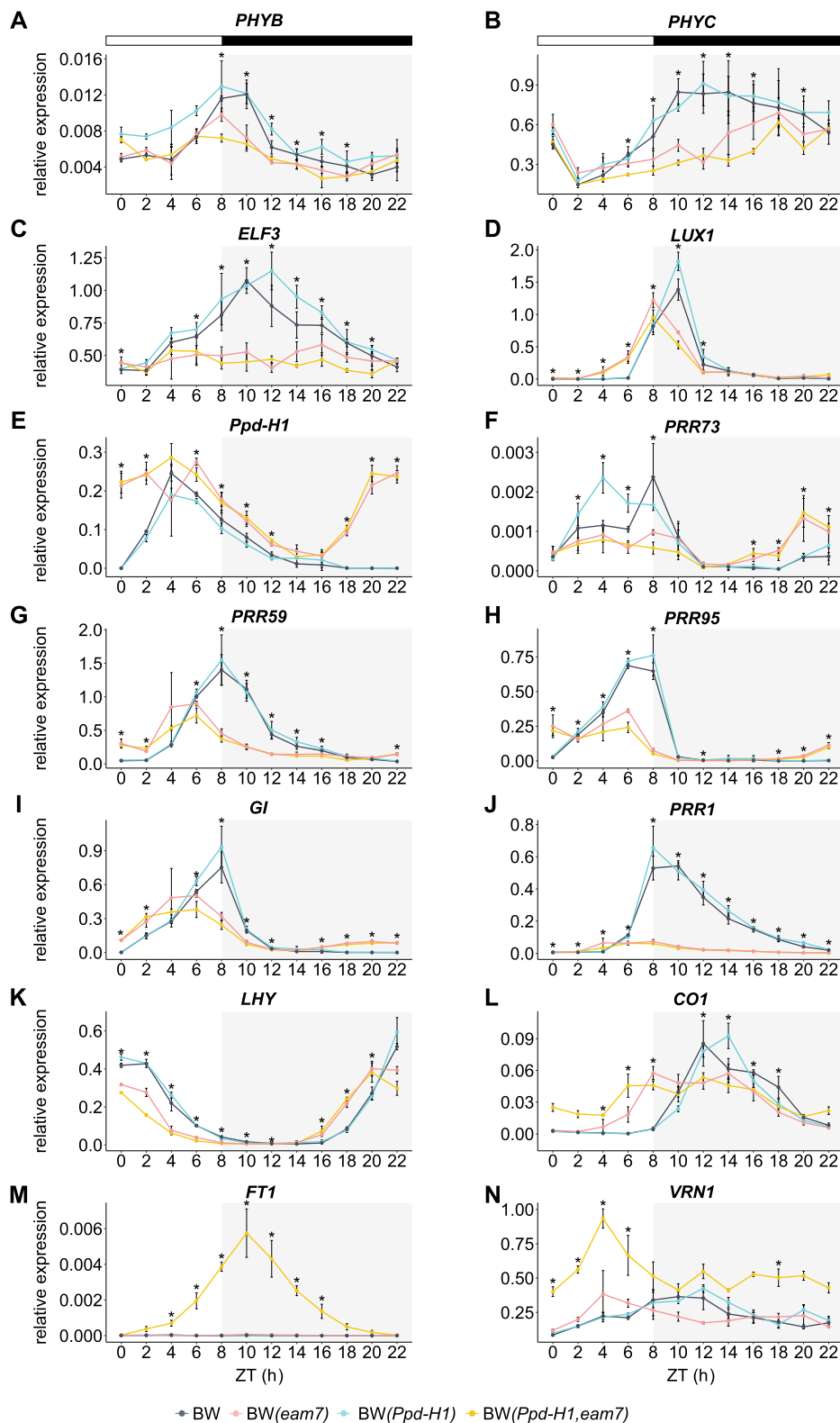


Figure 3. Gene expression pattern of circadian clock genes under SD conditions. Relative expression of *PHYB*, *PHYC*, *ELF3*, *LUX1*, *Ppd-H1*, *PRR73*, *PRR59*, *PRR95*, *GI*, *PRR1*, *LHY*, *CO1*, *FT1*, and *VRN1* in Bowman (gray), BW(Ppd-H1) (blue), BW(eam7) (pink), and BW(Ppd-H1, eam7) (yellow) under short-day conditions. Plants were sampled every 2 h from Zeitgeber Time (ZT) 0 to 22. White bars indicate day and black bars indicate night. Each value represents the mean of 3 independent biological replicates, each consisting of 2 pooled plants. Error bars indicate the standard deviation of the mean; significant differences are indicated by asterisks ($*P \leq 0.05$) comparing BW and BW(Ppd-H1) to BW(eam7) and BW(Ppd-H1, eam7) (A to L, N) or BW, BW(Ppd-H1), and BW(eam7) to BW(Ppd-H1, eam7) (M) with Student's *t*-test, $n = 3$.

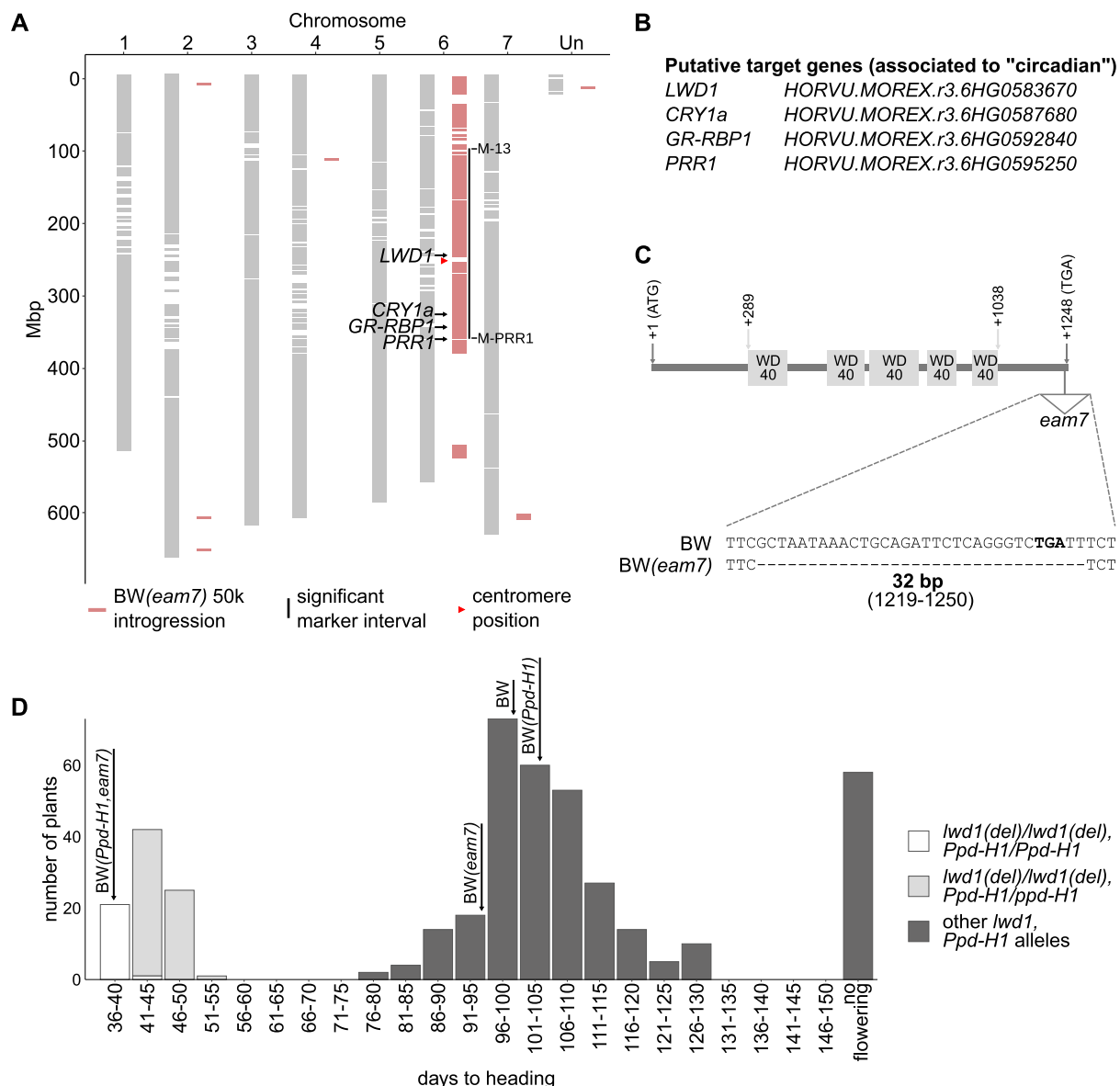


Figure 4. Mapping of *eam7* and identification of *LWD1* as a candidate gene. **A**) Overview of the *eam7* introgression in parent Bowman (BW), based on 50k Illumina Infinium iSelect SNP array. SNPs were mapped to Morex V3 (Mascher et al. 2021). Horizontal gray bars indicate SNPs that do not differ in BW and BW(*eam7*), while pink bars show SNPs polymorphic in BW(*eam7*) compared to BW. The vertical black line represents the significant marker interval determined by biparental mapping and its flanking markers (*M-13* and *M-PRR1*), and the red arrow indicates the predicted centromere position (256 Mbp, Mascher et al. 2021). Black arrows show the approximate position of candidate genes. **B**) Overview of putative *eam7* candidates related to the term "circadian" within the significant marker interval. **C**) Schematic overview of the *LWD1* gene. *LWD1* is a single-exon gene with 5 WD40 repeat domains. The *eam7* allele has a 32 bp deletion at the end of the coding sequence from position 1,219 to 1,250 (relative to the start codon). The stop codon is indicated in bold. **D**) Flowering time under short days of F2 plants of a biparental mapping population, segregating for *eam7* and *Ppd-H1*. This shows 100% co-segregation of the 32 bp *lwd1* deletion (*lwd1*(del)) with early flowering in the presence of a homozygous (white) or heterozygous (light gray) wild-type *Ppd-H1* allele. Plants with other allele combinations (homozygous for the mutated *Ppd-H1* allele, heterozygous for *lwd1*(del), or no deletion in *lwd1*) were grouped together (dark gray). Arrows indicate the approximate mean flowering time of parents BW(*Ppd-H1*, *eam7*) (37.8 ± 0.9 d), BW(*eam7*) (95.6 ± 5.7 d), BW (99.5 ± 6.4 d), and BW(*Ppd-H1*) (106.1 ± 9.7 d). Fifty-seven of 423 plants did not flower until the end of the experiment (130 DAE).

These candidates included 4 genes which are all associated with early flowering in barley or Arabidopsis: the clock gene *PRR1* (HORVU.MOREX.r3.6HG0595250), blue light receptor *CRYPTOCHROME 1a* (*CRY1a*, HORVU.MOREX.r3.6HG0587680), *GLYCIN-RICH RNA-BINDING-PROTEIN 1* (*GR-RBP1*, HORVU.

MOREX.r3.6HG0592840), and HORVU.MOREX.r3.6HG0583670 with high protein sequence identity (79% and 76%) to Arabidopsis *LIGHT-REGULATED WD 1* (*LWD1*) and *LWD2* (Fig. 4B; Supplemental Fig. S4). Due to the higher sequence similarity to *LWD1*, we termed the gene *HvLWD1*.

We Sanger sequenced these candidate genes in BW and the derived introgression lines BW(*Ppd-H1*), BW(*eam7*), and BW(*Ppd-H1, eam7*), the original *eam7.g* mutant Atsel and its parent, Atlas and the derived introgression donor GSHO579 which was introgressed into Bowman carrying the *eam7* mutation (Druka et al. 2011). *CRY1a* and *GR-RBP1* did not show any SNPs within the coding sequence between BW and BW(*eam7*) and were therefore excluded as candidates for *eam7*. For *PRR1*, we detected 2 non-synonymous SNPs (T215A and S434P) between BW(*eam7*) and BW (Supplemental Table S5). These SNPs were also present in *eam7* genotypes GSHO579 and Atsel, but likewise in the parent Atlas, which does not carry the *eam7* allele (Supplemental Fig. S5A). In addition, genotyping *PRR1* in the F2 population revealed one recombinant plant, which was with 104 DAE late flowering but carried the SNP haplotype from the introgressed segment (S434P, marker M-*PRR1*, Supplemental Table S3). We, therefore, excluded *PRR1* as a candidate for *eam7*. For *LWD1*, we identified a 32 bp deletion (position 1,219 to 1,252) in BW(*eam7*) and BW(*Ppd-H1, eam7*) but not in BW and BW(*Ppd-H1*) (Fig. 4C; Supplemental Table S5). This deletion is not within a conserved domain but shortens the protein length from 415 to 410 aa. The deletion was also present in *eam7* genotypes GSHO 579 and Atsel, but not in Atlas (Supplemental Fig. S5B). The complete co-segregation of *LWD1* with the early flowering phenotype was confirmed by genotyping the F2 population for the 32 bp deletion in *LWD1* (Fig. 4D; Supplemental Table S3). Sanger sequencing revealed that this deletion, however, was not present in the *eam7* introgression line BW287, suggesting that the causative mutations for early flowering under SD differed between BW(*eam7*) and BW287.

In summary, the genetic mapping reduced the introgression on chromosome 6H and revealed *LWD1* as a putative candidate gene for *eam7*.

CRISPR-generated mutants confirm *LWD1* as the gene underlying the *eam7* locus

To confirm *LWD1* as the gene underlying the *eam7* locus, we generated *lwd1* mutant plants using CRISPR-Cas9. GP-fast (spring cultivar Golden Promise with a dominant *Ppd-H1* introgressed from Igri, Gol et al. 2021) was transformed with 2 different constructs. These targeted either the start or the end of the CDS of *LWD1* to create either a complete knockout or a mutation similar to the 32 bp deletion present in BW(*eam7*). From 16 individual mutation events, 3 homozygous M2 lines were chosen for further experiments: *lwd1-26* and *lwd1-390*, with mutations early in the coding sequence and a total protein length of 26 and 390 aa, respectively, and *lwd1-402*, with modifications close to the C terminus and a total protein length of 402 aa (Supplemental Fig. S6).

Homozygous M2 and GP-fast plants were grown under SD conditions to test whether the mutant plants were early flowering under SD as observed for *eam7*. All mutant plants

flowered early in comparison to GP-fast: *lwd1-26* flowered 45 DAE, followed by *lwd1-402* with 51 DAE and *lwd1-390* with 67 DAE as compared to GP-fast, which flowered 104 DAE (3 plants) or had not flowered (20 plants) when the experiment was terminated (Fig. 5A). *lwd1* shoots and spikes were shorter than in GP-fast, similar to the differences in plant height and spike length between BW(*Ppd-H1, eam7*) and BW (Fig. 5, B and C). While *lwd1* plants produced fewer florets than GP-fast, grain set and spike fertility significantly increased (Supplemental Fig. S7).

We then tested if the *lwd1* mutant lines were also altered in phytochrome and clock gene expression as observed for the *eam7* genotypes. We grew GP-fast and *lwd1* mutant plants under SD for 2 wk and sampled them in 4 h intervals for a complete light–dark cycle. We could confirm that *lwd1* mutant plants were characterized by altered diurnal transcript patterns for phytochromes, clock, and flowering time genes comparable to those observed in *eam7* plants. The expression of phytochromes and *ELF3* showed a strong downregulation in the 3 *lwd1* mutant lines compared to GP-fast, as seen in *eam7* genotypes compared to BW (Fig. 5, D to F). The peak expression of *LUX1*, *PRR1*, and *LWD1* itself was reduced and advanced by 4 h in the *lwd1* mutants compared to GP-fast, similar to *eam7* plants (Fig. 5, G to I; Supplemental Fig. S3E). *Ppd-H1* transcription was de-repressed in *lwd1* mutants at night, which increased *Ppd-H1* expression levels in the night and morning (Fig. 5J). In *lwd1* mutants, *CO1* expression peaked earlier and at the end of the light phase (Fig. 5K). All *lwd1* lines showed low *FT1* expression levels, whereas no *FT1* transcripts could be detected for GP-fast (Fig. 5L).

To confirm that *lwd1* and *eam7* are allelic, complementation experiments were performed by crossing homozygous *lwd1-26*, *lwd1-390*, and *lwd1-402* in the background of GP-fast with homozygous BW(*Ppd-H1, eam7*). Since *eam7* and all 3 *lwd1* mutations are recessive, we expected that the resulting F1 plants would display the mutant phenotype if *eam7* and *lwd1* are allelic. As controls, we also crossed the *lwd1* mutants with the parental backgrounds GP-fast and BW(*Ppd-H1*), which are homozygous for the wild-type EAM7 allele.

All plants carrying at least one functional copy of *LWD1* flowered late under SD, between 98 and 114 DAE, or did not flower until the end of the experiment at 125 DAE (Fig. 6). A larger proportion of GP-fast plants failed to flower compared to BW(*Ppd-H1*), suggesting that additional minor variation for flowering time under SD segregated between GP-fast and BW. All F1 offspring plants from the 3 *lwd1*/BW(*Ppd-H1, eam7*) crosses flowered early under SD (Fig. 6; Supplemental Fig. S8). The F1 hybrids flowered on average 15 d earlier than the homozygous *lwd1* mutants in the GP-fast background, likely because BW carried additional variation for early flowering compared to GP-fast as observed in the control crosses. However, as only the *lwd1*/BW(*Ppd-H1, eam7*) crosses flowered early under SD and did not show any abortion of the main spike, these results suggested that *lwd1* and *eam7* are allelic.

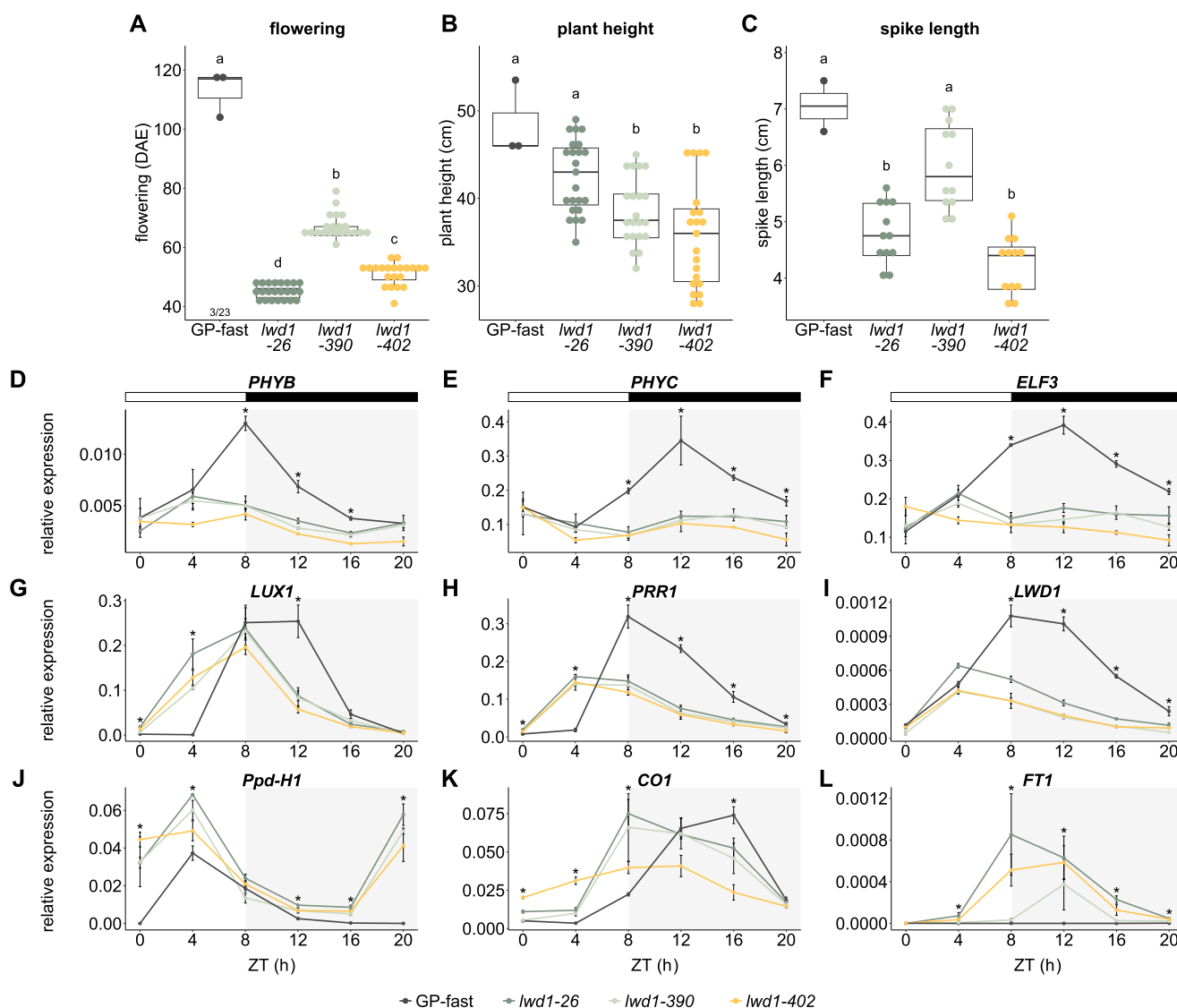


Figure 5. *lwd1* plants phenocopy BW(*Ppd-H1*, *eam7*). **A to C**) Spring cultivar GP-fast and the 3 *lwd1* mutants *lwd1-26*, *lwd1-390*, and *lwd1-402* were grown under short-day conditions. Flowering time (**A**), plant height at flowering (in cm) (**B**), and spike length (in cm) (**C**) were scored on the main culm. Boxplots show the median (central line), the upper and lower quartiles (box), the maximum values (whiskers), and individual values (points). Numbers below boxplots in (**A**) indicate the number of plants that flowered until the end of the experiment (130 days after emergence, DAE) compared to the total number of plants scored. Significance levels were determined by one-way ANOVA and subsequent Tukey's test, $P \leq 0.05$, $n = 3$ for GP-fast, $n = 12$ to 23 for *lwd1* plants. **D to L**) Diurnal gene expression in *lwd1* mutants and wild-type plants. Relative expression of *PHYB*, *PHYC*, *ELF3*, *LUX1*, *PRR1*, *LWD1*, *Ppd-H1*, *CO1*, and *FT1* in GP-fast (gray), *lwd1-26* (dark green), *lwd1-390* (light green), and *lwd1-402* (yellow) in short-day conditions. Plants were sampled every 4 h from zeitgeber time (ZT) 0 to 22. White bars indicate day and black bars indicate night. Each value represents the mean of 3 independent biological replicates, each consisting of 2 pooled plants. Error bars indicate the standard deviation of the mean; significant differences are indicated by asterisks ($*P \leq 0.05$) comparing the 3 *lwd1* lines to GP-fast with Student's *t*-test, $n = 3$.

In summary, *lwd1* mutants phenocopied Bowman's *eam7* plants. They were early flowering under SD, and the diurnal expression pattern of phytochromes, circadian clock, and flowering genes was altered. Complementation tests suggested that *eam7* and *lwd1* are allelic.

Natural variation of *LWD1*

LWD1 belongs to the WD40-repeat proteins, which are conserved across eukaryotes and are involved in highly diverse

processes, including flowering and floral development (van Nocker and Ludwig 2003). In *Arabidopsis*, 2 functionally redundant *LWD* proteins, *LWD1* and *LWD2*, control photoperiod response and flowering time under LD and SD (Wu et al. 2008). Barley and other *Triticeae* carry 2 paralogous genes, *WD40-1*, homologous to *LWD1* and *LWD2*, and *WD40-2* (*HORVU.MOREX.r3.6HG0604400*), homologous to *Arabidopsis* *TRANSPARENT TESTA GLABRA 1* (*TTG1*) (Strygina and Khlestkina 2019). Comparison of *LWD1* protein

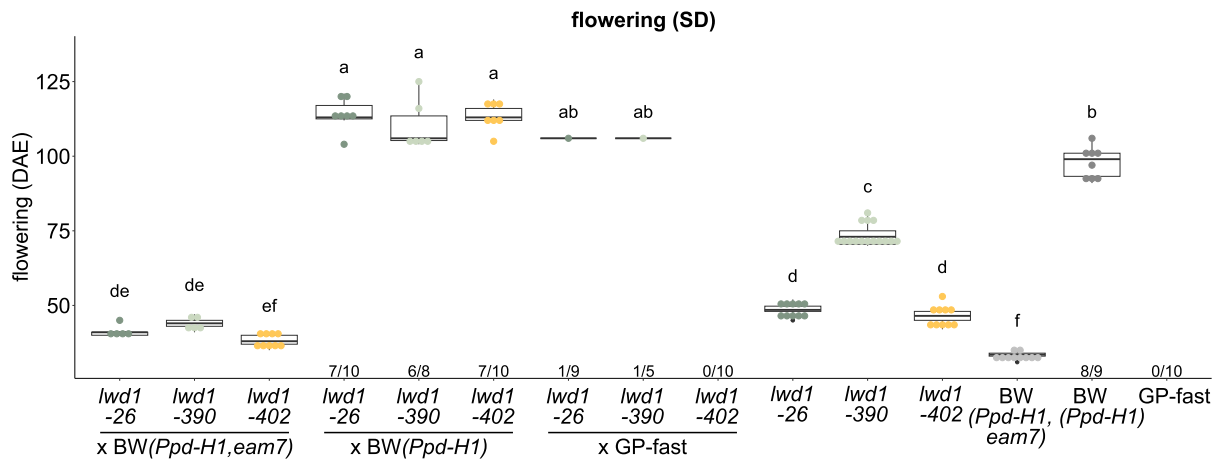


Figure 6. Allelism tests of *lwd1* and *eam7* mutants. F1 offspring of crosses between *lwd1* mutants and BW(*Ppd-H1*, *eam7*), BW(*Ppd-H1*), and GP-fast, and parent plants were grown under short-day (SD) conditions, and flowering was scored. Boxplots show the median (central line), the upper and lower quartiles (box), the maximum values (whiskers), and individual values (points). The numbers below boxplots indicate the number of plants that flowered until the end of the experiment (125 days after emergence, DAE) compared to the total number of plants scored. If no number is given, all plants flowered. Significance levels were determined by one-way ANOVA and subsequent Tukey's test, $P \leq 0.05$, $n = 1$ to 15 plants.

sequences across barley, bread wheat (*Triticum aestivum*) and emmer wheat (*Triticum didocum*), *Brachypodium distachyon*, rice, sorghum (*Sorghum bicolor*), and maize (*Zea mays*) demonstrated that the amino acid sequences of LWD1 are highly conserved in grasses (Supplemental Fig. S9, A and B). Furthermore, alignment of the last 15 amino acids from HvLWD1 with 281 homologous sequences from plant WD proteins showed that the protein terminus deleted in *eam7* is highly conserved even though located outside the WD repeats (Supplemental Fig. S9C).

We examined natural variation in the coding sequence of LWD1 by exploiting publicly available exome resequencing data from extensive collections of diverse barley germplasm (Russell et al. 2016; Bustos-Korts et al. 2019). Among the 670 investigated barley accessions, we identified 9 haplotypes in a haplotype network analysis (Supplemental Fig. S10, Supplemental Data Set 4). The 2 major haplotypes (I and II) comprised 97.8% of the analyzed accessions and were the only ones identified in elite barley cultivars. Haplotype I included LWD1 from the reference cultivar Morex and haplotype II carried a synonymous SNP. Seven additional minor haplotypes (III-IX) were identified in wild and landrace germplasm. Of these, only haplotypes VIII and IX carried non-synonymous changes in LWD1 and these were observed in only 4 and 2 genotypes, respectively. Their effect on protein function was assessed using the Sorting Intolerant from Tolerant (SIFT) algorithm (Sim et al. 2012), which predicted tolerated effects on the protein function for both amino acid substitutions (Supplemental Table S6).

In summary, natural variation in the coding sequence of LWD1 was low, and only a few landraces and wild barley accessions showed variation in LWD1 with no or predicted low-effect changes in the LWD1 protein. While we cannot exclude that natural variation in the regulatory sequences existed in the diverse germplasm set, this result suggested

that LWD1 is functionally conserved and under strong selection.

Discussion

LWD1 is a candidate for the *eam7* locus

We identified LIGHT-REGULATED WD 1 (LWD1) as a putative candidate gene underlying the *eam7* locus. We demonstrate that *eam7* in the background of a wild-type *Ppd-H1* allele causes rapid flowering and near day-length neutrality under SD.

Stracke and Börner (1998) mapped *eam7* close to the centromere on the short arm of chromosome 6H, and Druka et al. (2011) identified an introgression of 151.1 cM on 6H in the background of Bowman as the likely location of the causative *eam7* mutation. We narrowed down the genomic location of *eam7* to 2.98 cM using a biparental mapping population of a cross between the *eam7* introgression line BW(*eam7*) and the wild-type *Ppd-H1* introgression line BW(*Ppd-H1*). Within this mapping interval with more than 1,000 genes, we identified 4 putative candidate genes with functions in flowering time and circadian regulation based on the current barley reference (Mascher et al. 2021). We would like to point out that we might have excluded genes absent in the reference genome, and genes with unknown new functions in photoperiod control with this approach. Based on genetic mapping and sequencing of the 4 candidate genes, we revealed LWD1 with a 32 bp deletion in the C terminus of the gene as a promising candidate gene underlying the early flowering phenotype under SD (Fig. 4). To confirm LWD1 as a candidate for *eam7*, we used CRISPR-Cas9 to generate different *lwd1* mutants in the genotype GP-fast carrying a wild-type *Ppd-H1* allele. All analyzed homozygous *lwd1* mutants flowered significantly earlier than the wild-type under SD conditions, irrespective of the size of the protein

truncation (Fig. 5), confirming that *LWD1* controls flowering under SD in barley. In addition, all 3 *lwd1* mutants displayed the same changes in diurnal expression patterns of core clock genes and clock output genes as observed for *eam7* compared to the wild-type genotypes. Finally, we generated F1 hybrids between BW(*Ppd-H1*, *eam7*) and the *lwd1* mutant lines to show that *lwd1* did not complement *eam7*, suggesting that both mutations are allelic. The strong effects of C-terminal protein truncations in *eam7* and *lwd1-402* and the high degree of conservation of the C-terminal amino acids in WD proteins across different taxa indicated that the terminal part of the *LWD1* protein is crucial for its function. However, fine-mapping of *eam7* down to the 32 bp deletion would provide the ultimate evidence that this C-terminal truncation is causative for the *eam7* phenotype.

EAM7 is important for photoperiod sensing in barley

We demonstrated that *eam7* in the background of a wild-type *Ppd-H1* allele causes rapid flowering and near day-length neutrality under SD. We thus concluded that *eam7* is important for photoperiod perception in barley. This effect is reminiscent of the early maturity mutants *eam5*, *eam8*, and *eam10*, which are also early flowering under non-inductive photoperiods and were identified as mutant alleles of *PHYC* and the core clock components *ELF3* and *LUX1*, respectively (Faure et al. 2012; Campoli et al. 2013; Pankin et al. 2014).

In *eam7* plants, allelic variation at the major photoperiod response gene *Ppd-H1* strongly affected flowering time under SD; *eam7* plants with a wild-type *Ppd-H1* allele flowered more than 50 d earlier than those with a mutated *Ppd-H1* allele (Fig. 1). Furthermore, *eam7* plants were characterized by a strong upregulation of *Ppd-H1* in the night and the morning, which was linked to the expression of *FT1* and early flowering under SD (Fig. 3). We thus propose that *eam7* is an upstream transcriptional regulator of *Ppd-H1*. The upregulation of *Ppd-H1* in the night has already been associated with *FT1* expression under SD and day-neutral flowering in *eam5*, *eam8*, and *eam10* and photoperiod insensitive wheat lines (Faure et al. 2012; Shaw et al. 2012; Campoli et al. 2013; Pankin et al. 2014). *eam7* thus likely alters photoperiodic flowering by controlling the diurnal expression pattern of *Ppd-H1*. However, in contrast to *eam8* (*elf3*), which causes day-neutral flowering irrespective of allelic variation at *Ppd-H1*, *eam7* has only a minor effect on flowering time in the background of a mutated *Ppd-H1* allele. Early flowering under SD in *eam7* mutants was thus dependent on the presence of the wild-type *Ppd-H1* allele and the night-time upregulation of *Ppd-H1*.

It has been demonstrated that the repression of *Ppd-H1* at night is controlled by *ELF3* (*EAM8*) and *LUX1* (*EAM10*) in barley and wheat (Faure et al. 2012; Campoli et al. 2013; Alvarez et al. 2023). In Arabidopsis, *ELF3* and *LUX* interact to bind the promoter of the *Ppd-H1* ortholog *PRR7* to repress the expression during the night (Mizuno et al. 2014), and this function is likely conserved in barley and wheat (Faure et al. 2012; Campoli et al. 2013; Alvarez et al. 2023). *ELF3* expression

was strongly downregulated in *eam7* plants suggesting that *LWD1* controls *Ppd-H1* expression through *ELF3* (Fig. 3). However, *EAM7* might also directly regulate *Ppd-H1* expression, since in Arabidopsis the paralogs *LWD1* and *LWD2* directly bind to the promoters of *PRR* genes (Wang et al. 2011). In contrast to *EAM7* in barley, Arabidopsis *LWD1* and *LWD2* act as positive regulators of *PRR* expression (Wang et al. 2011). In addition to *ELF3*, we also observed the downregulation of *PHYC* and *PHYB* in *eam7* plants. *PHYB* and *PHYC* are necessary for the light activation of *Ppd-H1* and act as upstream repressors of *ELF3* in barley, wheat, and *Brachypodium* (Chen et al. 2014; Pankin et al. 2014; Alvarez et al. 2023; Woods et al. 2023). *EAM7* might therefore affect flowering time by modifying the expression of phytochromes and *ELF3* and, thus, the light input into the photoperiod pathway.

In Arabidopsis *thaliana*, *LWD1* and *LWD2* regulate photoperiodic flowering by advancing the expression phase of core clock and clock output genes under light/dark conditions (Wu et al. 2008). The early flowering phenotype of the Arabidopsis *lwd1lwd2* double mutant was attributed to a phase shift of the clock target and central photoperiod response gene *CONSTANS* (*CO*) and a consequent increase in *FT* expression. Similarly, in *eam7* mutants, the expression phase of evening-expressed clock genes *PRR59/95* and *GI* shifted approximately 4 h forward, suggesting that *LWD1* controls the expression phase of the central oscillator genes in barley (Fig. 3). This phase shift was associated with a forward shift and day-time expression of *CO1* under SD in the *eam7* mutants (Fig. 3). In Arabidopsis, the coincidence of *CO* expression with the light period is crucial for stabilizing the protein and expressing the florigen *FT* (Sawa et al. 2007; Jang et al. 2008). Similar to the Arabidopsis *lwd1lwd2* double mutants, the *eam7* mutants with an altered diurnal expression of *CO1* were characterized by *FT1* expression in non-inductive photoperiods. However, in barley and wheat, *CO1* mainly acts as a weak heading time repressor and accelerates flowering only in the absence of *Ppd-H1* (Shaw et al. 2020). Furthermore, night-break experiments have revealed that the length of the night and not of the light period is critical for the perception of inductive photoperiods in monocots (Pearce et al. 2017; Gao et al. 2019). Furthermore, BW(*eam7*) also displayed a shift in *CO1* phase expression into the day as observed in BW(*Ppd-H1*, *eam7*), but no *FT1* expression and only a minor acceleration in flowering under SD. Night-breaks during long nights cause the rapid upregulation of *Ppd-H1*, followed by *FT1* expression and flowering (Pearce et al. 2017). Similarly, *Ppd-H1* is upregulated during a long night in *eam7* and *lwd1* mutants but strongly downregulated in wild-type plants. These parallels in the molecular and flowering phenotype between night-break experiments and *eam7/lwd1* mutants suggested that *eam7* alters photoperiod sensing or downstream signaling. Further, the night-time de-repression of *Ppd-H1* either by night-breaks or mutations in upstream regulators such as *eam7* might thus be relevant for early flowering under SDs

(Faure et al. 2012; Campoli et al. 2013; Pankin et al. 2014; Pearce et al. 2017). Nevertheless, the advance in phase expression of clock and clock output genes was comparable between barley *eam7* mutants and Arabidopsis *lwd1lwd2* double mutants, and the function of *LWD1* in controlling the light entrainment of the clock, is thus likely conserved across these taxa.

In summary, we have successfully identified *LWD1* as a promising candidate to underlie the *eam7* locus. We propose that *LWD1* functions as an upstream activator of the nighttime repressor *ELF3* in the light entrainment pathway of the barley circadian clock. *eam7* plants were early flowering in non-inductive photoperiods due to the reduced activation of *ELF3*, the upregulation of *Ppd-H1* during the night, and consecutive *FT1* expression under SD. *LWD1* is an interesting target to modulate photoperiod sensitivity to breed for barley cultivars adapted to short growing seasons.

Materials and methods

Plant material

Barley (*Hordeum vulgare*) spring cultivar Bowman (BW) with a mutated *Ppd-H1* allele and 3 Bowman-derived introgression lines were used in this study. The introgression line BW281 (GSHO 1872) carries a wild-type *Ppd-H1* allele introgressed from winter barley KT1031 (GSHO 1568) (Druka et al. 2011). BW288 (GSHO 2068, NGB 20572) is an introgression line with the *eam7.g* mutation introgressed from Club Mariout/6*California Mariout (GSHO579, Gallagher et al. 1991) in Bowman by 3 rounds of backcrossing (Druka et al. 2011). We termed these introgression lines BW(*Ppd-H1*) and BW(*eam7*). We crossed BW(*Ppd-H1*) and BW(*eam7*) to generate a line with a wild-type *Ppd-H1* allele and the mutation at *eam7.g*. The F2 generation of this cross was grown under SD to identify early flowering plants homozygous for the wild-type *Ppd-H1* allele and the *eam7* introgression. The *Ppd-H1* allele was determined by using the CAPS marker designed by Turner et al. (2005) (Supplemental Table S4), and the presence of the *eam7* introgression was genotyped based on the 32 bp deletion in *LWD1* and a CAPS marker placed within the introgression (M-*eam7*, Supplemental Table S4). An early flowering plant homozygous for *eam7* and *Ppd-H1* was used for single seed propagation by selfing the plants twice until used for experiments. We termed this genotype BW(*Ppd-H1*, *eam7*).

The F2 generation of the cross between BW(*Ppd-H1*) and BW(*eam7*) was used for segregation analysis and mapping of *eam7*. Furthermore, the *eam7* introgression donor GSHO579 and the original *eam7.g* mutant Atsel (Clho 6250) and its genetic background Atlas (PI 539108) were included to sequence potential candidate genes. We also included BW287 (NGB 20571), which was generated by backcrossing Club Mariout/6*California Mariout with *eam7.g* into Bowman by 2 cycles of crossing and was thus reported to be allelic to BW(*eam7*) (Druka et al. 2011).

The introgression line GP-fast, spring cultivar Golden Promise with a dominant *Ppd-H1* allele introgressed from

winter cultivar Igri (Gol et al. 2021), was transformed to generate mutants in *LIGHT-REGULATED WD 1* (*LWD1*, HORVU.MOREX.r3.6HG0583670) using CRISPR-Cas9. Three independent homozygous M2 lines, *lwd1-26*, *lwd1-390*, and *lwd1-402*, were selected for functional analyses and crossing to BW(*Ppd-H1*, *eam7*). *lwd1-26* has 2 deletions within the CDS (-C21, -C23) and one single insertion (+T114) that lead to a frameshift and premature stop codon, reducing the protein from 415 (WT) to 26 amino acids (aa). *lwd1-390* has 2 deletions (66 bp, position 15 to 80 and 9 bp, position 109 to 117) that are in frame and lead to the deletion of amino acids 6 to 27 and 37 to 39, reducing the protein size to 390 aa. *lwd1-402* has a 39 bp deletion (position 1,198 to 1,238) that reduces protein length to 402 aa.

Plant phenotyping and growth conditions

BW and the derived introgression lines BW(*Ppd-H1*), BW(*eam7*), and BW(*Ppd-H1*, *eam7*) were cultivated under controlled growth conditions for phenotyping and gene expression analyses. All plants were grown in soil (Einheitserde ED73, Einheitserde Werkverband e.V., with 7% sand and 4 g/L Osmocote Exact Hi.End 3 to 4 M, 4th generation, ICL Group Ltd.) and were stratified for 4 d in 4 °C before moving them to controlled growth conditions.

For phenotyping, plants were grown in plant growth chambers under long-day (LD, 16 h light, 20 °C, photosynthetically active radiation (PAR) $\sim 250 \mu\text{mol m}^{-2} \text{s}^{-1}$; 8 h dark, 16 °C) and short-day (SD, 8 h light, 20 °C, PAR $\sim 250 \mu\text{mol m}^{-2} \text{s}^{-1}$; 16 h dark, 16 °C) conditions in QuickPot E 24/10 trays (HerkuPlast Kubern GmbH). Flowering was scored in DAE as the period between emergence from soil and reaching Zadoks stage 49 when the awns exited the leaf sheath (Zadoks et al. 1974). Plant height, leaf number on the first emerging shoot (main culm), and tiller number were scored at flowering. Plant height was scored as the distance from soil to the flag leaf ligule of the main culm. Leaf number was scored on the main culm, and tiller number as all tillers emerging after the main culm. The length and width of the flag leaf on the main culm were measured as the leaf blade length (from the ligule to the leaf tip) and the maximum width of the blade under SD. Spike length, floret number, and grain number of the main culm were scored at maturity. Fertility was calculated as the percentage of florets on the mature spike that developed into grains. The experiment was stopped 125 DAE, and all plants that had not flowered up to this point were scored as “not flowering”.

MSA development of all 4 genotypes was monitored and quantified based on the scale by Waddington et al. (1983). Once or twice a week, the development of the MSA of the main stem of 4 randomly chosen plants per genotype was dissected. MSA development was documented using the stereo microscope Nikon SMZ18 with a Nikon DS-Fi2 camera and was analyzed with the NIS-Elements Software (version 5.21.03, Nikon Instruments Europe BV). Under LD, plants were dissected every 2 to 10 d starting from 5 DAE until pollination (W10.0). Under SD, plants were dissected every 6 to

8 d between 6 and 47 DAE and every 4 to 13 d from 48 DAE until pollination. The number of developing SM, including those that had initiated floret meristems (FM) or developed into florets, was determined on the main inflorescence. The R package *segmented* (version 1.6-2, Muggeo 2008) was used to calculate broken-line regressions for SM initiation and FM abortion by plotting the number of SM against the Waddington stage. One breakpoint was calculated automatically to separate initiation from abortion and was set as the maximum SM number stage. The corresponding maximum SM number was calculated using linear regression calculated with *segmented*.

The *lwd1* mutant and wild-type plants were grown in controlled plant growth chambers under SD in QuickPot 96 T trays (HerkuPlast Kubern GmbH) until maturity. Flowering, plant height, leaf and tiller number, leaf size, and yield parameter were scored as described above. Plants that did not flower until 130 DAE were scored as “not flowering”.

Gene expression analysis

Gene expression analysis was performed in 2 independent experiments in Bowman and derived introgression lines BW(*Ppd-H1*), BW(*eam7*), and BW(*Ppd-H1*, *eam7*) and in the CRISPR-Cas9-generated mutants *lwd1-26*, *lwd1-390*, *lwd1-402*, and wild-type GP-fast.

Plants were sown in QuickPot 96 T trays (HerkuPlast Kubern GmbH) and transferred to plant growth chambers after 4 d of stratification at 4 °C. Plants were cultivated under SD conditions until 14 DAE. BW and derived introgression lines were sampled every 2 h, the *lwd1* mutants and wild-type GP-fast every 4 h over a complete light/dark cycle of 24 h (light from ZT0-8, dark from ZT8-24). For each replicate, the middle sections of the youngest, fully elongated leaf of 2 plants were pooled. Three biological replicates were sampled, frozen immediately in liquid nitrogen, and stored at –80 °C until further analysis. In addition, the middle sections of the youngest, fully elongated leaf of the same genotypes were sampled at ZT9 once a week for 6 wk, starting at 19 DAE. These leaf samples were used to monitor *FT1*, *FT2*, *FT3*, and *VRN1* transcript levels during plant development.

RNA was extracted by grinding the samples using TRIzol (Thermo Fisher Scientific) according to the manufacturer's instructions. RNA was resuspended in 60 µL of diethyl dicarbonate-treated water at 4 °C overnight. The remaining DNA was removed by subsequent DNase I treatment (Thermo Fisher Scientific) according to the manufacturer's instructions. cDNA was synthesized on 2 µg of total RNA using ProtoScript II First Strand cDNA Synthesis Kit (NEB) following the manufacturer's instructions. Gene expression levels were determined by RT-qPCR in a LightCycler 480 (Roche) using gene-specific primers (Supplemental Table S7). The reaction was performed using 4 µL of cDNA, 5 µL of 2X Luna qPCR Master Mix (NEB), 0.02 mM of forward and reverse primer, and 0.75 µL of water with the amplification conditions 95 °C for 5 min, 40 cycles of 95 °C (10 s), 60 °C (10 s) and 72 °C (10 s). Non-template controls were added to each

plate, and dissociation analysis was performed at the end of each run to confirm the specificity of the reaction. Starting amounts for transcript levels were calculated based on the titration curve for each target gene using the LightCycler 480 Software (Roche; version 1.5.1.62). Two technical replicates were used and averaged in analyses for each biological replicate. The expression of *Actin* was used as a reference to calculate the relative gene expression of the target genes.

Identification of a candidate gene underlying *eam7*

DNA was extracted from BW(*eam7*) leaf using the DNeasy Plant Mini Kit (QIAGEN) according to the manufacturer's instructions, and plants were genotyped with the 50k Illumina Infinium iSelect SNP Array (Bayer et al. 2017). The *eam7* introgression area was visualized by comparing the BW(*eam7*) allele to the Bowman allele for each SNP. SNPs were plotted against their respective position within the Morex V3 genome assembly in Megabase pairs (Mbp, Mascher et al. 2021). Ambiguous (including heterozygous) and failed SNPs were removed. The *eam7* introgression was defined as the region between the flanking SNPs carrying the Bowman allele.

For segregation analyses, the Bowman introgression lines BW(*eam7*) and BW(*Ppd-H1*) were crossed, and 423 F2 plants together with 9 plants each of BW, BW(*eam7*), and BW(*Ppd-H1*) were sown in QuickPot E24/10 trays. After 4 d of stratification at 4 °C, plants were cultivated under SD conditions, and DNA was extracted using the KingFisher Flex (Thermo Fisher Scientific) and the BioSprint 96 DNA Plant Kit (QIAGEN). Flowering time was scored as described above. Plants that did not flower until the end of the experiment (130 DAE) were scored as “not flowering”.

Based on the introgression area determined with the 50k SNP array, several CAPS markers were designed on chromosome 6 with indCAPS and Primer3Plus to localize *eam7* (Untergasser et al. 2007; Hodgens et al. 2017). In addition, the CAPS marker designed by Turner et al. (2005) was used to determine whether the plants carried a wild-type or mutated *Ppd-H1* allele. Co-segregation of early flowering with a 32 bp deletion in *LWD1* was tested by amplifying the surrounding area with the primer pair *lwd1-del* and comparing fragment sizes on an agarose gel. All used CAPS markers and primers are listed in Supplemental Table S4.

eam7 candidate genes *CRY1a*, *GR-RBP1*, *LWD1*, and *PRR1* were amplified in Bowman and the derived introgression lines BW(*Ppd-H1*), BW(*eam7*), BW287 and BW(*Ppd-H1*, *eam7*), in GSHO 579 and the original *eam7* mutant Atsel and its parent Atlas. The full genomic sequence was Sanger sequenced to identify mutations. Primers used for amplification and Sanger sequencing can be found in Supplemental Table S8.

Generating *lwd1* mutants using CRISPR-Cas9

To confirm *LWD1* as a candidate gene for *eam7*, *lwd1* mutants were generated using CRISPR-Cas9. The vector system by Kumar et al. (2018) was used to design transformation vectors targeting *LWD1*. Two approaches were used:

Approach 1 included 2 guide RNAs (gRNAs) targeting the start of the CDS of *LWD1* (CDS position 7 and 97). The second approach targeted the end of the coding sequence (CDS position 1,182 and 1,222, Supplemental Table S9) to generate mutations comparable to BW(*eam7*). gRNAs were designed using RGEN Tools Cas-Designer (Bae et al. 2014; Park et al. 2015). Cloning was performed according to the protocol by Kumar et al. (2018): The single gRNA strands were hybridized and cloned into the shuttle vectors pMGE625 or pMGE627 by a Bpil cut/ligation reaction. A second cut/ligation reaction (BsaI) was used to transfer the gRNA transformation units (TUs) to the recipient vector pMGE599. The final vectors were used to transform GP-fast via embryo transformation according to the protocol by Hensel et al. (2009). Successful insertion of the transformation vector into the genome was tested by PCR (primer Hyg-156 and Hyg-047, Supplemental Table S8) on M0 plants. M2 plants were genotyped for mutations by amplifying the entire genomic sequence of *LWD1* (primer *LWD1_72us_F* and *LWD1_21ds_R*) and subsequent Sanger sequencing (Supplemental Table S8). Three lines that showed different mutations were selected for further experiments and were termed *lwd1-26*, *lwd1-390*, and *lwd1-402*.

Allelism tests

Allelism tests were performed by generating F1 crosses of the mutant lines *lwd1-26*, *lwd1-390*, and *lwd1-402* with BW(*Ppd-H1*, *eam7*). As controls, plants were crossed with BW(*Ppd-H1*) and GP-fast. Five to ten plants per cross of the resulting F1 generation were grown in 7 × 7 × 7.5 cm pots with the parental plants under SD conditions in plant growth chambers, and flowering time was scored as described above. The experiment was terminated after 125 DAE and all plants that did not flower were scored as “not flowering”. DNA was extracted from all F1 and parent plants using the KingFisher Flex (Thermo Fisher Scientific) and the BioSprint 96 DNA Plant Kit (QIAGEN). The complete *LWD1* CDS was amplified by PCR and sequenced using Sanger sequencing with the same primers described above (Supplemental Table S8).

Natural variation

A haplotype network analysis was conducted based on combined exome resequencing data from Russell et al. (2016) and the WHEALBI collection (Bustos-Korts et al. 2019). This combined set includes 213 cultivars, 303 landraces, 111 wild barley accessions (*H. vulgare* ssp. *spontaneum*), one *H. agriocrithon* accession, and 42 *H. vulgare* spp. *vulgare* accessions with unassigned breeding history (referred to as “unknown”). The haplotype network was constructed as described by Walla et al. (2020).

Putative orthologs of HvLWD1 in other grasses were identified in the Ensembl Plants database (Bolser et al. 2016). The multiple protein sequence alignment was performed using CLUSTAL Omega (1.2.4) (Madeira et al. 2022), and conserved domains were identified with NCBI conserved domains (Marchler-Bauer et al. 2017). Sequence conservation analysis

was performed as described in Pankin et al. (2014). The last 15 amino acids from HvLWD1 were used to extract 281 sequences of proteins annotated as WD proteins from plants using NCBI Blastp (e-value cutoff: 0.05). Sequences were mapped using MAFFT v7 (“auto” method, Katoh et al. 2019), and the sequence logo was visualized with WebLogo 3 (Crooks et al. 2004).

Statistical analyses

All statistical tests were performed using R Studio (RStudio Team 2022). A 2-tailed, unpaired Student's *t*-test (function *t.test* from the package *rstatix*, v0.7.2) was used to determine the significance between 2 group means, with a *P*-value cutoff at ≤ 0.05 . Significance between more than 2 groups was determined using a one-way ANOVA (function *aov*) and a subsequent Tukey test (function *HSD.test* from package *agricolae*, v1.3-5), *P*-value cutoff at ≤ 0.05 . Polynomial regressions (Loess smooth line) were calculated with a 95% confidence interval.

Accession numbers

Accession numbers of genes described in the text can be found in Supplemental Table S10.

Acknowledgments

We would like to thank Einar B. Haraldsson for providing the BLASTp results of barley against *Arabidopsis thaliana* and Kumsal Ecem Çolpan Karışan for the critical reading of the manuscript. The funders had no role in study design, data collection and interpretation, or the decision to submit the work for publication.

Author contributions

Gesa H. and M.v.K. conceived and designed the experiments. Gesa H. conducted plant phenotypic analyses, generated BW(*Ppd-H1*, *eam7*) crosses, designed CAPS markers, cloned CRISPR-Cas9 transformation vectors, did sequence analyses, and analyzed the data. A.W. performed the haplotype analysis. T.R. and Gesa H. performed RT-qPCR experiments and genotyping of the mapping population. G.B. and Götz H. transformed plants and regenerated *lwd1* mutants. R.S. generated allelic *lwd1* crosses. Gesa H. wrote the manuscript with the help of A.W. and M.v.K.

Supplemental data

The following materials are available in the online version of this article.

Supplemental Figure S1. Effect of *eam7* on spikelet meristem (SM) number.

Supplemental Figure S2. Effects of *eam7* and *Ppd-H1* on plant architecture under LD and SD.

Supplemental Figure S3. Gene expression pattern of *FT*-like genes, *VRN1* over development, and diurnal expression of *LWD1* under SD conditions.

Supplemental Figure S4. Amino acid sequence comparison of HvLWD1 with AtLWD1 and AtLWD2.

Supplemental Figure S5. Nucleotide alignment of *eam7* candidate genes.

Supplemental Figure S6. Protein sequence alignment of wild-type, *eam7*, and *lwd1* mutants.

Supplemental Figure S7. Effect of *lwd1* mutations on spike morphology under SD.

Supplemental Figure S8. Allelism tests of *lwd1* and *eam7* mutants.

Supplemental Figure S9. Sequence comparison of barley LWD1 orthologs in grasses.

Supplemental Figure S10. Median-joining network of 9 LWD1 haplotypes identified in a diverse collection of 670 barley accessions.

Supplemental Table S1. Spikelet meristem number on MSA of plants grown under LD and SD.

Supplemental Table S2. Introgression areas on chromosome 6 in BW(*eam7*).

Supplemental Table S3. Mapping of *eam7* in a segregating F2 population.

Supplemental Table S4. CAPS and PCR marker used to map the position of *eam7*.

Supplemental Table S5. Candidate genes for *eam7*.

Supplemental Table S6. SIFT results for LWD1 haplotypes.

Supplemental Table S7. RT-qPCR primer used in this study.

Supplemental Table S8. PCR primer used in this study.

Supplemental Table S9. Guide RNAs for CRISPR-Cas9 used in this study.

Supplemental Table S10. NCBI GenBank accession numbers of genes.

Supplemental Data Set 1. SNP data from the 50k Illumina Infinium iSelect SNP Array.

Supplemental Data Set 2. Flowering time and results of genotyping of biparental mapping population in short-day conditions.

Supplemental Data Set 3. High-confidence genes (Morex V3) within the introgression “6H-1-reduced”.

Supplemental Data Set 4. List of accessions used for haplotype analysis and the respective haplotype.

Funding

This work was funded by the Deutsche Forschungsgemeinschaft (DFG) under Germany's Excellence Strategy—EXC-2048/1—Project ID: 390686111, grant KO3498/13-1 and the IRTG 2466: Network, exchange, and training program to understand plant resource allocation—Project ID: 391465903.

Conflict of interest statement. None declared.

Data availability

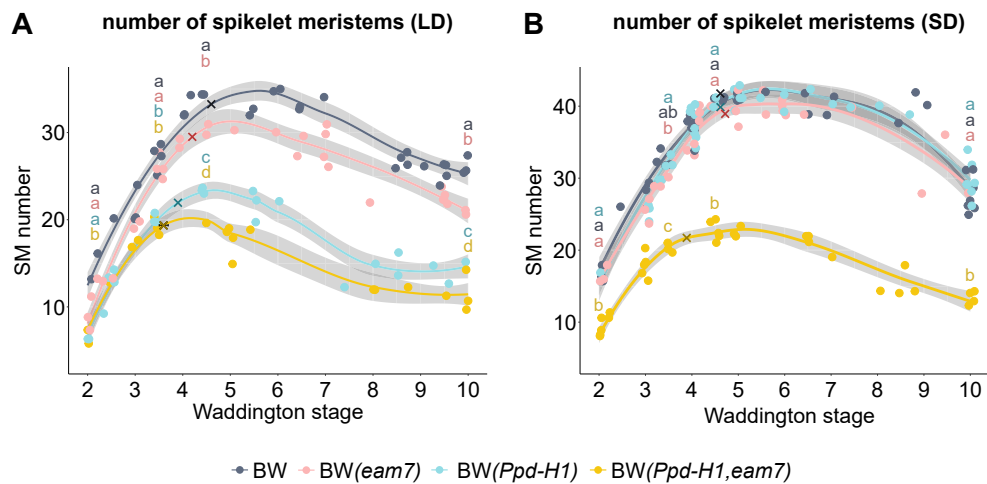
The data underlying this article are available in the article and in its online supplementary material.

References

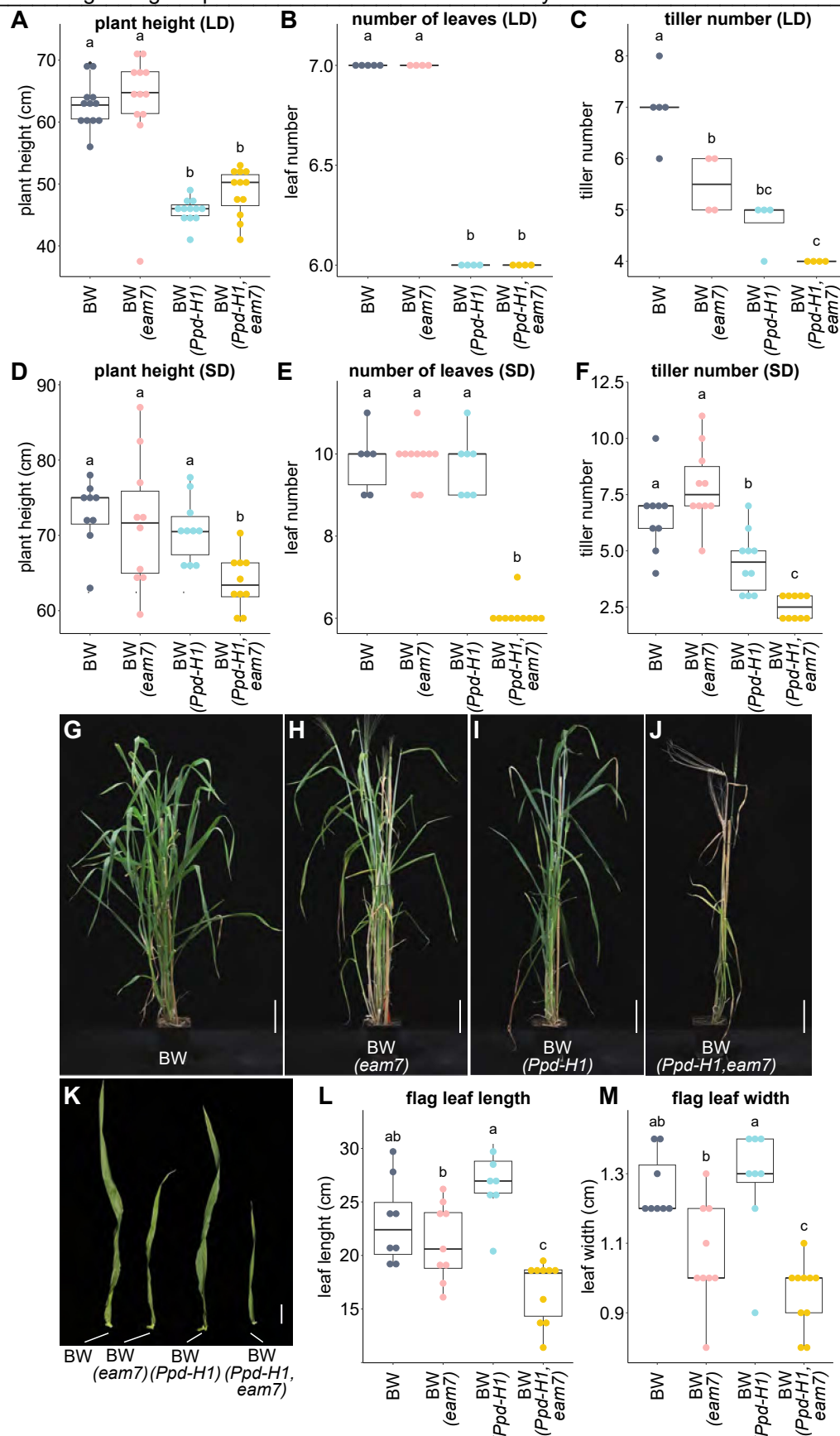
- Alvarez MA, Li C, Lin H, Joe A, Padilla M, Woods DP, Dubcovsky J. Early FLOWERING 3 interactions with PHYTOCHROME B and PHOTOPERIOD1 are critical for the photoperiodic regulation of wheat heading time. *PLoS Genet.* 2023;**19**(5):e1010655. <https://doi.org/10.1371/journal.pgen.1010655>
- Andrade L, Lu Y, Cordeiro A, Costa JMF, Wigge PA, Saibo NJM, Jaeger KE. The evening complex integrates photoperiod signals to control flowering in rice. *Proc Natl Acad Sci U S A.* 2022;**119**(26):e2122582119. <https://doi.org/10.1073/pnas.2122582119>
- Bae S, Park J, Kim J-S. Cas-OFFinder: a fast and versatile algorithm that searches for potential off-target sites of Cas9 RNA-guided endonucleases. *Bioinformatics.* 2014;**30**(10):1473–1475. <https://doi.org/10.1093/bioinformatics/btu048>
- Bayer MM, Rapazote-Flores P, Ganal M, Hedley PE, Macaulay M, Plieske J, Ramsay L, Russell J, Shaw PD, Thomas W, et al. Development and evaluation of a barley 50k iSelect SNP array. *Front Plant Sci.* 2017;**8**:1792. <https://doi.org/10.3389/fpls.2017.01792>
- Bolser D, Staines DM, Pritchard E, Kersey P. Ensembl plants: integrating tools for visualizing, mining, and analyzing plant genomics data. *Methods Mol Biol.* 2016;**1374**:115–140. https://doi.org/10.1007/978-1-4939-3167-5_6
- Bustos-Korts D, Dawson IK, Russell J, Tondelli A, Guerra D, Ferrandi C, Strozzi F, Nicolazzi EL, Molnar-Lang M, Ozkan H, et al. Exome sequences and multi-environment field trials elucidate the genetic basis of adaptation in barley. *Plant J.* 2019;**99**(6):1172–1191. <https://doi.org/10.1111/tj.14414>
- Campoli C, Pankin A, Drosse B, Casao CM, Davis SJ, von Korff M. *Hvlux1* is a candidate gene underlying the *early maturity 10* locus in barley: phylogeny, diversity, and interactions with the circadian clock and photoperiodic pathways. *New Phytol.* 2013;**199**(4):1045–1059. <https://doi.org/10.1111/nph.12346>
- Campoli C, Shtaya M, Davis SJ, von Korff M. Expression conservation within the circadian clock of a monocot: natural variation at barley *Ppd-H1* affects circadian expression of flowering time genes, but not clock orthologs. *BMC Plant Biol.* 2012;**12**(1):97. <https://doi.org/10.1186/1471-2229-12-97>
- Chen A, Li C, Hu W, Lau MY, Lin H, Rockwell NC, Martin SS, Jernstedt JA, Lagarias JC, Dubcovsky J. *Phytochrome C* plays a major role in the acceleration of wheat flowering under long-day photoperiod. *Proc Natl Acad Sci U S A.* 2014;**111**(28):10037–10044. <https://doi.org/10.1073/pnas.1409795111>
- Cheng C-Y, Krishnakumar V, Chan AP, Thibaud-Nissen F, Schobel S, Town CD. Araport11: a complete reannotation of the *Arabidopsis thaliana* reference genome. *Plant J.* 2017;**89**(4):789–804. <https://doi.org/10.1111/tj.13415>
- Cockram J, Jones H, Leigh FJ, O'Sullivan D, Powell W, Laurie DA, Greenland AJ. Control of flowering time in temperate cereals: genes, domestication, and sustainable productivity. *J Exp Bot.* 2007;**58**(6):1231–1244. <https://doi.org/10.1093/jxb/erm042>
- Corbesier L, Vincent C, Jang S, Fornara F, Fan Q, Searle I, Giakountis A, Farrona S, Gissot L, Turnbull C, et al. Ft protein movement contributes to long-distance signaling in floral induction of *Arabidopsis*. *Science.* 2007;**316**(5827):1030–1033. <https://doi.org/10.1126/science.1141752>
- Crooks GE, Hon G, Chandonia J-M, Brenner SE. Weblogo: a sequence logo generator. *Genome Res.* 2004;**14**(6):1188–1190. <https://doi.org/10.1101/gr.849004>
- Digel B, Pankin A, von Korff M. Global transcriptome profiling of developing leaf and shoot apices reveals distinct genetic and environmental control of floral transition and inflorescence development in barley. *Plant Cell.* 2015;**27**(9):2318–2334. <https://doi.org/10.1105/tpc.15.00203>
- Druka A, Franckowiak J, Lundqvist U, Bonar N, Alexander J, Houston K, Radovic S, Shahinnia F, Vendramin V, Morgante M, et al. Genetic dissection of barley morphology and development.

- Plant Physiol. 2011;155(2):617–627. <https://doi.org/10.1104/pp.110.166249>
- Farré EM, Harmer SL, Harmon FG, Yanovsky MJ, Kay SA.** Overlapping and distinct roles of *PRR7* and *PRR9* in the *Arabidopsis* circadian clock. *Curr Biol*. 2005;15(1):47–54. <https://doi.org/10.1016/j.cub.2004.12.067>
- Faure S, Turner AS, Gruszka D, Christodoulou V, Davis SJ, von Korff M, Laurie DA.** Mutation at the circadian clock gene *EARLY MATURITY 8* adapts domesticated barley (*Hordeum vulgare*) to short growing seasons. *Proc Natl Acad Sci U S A*. 2012;109(21):8328–8333. <https://doi.org/10.1073/pnas.1120496109>
- Frankowiak JD, Lundqvist U.** Description of stock number BGS252 (Early maturity 7). *Barley Genet Newslett*. 2015;45:118–119.
- Gallagher LW, Soliman KM, Vivar H.** Interactions among loci conferring photoperiod insensitivity for heading time in spring barley. *Crop Sci*. 1991;31(2):256–261. <https://doi.org/10.2135/cropsci1991.0011183X003100020003x>
- Gao M, Geng F, Klose C, Staudt A-M, Huang H, Nguyen D, Lan H, Mockler TC, Nusinow DA, Hiltbrunner A, et al.** Phytochromes measure photoperiod in *Brachypodium*. *bioRxiv*. <https://doi.org/10.1101/697169>, 9 July 2019, preprint: not peer reviewed.
- Gol L, Haraldsson EB, von Korff M.** Ppd-H1 integrates drought stress signals to control spike development and flowering time in barley. *J Exp Bot*. 2021;72(1):122–136. <https://doi.org/10.1093/jxb/eraa261>
- He T, Angessa T, Hill CB, Zhang X-Q, Telfer P, Westcott S, Li C.** Genetic solutions through breeding counteract climate change and secure barley production in Australia. *Crop Des*. 2022;1(1):10001. <https://doi.org/10.1016/j.cropd.2021.12.001>
- Hensel G, Kastner C, Oleszczuk S, Riechen J, Kumlehn J.** *Agrobacterium*-mediated gene transfer to cereal crop plants: current protocols for barley, wheat, triticale, and maize. *Int J Plant Genomics*. 2009;2009:835608. <https://doi.org/10.1155/2009/835608>
- Hodgens C, Nimchuk ZL, Kieber JJ.** Indcaps: a tool for designing screening primers for CRISPR/Cas9 mutagenesis events. *PLoS One*. 2017;12(11):e0188406. <https://doi.org/10.1371/journal.pone.0188406>
- Huang W, Pérez-García P, Pokhilko A, Millar AJ, Antoshechkin I, Riechmann JL, Mas P.** Mapping the core of the *Arabidopsis* circadian clock defines the network structure of the oscillator. *Science*. 2012;336(6077):75–79. <https://doi.org/10.1126/science.1219075>
- Jang S, Marchal V, Panigrahi KCS, Wenkel S, Soppe W, Deng X-W, Valverde F, Coupland G.** *Arabidopsis* COP1 shapes the temporal pattern of CO accumulation conferring a photoperiodic flowering response. *EMBO J*. 2008;27(8):1277–1288. <https://doi.org/10.1038/emboj.2008.68>
- Jones H, Leigh FJ, Mackay I, Bower MA, Smith LMJ, Charles MP, Jones G, Jones MK, Brown TA, Powell W.** Population-based resequencing reveals that the flowering time adaptation of cultivated barley originated east of the Fertile Crescent. *Mol Biol Evol*. 2008;25(10):2211–2219. <https://doi.org/10.1093/molbev/msn167>
- Kardailsky I, Shukla VK, Ahn JH, Dagenais N, Christensen SK, Nguyen JT, Chory J, Harrison MJ, Weigel D.** Activation tagging of the floral inducer *FT*. *Science*. 1999;286(5446):1962–1965. <https://doi.org/10.1126/science.286.5446.1962>
- Katoh K, Rozewicki J, Yamada KD.** Mafft online service: multiple sequence alignment, interactive sequence choice and visualization. *Brief Bioinform*. 2019;20(4):1160–1166. <https://doi.org/10.1093/bib/bbx108>
- Kikis EA, Khanna R, Quail PH.** *Elf4* is a phytochrome-regulated component of a negative-feedback loop involving the central oscillator components *CCA1* and *LHY*. *Plant J*. 2005;44(2):300–313. <https://doi.org/10.1111/j.1365-3113X.2005.02531.x>
- Kippes N, VanGessel C, Hamilton J, Akpinar A, Budak H, Dubcovsky J, Pearce S.** Effect of *phyB* and *phyC* loss-of-function mutations on the wheat transcriptome under short and long day photoperiods. *BMC Plant Biol*. 2020;20(1):297. <https://doi.org/10.1186/s12870-020-02506-0>
- Kumar N, Galli M, Ordon J, Stuttmann J, Kogel K-H, Imani J.** Further analysis of barley *MORC1* using a highly efficient RNA-guided Cas9 gene-editing system. *Plant Biotechnol J*. 2018;16(11):1892–1903. <https://doi.org/10.1111/pbi.12924>
- Laurie DA, Pratchett N, Snape JW, Bezant JH.** RFLP Mapping of five major genes and eight quantitative trait loci controlling flowering time in a winter × spring barley (*Hordeum vulgare* L.) cross. *Genome*. 1995;38(3):575–585. <https://doi.org/10.1139/g95-074>
- Lundqvist U.** Eighty years of Scandinavian barley mutation genetics and breeding. In: **Shu QY**, editor. *Joint FAO/IAEA Programme. Induced plant mutations in the genomics era*. Rome: FAO; 2009. p. 39–43.
- Madeira F, Pearce M, Tivey ARN, Basutkar P, Lee J, Edbali O, Madhusoodanan N, Kolesnikov A, Lopez R.** Search and sequence analysis tools services from EMBL-EBI in 2022. *Nucleic Acids Res*. 2022;50(W1):W276–W279. <https://doi.org/10.1093/nar/gkac240>
- Marchler-Bauer A, Bo Y, Han L, He J, Lanczycki CJ, Lu S, Chitsaz F, Derbyshire MK, Geer RC, Gonzales NR, et al.** CDD/SPARCLE: functional classification of proteins via subfamily domain architectures. *Nucleic Acids Res*. 2017;45(D1):D200–D203. <https://doi.org/10.1093/nar/gkw1129>
- Mascher M, Wicker T, Jenkins J, Plott C, Lux T, Koh CS, Ens J, Gundlach H, Boston LB, Tulpová Z, et al.** Long-read sequence assembly: a technical evaluation in barley. *Plant Cell*. 2021;33(6):1888–1906. <https://doi.org/10.1093/plcell/koab077>
- McClung CR.** Circadian clock components offer targets for crop domestication and improvement. *Genes (Basel)*. 2021;12(3):374. <https://doi.org/10.3390/genes12030374>
- Mizuno T, Nomoto Y, Oka H, Kitayama M, Takeuchi A, Tsubouchi M, Yamashino T.** Ambient temperature signal feeds into the circadian clock transcriptional circuitry through the EC night-time repressor in *Arabidopsis thaliana*. *Plant Cell Physiol*. 2014;55(5):958–976. <https://doi.org/10.1093/pcp/pcu030>
- Mugge VMR.** Segmented: an R package to fit regression models with broken-line relationships. *R News*. 2008;8(1):20–25.
- Müller LM, Mombaerts L, Pankin A, Davis SJ, Webb AAR, Goncalves J, von Korff M.** Differential effects of day/night cues and the circadian clock on the barley transcriptome. *Plant Physiol*. 2020;183(2):765–779. <https://doi.org/10.1104/pp.19.01411>
- Müller NA, Wijnen CL, Srinivasan A, Ryngajillo M, Ofner I, Lin T, Ranjan A, West D, Maloof JN, Sinha NR, et al.** Domestication selected for deceleration of the circadian clock in cultivated tomato. *Nat Genet*. 2016;48(1):89–93. <https://doi.org/10.1038/ng.3447>
- Pankin A, Campoli C, Dong X, Kilian B, Sharma R, Himmelbach A, Saini R, Davis SJ, Stein N, Schneeberger K, et al.** Mapping-by-sequencing identifies *HvPHYTOCHROME C* as a candidate gene for the *early maturity 5* locus modulating the circadian clock and photoperiodic flowering in barley. *Genetics*. 2014;198(1):383–396. <https://doi.org/10.1534/genetics.114.165613>
- Park J, Bae S, Kim J-S.** Cas-Designer: a web-based tool for choice of CRISPR-Cas9 target sites. *Bioinformatics*. 2015;31(24):4014–4016. <https://doi.org/10.1093/bioinformatics/btv537>
- Pearce S, Shaw LM, Lin H, Cotter JD, Li C, Dubcovsky J.** Night-break experiments shed light on the photoperiod1-mediated flowering. *Plant Physiol*. 2017;174(2):1139–1150. <https://doi.org/10.1104/pp.17.00361>
- RStudio Team.** RStudio: Integrated Development for R. RStudio [Computer software]. Boston, MA: PBC; 2022. <http://www.rstudio.com/>.
- Russell J, Mascher M, Dawson IK, Kyriakidis S, Calixto C, Freund F, Bayer M, Milne I, Marshall-Griffiths T, Heinen S, et al.** Exome sequencing of geographically diverse barley landraces and wild relatives gives insights into environmental adaptation. *Nat Genet*. 2016;48(9):1024–1030. <https://doi.org/10.1038/ng.3612>
- Sawa M, Nusinow DA, Kay SA, Imaizumi T.** Fkf1 and GIGANTEA complex formation is required for day-length measurement in *Arabidopsis*. *Science*. 2007;318(5848):261–265. <https://doi.org/10.1126/science.1146994>

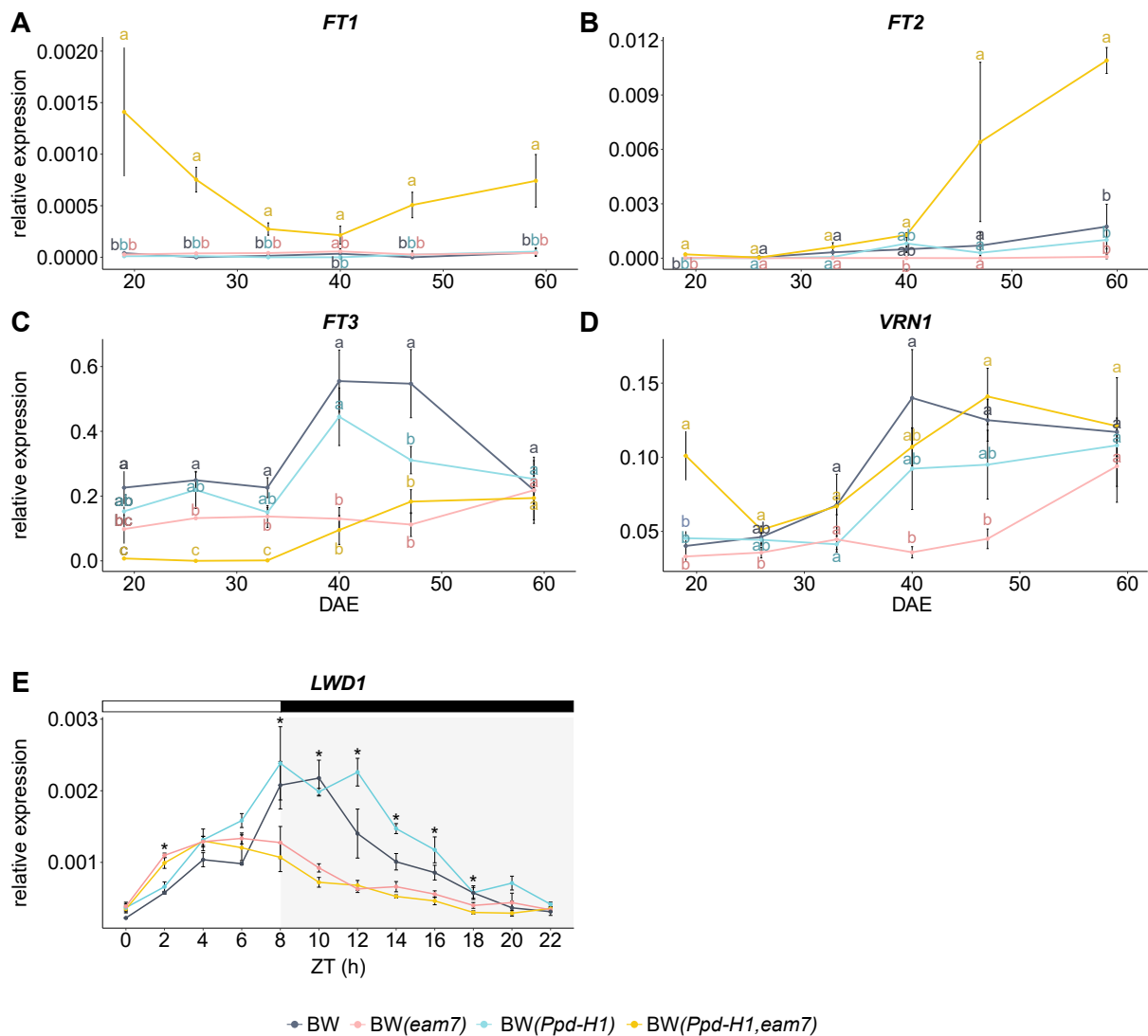
- Shaw LM, Li C, Woods DP, Alvarez MA, Lin H, Lau MY, Chen A, Dubcovsky J.** Epistatic interactions between PHOTOPERIOD1, CONSTANS1 and CONSTANS2 modulate the photoperiodic response in wheat. *PLoS Genet.* 2020;**16**(7):e1008812. <https://doi.org/10.1371/journal.pgen.1008812>
- Shaw LM, Turner AS, Laurie DA.** The impact of photoperiod insensitive Ppd-1a mutations on the photoperiod pathway across the three genomes of hexaploid wheat (*Triticum aestivum*). *Plant J.* 2012;**71**(1): 71–84. <https://doi.org/10.1111/j.1365-313X.2012.04971.x>
- Sim N-L, Kumar P, Hu J, Henikoff S, Schneider G, Ng PC.** Sift web server: predicting effects of amino acid substitutions on proteins. *Nucleic Acids Res.* 2012;**40**(W1):W452–W457. <https://doi.org/10.1093/nar/gks539>
- Song YH, Ito S, Imaizumi T.** Similarities in the circadian clock and photoperiodism in plants. *Curr Opin Plant Biol.* 2010;**13**(5): 594–603. <https://doi.org/10.1016/j.pbi.2010.05.004>
- Stracke S, Börner A.** Molecular mapping of the photoperiod response gene *ea7* in barley. *Theor Appl Genet.* 1998;**97**(5–6):797–800. <https://doi.org/10.1007/s001220050958>
- Strygina KV, Khlestkina EK.** Structural and functional organization and evolution of the *WD40* genes involved in the regulation of flavonoid biosynthesis in the Triticeae tribe. *Russian J Genet.* 2019;**55**(11):1398–1405. <https://doi.org/10.1134/S1022795419110152>
- Suárez-López P, Wheatley K, Robson F, Onouchi H, Valverde F, Coupland G.** *Constans* mediates between the circadian clock and the control of flowering in *Arabidopsis*. *Nature.* 2001;**410**(6832): 1116–1120. <https://doi.org/10.1038/35074138>
- Tamaki S, Matsuo S, Wong HL, Yokoi S, Shimamoto K.** Hd3a protein is a mobile flowering signal in rice. *Science.* 2007;**316**(5827): 1033–1036. <https://doi.org/10.1126/science.1141753>
- Tewolde H, Fernandez CJ, Erickson CA.** Wheat cultivars adapted to post-heading high temperature stress. *J Agron Crop Sci.* 2006;**192**(2):111–120. <https://doi.org/10.1111/j.1439-037X.2006.00189.x>
- Turner A, Beales J, Faure S, Dunford RP, Laurie DA.** The pseudo-response regulator *Ppd-H1* provides adaptation to photoperiod in barley. *Science.* 2005;**310**(5750):1031–1034. <https://doi.org/10.1126/science.1117619>
- Untergasser A, Nijveen H, Rao X, Bisseling T, Geurts R, Leunissen JAM.** Primer3plus, an enhanced web interface to Primer3. *Nucleic Acids Res.* 2007;**35**(Web Server):W71–W74. <https://doi.org/10.1093/nar/gkm306>
- Valverde F, Mouradov A, Soppe W, Ravenscroft D, Samach A, Coupland G.** Photoreceptor regulation of CONSTANS protein in photoperiodic flowering. *Science.* 2004;**303**(5660):1003–1006. <https://doi.org/10.1126/science.1091761>
- Van Nocker S, Ludwig P.** The WD-repeat protein superfamily in Arabidopsis: conservation and divergence in structure and function. *BMC Genomics.* 2003;**4**(1):50. <https://doi.org/10.1186/1471-2164-4-50>
- Von Korff M, Grando S, Del Greco A, This D, Baum M, Ceccarelli S.** Quantitative trait loci associated with adaptation to Mediterranean dryland conditions in barley. *Theor Appl Genet.* 2008;**117**(5): 653–669. <https://doi.org/10.1007/s00122-008-0787-2>
- Waddington SR, Cartwright PM, Wall PC.** A quantitative scale of spike initial and pistil development in barley and wheat. *Ann Bot.* 1983;**51**(1):119–130. <https://doi.org/10.1093/oxfordjournals.aob.a086434>
- Walla A, van Wilma Esse G, Kirschner GK, Guo G, Brünje A, Finkemeier I, Simon R, von Korff M.** An acyl-CoA N-acyltransferase regulates meristem phase change and plant architecture in barley. *Plant Physiol.* 2020;**183**(3):1088–1109. <https://doi.org/10.1104/pp.20.00087>
- Wang Y, Wu J-F, Nakamichi N, Sakakibara H, Nam H-G, Wu S-H.** Light-REGULATED WD1 and PSEUDO-RESPONSE REGULATOR9 form a positive feedback regulatory loop in the *Arabidopsis* circadian clock. *Plant Cell.* 2011;**23**(2):486–498. <https://doi.org/10.1105/tpc.110.081661>
- Woods DP, Li W, Sibout R, Shao M, Laudencia-Chingcuanco D, Vogel JP, Dubcovsky J, Amasino RM.** Phytochrome C regulation of photoperiodic flowering via PHOTOPERIOD1 is mediated by EARLY FLOWERING 3 in *Brachypodium distachyon*. *PLoS Genet.* 2023;**19**(5):e1010706. <https://doi.org/10.1371/journal.pgen.1010706>
- Wu J-F, Wang Y, Wu S-H.** Two new clock proteins, LWD1 and LWD2, regulate *Arabidopsis* photoperiodic flowering. *Plant Physiol.* 2008;**148**(2):948–959. <https://doi.org/10.1104/pp.108.124917>
- Zadoks JC, Chang TT, Konzak CF.** A decimal code for the growth stages of cereals. *Weed Res.* 1974;**14**(6):415–421. <https://doi.org/10.1111/j.1365-3180.1974.tb01084.x>
- Zakhrabekova S, Gough SP, Braumann I, Müller AH, Lundqvist J, Ahmann K, Dockter C, Matyszczyk I, Kurowska M, Druka A, et al.** Induced mutations in circadian clock regulator *Mat-a* facilitated short-season adaptation and range extension in cultivated barley. *Proc Natl Acad Sci U S A.* 2012;**109**(11):4326–4331. <https://doi.org/10.1073/pnas.1113009109>



Supplemental Figure S1. Effect of *eam7* on spikelet meristem (SM) number. SM number scored on the main developing inflorescences in plants grown under long-day (LD) (**A**) and short-day (SD) (**B**) conditions, plotted against the developmental stage of the inflorescence according to Waddington et al. (1983). Depending on the developmental stage, either spikelet meristems, central spikelet meristems, central floret meristems, central florets, or a combination were scored from 4 plants for each time point and genotype. Each dot represents a single value. Significance levels were determined by one-way ANOVA and subsequent Tukey's test, $p \leq 0.05$, $n = 1-7$ at developmental stages W2.0, W3.5, W4.5 and W10.0. Grey areas show a 95% confidence interval of a polynomial regression (Loess smooth line) and crosses indicate the position of the maximum SM stage, calculated with broken-line linear regressions. Corresponding values can be found in Supplemental Table S1.



Supplemental Figure S2. Effects of *eam7* and *Ppd-H1* on plant architecture under LD and SD. Phenotypic parameters scored at flowering of plants grown under long-day (A-C) or short-day (D-F) conditions. Plant height (in cm) and the total number of leaves were scored on the main culm, the number of tillers as all shoots appearing after the main culm. **G-J** Representative images of BW, BW(*eam7*), BW(*Ppd-H1*), and BW(*Ppd-H1,eam7*) plants 17 weeks after emergence, grown under short-day conditions. Scale = 10 cm. **K** Representative images of the flag leaf from plants grown under short days, scale = 2 cm. **L-M** Flag leaf length and width (in cm) of plants grown under short-day conditions. Boxplots show the median (central line), the upper and lower quartiles (box), the maximum values (whiskers) and individual values (points). Significance levels were determined by one-way ANOVA and subsequent Tukey's test, $p \leq 0.05$, $n = 4-12$ plants (A-F) and $n = 8-10$ plants (L-M)



Supplemental Figure S3. Gene expression pattern of FT-like genes, VRN1 over development, and diurnal expression of LWD1 under SD conditions. Relative expression of FT1 (A), FT2 (B), FT3 (C) and VRN1 (D) in BW (grey), BW(*Ppd-H1*) (blue), BW(*eam7*) (pink), and BW(*Ppd-H1,eam7*) (yellow). Plants were grown under short-day conditions and sampled at zeitgeber time (ZT) 9 every 1-2 weeks for a total period of 60 days. Each value represents the mean of three independent biological replicates, each consisting of two pooled plants. Error bars indicate standard deviation of the mean; significance levels were determined by one-way ANOVA and subsequent Tukey's test, $p \leq 0.05$, $n = 3$. E Relative expression of LWD1 in BW (grey), BW(*Ppd-H1*) (blue), BW(*eam7*) (pink), and BW(*Ppd-H1,eam7*) (yellow). Plants were grown for 14 days under short days and then sampled every 2 h for a total period of 24 h. The white bar indicates day and the black bar indicates night. Each value represents the mean of three independent biological replicates, each consisting of two pooled plants. Error bars indicate the standard deviation of the mean; significant differences are indicated by asterisks (* $p \leq 0.05$) comparing BW and BW(*Ppd-H1*) to BW(*eam7*) and BW(*Ppd-H1,eam7*) with Student's *t*-test, $n = 3$

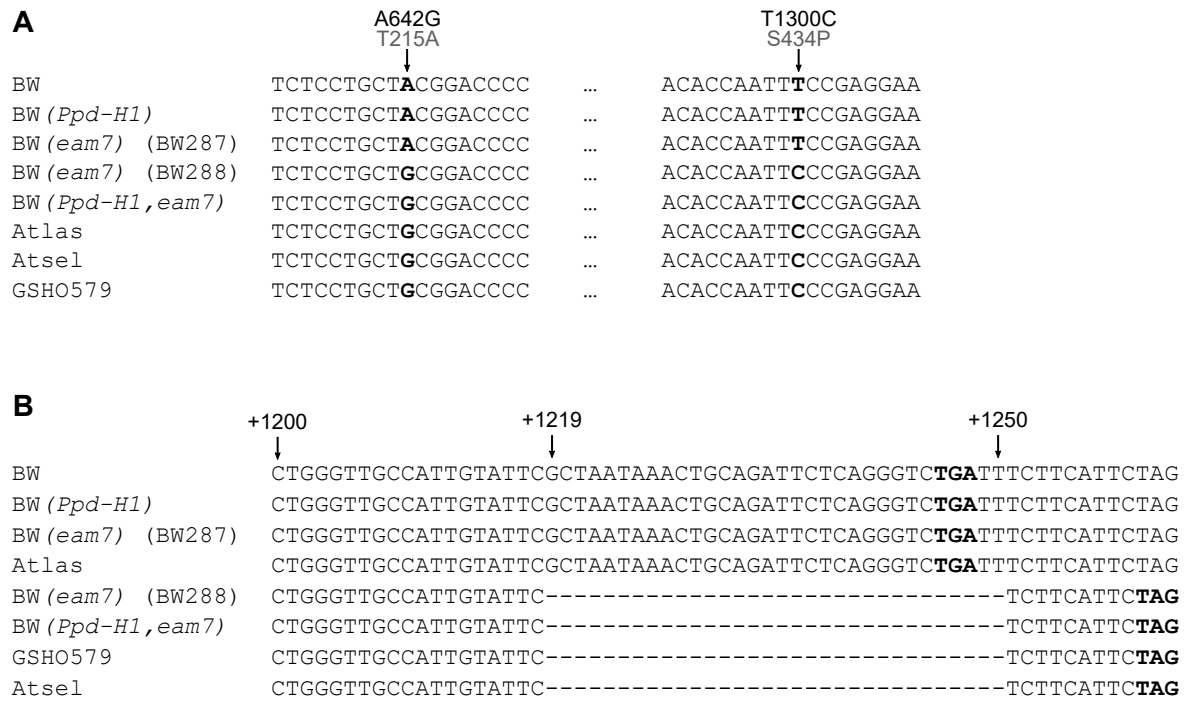
A

HvLWD1	MGGGGAAADGDGWADQDQNGGSRGGGEAKRSEIYTYEAGW HI YGMNWSVRRDKKYRLAI	60
AtLWD1	MG T SS-----DPIQDGSDEQQKRSEIYTYEAPW HI YAMNWSVRRDKKYRLAI	47
AtLWD2	M V TSS-----DQIQNGSEEQSKRSEIYTYEAPW QI YAMNWS I RRDKKYRLAI	47
	* : ***** *:*.*.*****:*****	
HvLWD1	ASL LE QLVNRVEVVQLDESTGDI--APVLSFDHFPFPPT KTMFV PDQPQGLRPDLLATSADL	118
AtLWD1	TS L EQYPNRVEIVQLDESNGEIRSDPNLS FE HPYPPTKT IF IPDKECQRPDLLATSSDF	107
AtLWD2	TS L IEQYPNRVEIVQLDESNGEIRSDPNL CF EHYPPTKT SF IPDKECQRPDLLATSSDF	107
	:**:* *:*:*:*:*:*:*:* * *.*:*:*:*:*:*:*:*:* : *****:*	
HvLWD1	LRIWRITDDDAAPGAADS NNGSVRCNGVGGPAGQQPGVKLCCELNGNRNSDFCG PLT TSF	178
AtLWD1	LRLWRIAD DHSR-----VELK SCLNS KNSE FCG PLTSF	141
AtLWD2	LRLWRI SDDSR-----VELK SCL SSDKNSE FSG PI T TSF	141
	**:*:*:*:*:*:*:* *:* . *..:*:*:*:*:*:*:*	
HvLWD1	D WN DADPRRIGTSSIDTTCTIWDVEREVVD TQLIA HDKE VYD I AWGGAGVFASV ADGSV	238
AtLWD1	D W NEAEP R IGTSSIDTTCTIWDI ERE AVDT QLIA HDKE V FDI AWGGVGVFASV ADGSV	201
AtLWD2	D W NEAEP R IGTSSIDTTCTIWDI ERE VVD TQLIA HDKE V YD I AWGGVGVFASV ED GSV	201
	***:*:*:*:*:*:* *:*:*:*:*:*:*:*:*:*:*:*:*:*:*:*:* *:*	
HvLWD1	RVFDLRDKEHSTIIYESS GGGSNSAVTDGGSVSPT PLVRLGWNKQDPRYMATI IMDSPK	298
AtLWD1	RVFDLRDKEHSTIIYESS E-----PDT PLVRLGWNKQDPRYMATI IMDSAK	247
AtLWD2	RVFDLRDKEHSTIIYESS E-----P S T PLVRLS WNKQDPRYMAT V IMGSAK	247
	*****.*	
HvLWD1	VV VLDIRYPTLPV VELHRH HAFV N AI A W A PHSS CHIC TAGD S Q AL I W DLSSMG T G N NSG	358
AtLWD1	VV VLDIRFPALPV VELQRHQ ASV N AI A W A PHSS CHIC TAGD S Q AL I W DISSMG Q ----	302
AtLWD2	I VVLDIRFPALPV VELQRHQ ASV N AI A W A PHSS SHIC SAGD S Q AL I W DISSMG Q ----	302
	:*****:*:*:*:*:*:*:* *:*:*:*:*:*:*:*:*:*:*:*:*:*:*:*	
HvLWD1	GNGNGNAAAAAAAAAEGGLDPILAYTAGAEVEQLQWSATQPDWVAIVFANKLQILRV	415
AtLWD1	-----HVEGGLDPILAYTAGAEIEQLQWSSSQPDWVAIAFSTKLQILRV	346
AtLWD2	-----HVEGGLDPILAYTAGAEVEQLQWSSSQPDWVAIAFSNKLQILRV	346
	.*****.*.*.*.*.*.*.*.*.*:*:*:*:*:*:*.*:*.*.*.*.*.*	

B

HvLWD1	100.00		
AtLWD1	79.07	100.00	
AtLWD2	75.58	91.33	100.00

Supplemental Figure S4: Amino acid sequence comparison of HvLWD1 with AtLWD1 and AtLWD2.
A Protein sequences from *Arabidopsis thaliana* AtLWD1 (AT1G12910), Arabidopsis AtLWD2 (AT3G26640), and barley HvLWD1 (HORVU.MOREX.r3.6HG0583670) were compared with CLUSTAL Omega (1.2.4, Madeira et al., 2022). The conserved WD40 repeats are shown in white on black background (barley, based on NCBI conserved domains, Marchler-Bauer et al., 2017) and black on grey background (Arabidopsis, based on Wu et al., 2008). Residues matching in HvLWD1 and AtLWD1, but not AtLWD2, are indicated in bold. Asterisks indicate positions that are conserved across all sequences, colons indicate positions with conservation between groups of strongly similar properties, and periods indicate positions with conservation between groups of weakly similar properties. **B** Percent identity matrix of the protein sequences aligned in (A).

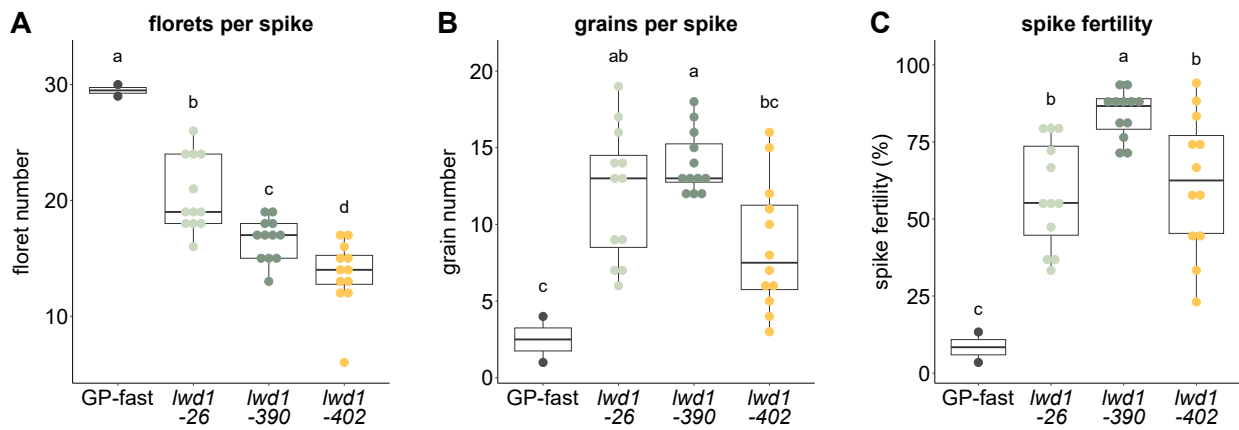


Supplemental Figure S5. Nucleotide alignment of *eam7* candidate genes. **A** Nucleotide alignment of the area surrounding the predicted non-synonymous SNPs in the CDS of *PRR1* (*HORVU.MOREX.r3.6HG0595250*). Sequences shown are from position 633 to 650, including the SNP A642G (T251A on protein level) and from position 1291 to 1308, including the SNP T1300C (S434P on protein level). The positions are relative to the start codon of the CDS of *PRR1*. SNPs are indicated in bold. **B** Nucleotide alignment of the terminal 60 nucleotides of *LWD1* (*HORVU.MOREX.r3.6HG0583670*) in wild-type and mutant plants. Sequences show the C-terminal sequence (position 1200 to 1262) of *LWD1*, including the 32 bp deletion (position 1219 to 1250) in BW(*eam7*), BW(*Ppd-H1,eam7*), GSHO 579, and Atsel. The indicated positions are relative to the start codon of the CDS of *LWD1*. Stop codons are indicated in bold.

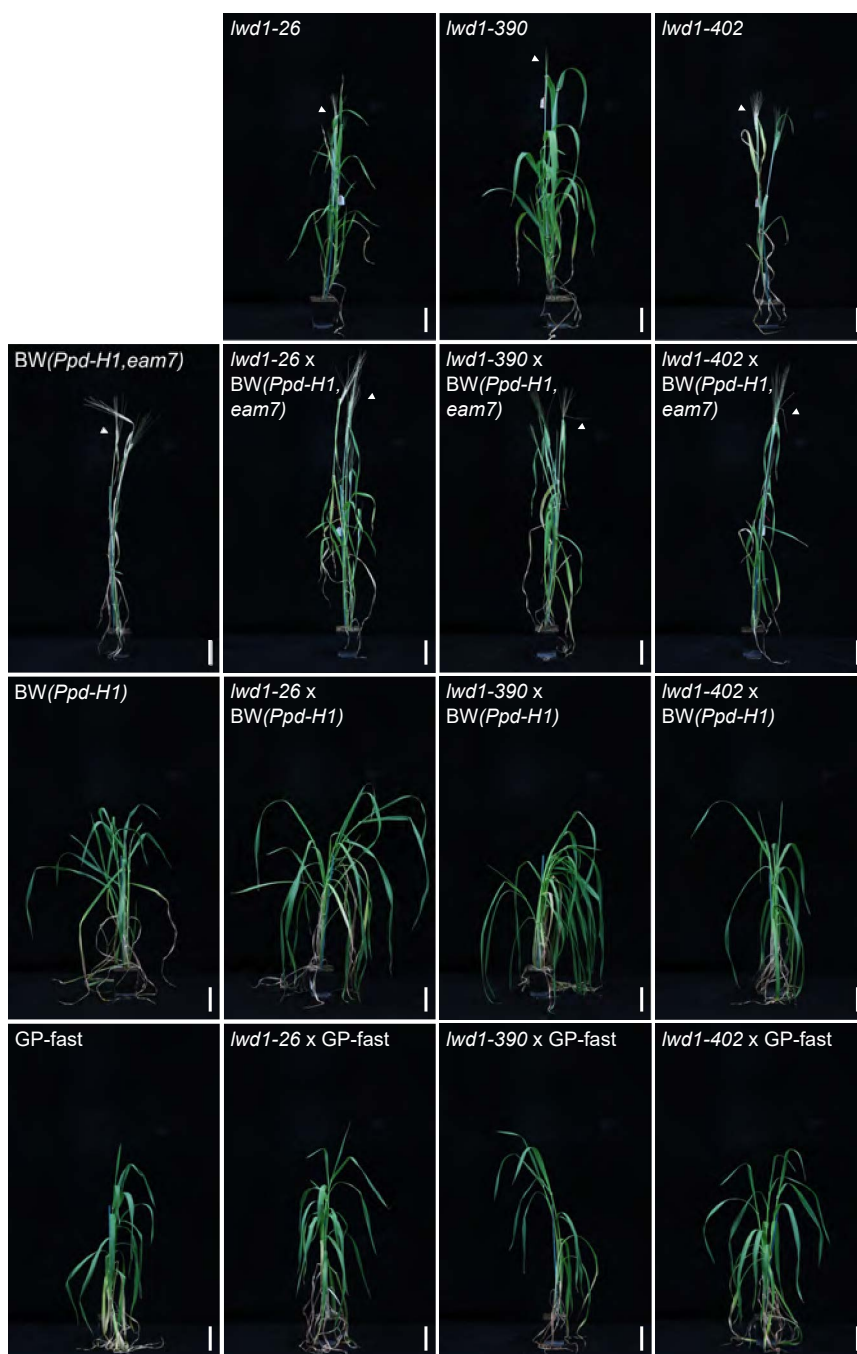
**early maturity 7 promotes early flowering by
controlling the light input into the circadian clock in barley**

GP-fast	MGGGGAAADGDGWADQDQNGGSRGGGEAKRSEIYTYEAGWHIYGMNWSVRRDKKYRLAI	60
BW	MGGGGAAADGDGWADQDQNGGSRGGGEAKRSEIYTYEAGWHIYGMNWSVRRDKKYRLAI	60
BW (<i>eam7</i>)	MGGGGAAADGDGWADQDQNGGSRGGGEAKRSEIYTYEAGWHIYGMNWSVRRDKKYRLAI	60
<i>lwd1-402</i>	MGGGGAAADGDGWADQDQNGGSRGGGEAKRSEIYTYEAGWHIYGMNWSVRRDKKYRLAI	60
<i>lwd1-390</i>	MGGGG-----EAKRSEIYT---GWHIYGMNWSVRRDKKYRLAI	35
<i>lwd1-26</i>	MGGGGAA GWRRVGRSGPGQRREPRW *-----	26
GP-fast	ASLLEQLVNRVEVVQLDESTGDIAPVLSFDHFPPTKTMFVPDPQGLRPDLLATSADLLR	120
BW	ASLLEQLVNRVEVVQLDESTGDIAPVLSFDHFPPTKTMFVPDPQGLRPDLLATSADLLR	120
BW (<i>eam7</i>)	ASLLEQLVNRVEVVQLDESTGDIAPVLSFDHFPPTKTMFVPDPQGLRPDLLATSADLLR	120
<i>lwd1-402</i>	ASLLEQLVNRVEVVQLDESTGDIAPVLSFDHFPPTKTMFVPDPQGLRPDLLATSADLLR	120
<i>lwd1-390</i>	ASLLEQLVNRVEVVQLDESTGDIAPVLSFDHFPPTKTMFVPDPQGLRPDLLATSADLLR	95
<i>lwd1-26</i>	-----	
GP-fast	IWRITDDDDAAAPGAADSNNGSVRCNGVGGPAGQQPGVKLCCELNGNRNSDFCGPLTSFDW	180
BW	IWRITDDDDAAAPGAADSNNGSVRCNGVGGPAGQQPGVKLCCELNGNRNSDFCGPLTSFDW	180
BW (<i>eam7</i>)	IWRITDDDDAAAPGAADSNNGSVRCNGVGGPAGQQPGVKLCCELNGNRNSDFCGPLTSFDW	180
<i>lwd1-402</i>	IWRITDDDDAAAPGAADSNNGSVRCNGVGGPAGQQPGVKLCCELNGNRNSDFCGPLTSFDW	180
<i>lwd1-390</i>	IWRITDDDDAAAPGAADSNNGSVRCNGVGGPAGQQPGVKLCCELNGNRNSDFCGPLTSFDW	155
<i>lwd1-26</i>	-----	
GP-fast	NDADPRRIGTSSIDTTCTIWDVEREVVDTQLIAHDKEVYDIAWGGAGVFASVSADGSVRV	240
BW	NDADPRRIGTSSIDTTCTIWDVEREVVDTQLIAHDKEVYDIAWGGAGVFASVSADGSVRV	240
BW (<i>eam7</i>)	NDADPRRIGTSSIDTTCTIWDVEREVVDTQLIAHDKEVYDIAWGGAGVFASVSADGSVRV	240
<i>lwd1-402</i>	NDADPRRIGTSSIDTTCTIWDVEREVVDTQLIAHDKEVYDIAWGGAGVFASVSADGSVRV	240
<i>lwd1-390</i>	NDADPRRIGTSSIDTTCTIWDVEREVVDTQLIAHDKEVYDIAWGGAGVFASVSADGSVRV	215
<i>lwd1-26</i>	-----	
GP-fast	FDLRDKEHSTIIYESSGGGSNSAVTDGGSVSPTPLVRLGWNKQDPRYMATIIMDSPKVV	300
BW	FDLRDKEHSTIIYESSGGGSNSAVTDGGSVSPTPLVRLGWNKQDPRYMATIIMDSPKVV	300
BW (<i>eam7</i>)	FDLRDKEHSTIIYESSGGGSNSAVTDGGSVSPTPLVRLGWNKQDPRYMATIIMDSPKVV	300
<i>lwd1-402</i>	FDLRDKEHSTIIYESSGGGSNSAVTDGGSVSPTPLVRLGWNKQDPRYMATIIMDSPKVV	300
<i>lwd1-390</i>	FDLRDKEHSTIIYESSGGGSNSAVTDGGSVSPTPLVRLGWNKQDPRYMATIIMDSPKVV	275
<i>lwd1-26</i>	-----	
GP-fast	VLDIRYPTLPVVELHRHHAPVNAIAWAPHSSCHICTAGDQSALIWDLSSMGTGNNSGGN	360
BW	VLDIRYPTLPVVELHRHHAPVNAIAWAPHSSCHICTAGDQSALIWDLSSMGTGNNSGGN	360
BW (<i>eam7</i>)	VLDIRYPTLPVVELHRHHAPVNAIAWAPHSSCHICTAGDQSALIWDLSSMGTGNNSGGN	360
<i>lwd1-402</i>	VLDIRYPTLPVVELHRHHAPVNAIAWAPHSSCHICTAGDQSALIWDLSSMGTGNNSGGN	360
<i>lwd1-390</i>	VLDIRYPTLPVVELHRHHAPVNAIAWAPHSSCHICTAGDQSALIWDLSSMGTGNNSGGN	335
<i>lwd1-26</i>	-----	
GP-fast	GNGNAAAAAAAAAEGGLDPI LAYTAGAEVEQLQWSATQPDWVAIVFANKLQILRV*	415
BW	GNGNAAAAAAAAAEGGLDPI LAYTAGAEVEQLQWSATQPDWVAIVFANKLQILRV*	415
BW (<i>eam7</i>)	GNGNAAAAAAAAAEGGLDPI LAYTAGAEVEQLQWSATQPDWVAIVF SSF *-----	409
<i>lwd1-402</i>	GNGNAAAAAAAAAEGGLDPI LAYTAGAEVEQLQWSATQ PLRV *-----	402
<i>lwd1-390</i>	GNGNAAAAAAAAAEGGLDPI LAYTAGAEVEQLQWSATQPDWVAIVFANKLQILRV*	390
<i>lwd1-26</i>	-----	

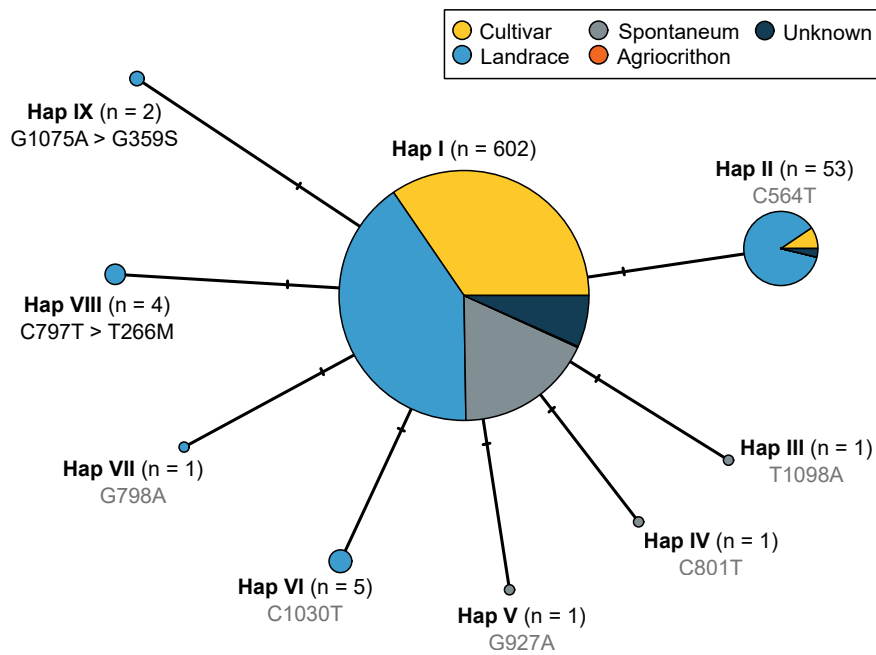
Supplemental Figure S6. Protein sequence alignment of wild-type, *eam7*, and *lwd1* mutants. The protein sequence of HvLWD1 of CRISPR-Cas9-generated mutants *lwd1-402*, *lwd1-390*, and *lwd1-26* are compared to BW, BW(*eam7*), and wild-type GP-fast. Amino acids that differ from the BW sequence in *lwd1* mutants are shown in white on black background. Asterisks indicate stop codons, and dashes gaps in the sequences.



Supplemental Figure S7. Effect of *lwd1* mutations on spike morphology under SD. Spring cultivar GP-fast and the three *lwd1* mutants *lwd1*-26, *lwd1*-390, and *lwd1*-402 were grown under short-day conditions. Floret number (A), grain number (B) and spike fertility (in %) (C) were scored on the main culm. Boxplots show the median (central line), the upper and lower quartiles (box), the maximum values (whiskers) and individual values (points), significance levels were determined by one-way ANOVA and subsequent Tukey's test, $p \leq 0.05$, $n = 2$ for GP-fast, $n = 12-23$ for *lwd1* plants.



Supplemental Figure S8. Allelism tests of *lwd1* and *eam7* mutants. F1 offspring of crosses between *lwd1* mutants and *BW(Ppd-H1,eam7)*, *BW(Ppd-H1)*, and *GP-fast*, and parent plants were grown under short-day conditions. Shown are images of representative plants, taken 86 DAE. Emerged spikes are marked with white arrows. Scale = 10 cm.



Supplemental Figure S10. Median-joining network of nine *LWD1* haplotypes identified in a diverse collection of 670 barley accessions. The number of accessions carrying the corresponding haplotype is indicated with n. Haplotype frequencies are also indicated in node sizes. Mutations are represented with marks on edges. SNPs for each haplotype are given based on their position in the *LWD1* CDS. Grey polymorphisms are synonymous, polymorphisms in black are non-synonymous, and respective amino acid substitutions are shown.

Supplemental Table S1. Spikelet meristem number on MSA of plants grown under LD and SD. Broken-line regressions were calculated on spikelet meristem (SM) initiation and floret meristem abortion under short-day (SD) and long-day (LD) conditions using the R package *segmented*. The maximum SM stage was determined at the breakpoint, and the maximum SM number was calculated with the linear models of the regression. Final floret and grain number were counted on mature spikes and averaged for each genotype. Aborted SM were calculated by subtracting final floret number from initiated SM. Spike fertility was calculated as the percentage of florets on the mature spike that developed into grains. All values were rounded to the next full number.

Genotype	Photo-period	Maximum SM stage	Maximum SM number	Final floret number	Aborted SM	Final grain number	Spike fertility (%)
Bowman	LD	4.5	37	23	14	17	73
BW(<i>eam7</i>)		4.0	32	19	13	13	69
BW(<i>Ppd-H1</i>)		4.0	24	14	10	10	76
BW(<i>Ppd-H1,eam7</i>)		3.5	20	9	11	3	30
Bowman	SD	4.5	43	30	13	11	37
BW(<i>eam7</i>)		4.5	42	23	19	14	61
BW(<i>Ppd-H1</i>)		4.5	43	27	16	8	26
BW(<i>Ppd-H1,eam7</i>)		4.0	24	14	10	7	49

Supplemental Table S2. Introgression areas on chromosome 6 in BW(*eam7*). Flanking SNP markers are from the 50k Illumina Infinium iSelect SNP array. 6H-1-reduced = area from marker M-13 to the flanking introgression marker. The number of 50k SNPs equals the number of polymorphic SNPs compared to BW. The number of high-confidence (HC) genes was determined by screening for HC genes in the Morex V3 annotation (Mascher et al., 2021) within the introgression area.

Introgression	Size (start - end in Mbp)	Flanking SNP markers	Size (start - end in cM)	Number of 50k SNPs	Number of HC genes
6H-1	380.6 (2.2-382.8)	JHI-Hv50k-2016-369341; JHI-Hv50k-2016-401705	54.75 (0.28-55.03)	802	2329
6H-2	16.53 (511.4-527.93)	JHI-Hv50k-2016-414738; JHI-Hv50k-2016-418647	13.38 (75.5-88.88)	185	236
6H-1-reduced	286.16 (96.64-382.8)	JHI-Hv50k-2016-390119; JHI-Hv50k-2016-401705	2.98 (52.05-55.03)	382	1084

Supplemental Table S3. Mapping of *eam7* in a segregating F2 population. Counted were early (≤ 60 DAE) or late (> 60 DAE) flowering plants carrying either the BW(*eam7*) allele, the BW allele, or are heterozygous at the respective marker position. Only plants with a confirmed dominant *Ppd-H1* allele (homo- or heterozygous, 319 plants in total) were considered. More detailed information on CAPS markers can be found in Supplemental Table S4.

Marker	SNP target (50k)	Position chr6H (Mbp)	Flowering	BW(<i>eam7</i>) allele	BW allele	heterozygous
M-13	JHI-Hv50k-2016-390119	96	Early	82	0	7
			Late	3	73	154
M-16	JHI-Hv50k-2016-393938	178	Early	89	0	0
			Late	0	76	154
lwd1-del	-	245	Early	89	0	0
			Late	0	76	154
M-11	JHI-Hv50k-2016-395274	262	Early	89	0	0
			Late	0	76	154
M-39	JHI-Hv50k-2016-398102	345	Early	89	0	0
			Late	0	76	154
M-PRR1	-	368	Early	89	0	0
			Late	1	75	154

Supplemental Table S4. CAPS and PCR marker used to map the position of *eam7*. SNP target and genetic position refer to the corresponding SNP in the 50k Illumina Infinium iSelect SNP array or the gene. The physical position of the SNP (*M-13*, *M-16*, *M-11*, *M-39*, *M-PRR1* and *M-*eam7**) or the gene (*M-PPD-H1* and *lwd1-del*) is given according to the Morex V3 assembly (Mascher et al., 2021). ¹Marker from Turner et al. (2005)

Marker	Primer	Sequence 5'-3'	SNP target	Enzyme	Physical position	Genetic position
M-13	F	GTAATTGCCCTAGCGTTGGA	JHI-Hv50k-2016-390119	MnII	6H:96,639,872	52.05
	R	CAGAACCCGGGAATTAGGAT				
M-16	F	AAAACGGTGGCATTAGCAAG	JHI-Hv50k-2016-393938	HindIII	6H:178,729,018	54.96
	R	CGGAGGCATGATCAGGTATT				
M-11	F	AAAGGCCACACTAGTGCAT	JHI-Hv50k-2016-395274	BstUI	6H:262,872,248	55.38
	R	ACGCTCACTCCCTGCATCT				
M-39	F	CTAAATTCAGCCCCGAACA	JHI-Hv50k-2016-398102	Ddel	6H:345,516,784	55.45
	R	TGCCTGGACTTGTTCTGATG				
M-PRR1	F	GAGCATAGCATGGCACTTCA	PRR1 (S434P)	Hpy188I	6H:368,105,203	-
	R	GCCTGCCTAACAAACTGACC				
M-PPDH1 ¹	F	ACGTGAATGGTGGATCGGC	<i>Ppd-H1</i>	BstUI	2H:25,876,427-25,880,400	-
	R	TATAGCTAGGTGCGTGGCG				
M- <i>eam7</i>	F	GTGGAACGCCTTCTGAAAT	SCRI_RS_34440	MseI	6H:277,337,775	55.03
	R	CCTCCTGCTGAGCGACCT				
lwd1-del	F	TACCATCCTCCCATTGCCTG	<i>LWD1</i>	-	6H:245,548,819-245,550,556	-
	R	ATTGGCTTACACTGCAGGGG				

Supplemental Table S5. Candidate genes for *eam7*. Candidates were determined by screening HC genes in the *eam7* introgression area (6H-1-reduced, position 6H:96,639,872 - 6H:382,834,297 in Morex V3) for the term “circadian” in the closest *Arabidopsis thaliana* (Araport11) ortholog description. Pident/evalue: percentage of identical matches and expect value of MorexV3-Araport11 BLASTp; SNP position: indicates the position (relative to the start codon of the gene and based on MorexV3) of non-synonymous SNPs identified in *eam7* plants; changes in aa sequence: the effect of SNPs on amino acid sequence; “-” indicates that the CDS of these genes was not sequenced.

MorexV3 gene ID	pident	evalue	Araport11 gene ID	Gene name	SNP positions	Changes in aa sequence
<i>HORVU.MOREX.r3.6HG0592840</i>	73.75	2.26E-40	<i>AT2G21660</i>	<i>GR-RBP1</i>	None	None
<i>HORVU.MOREX.r3.6HG0583670</i>	69.309	0	<i>AT1G12910</i>	<i>LWD1</i>	32 bp del (1219-1250)	A407F N408S K409F L410*
<i>HORVU.MOREX.r3.6HG0587680</i>	66.082	0	<i>AT4G08920</i>	<i>CRY1</i>	None	None
<i>HORVU.MOREX.r3.6HG0595250</i>	38.475	3.92E-106	<i>AT5G61380</i>	<i>PRR1</i>	A642G T1300C	T215A S434P
<i>HORVU.MOREX.r3.6HG0578070</i>	55.367	0	<i>AT5G51200</i>	<i>EDS4</i>	-	-
<i>HORVU.MOREX.r3.6HG0589220</i>	34.855	9.66E-46	<i>AT3G07640</i>	<i>PBAC5</i>	-	-
<i>HORVU.MOREX.r3.6HG0571470</i>	36.735	1.3	<i>AT3G42170</i>	<i>DAY-SLEEPER</i>	-	-
<i>HORVU.MOREX.r3.6HG0582650</i>	30.108	1.00E-12	<i>AT3G42170</i>	<i>DAY-SLEEPER</i>	-	-
<i>HORVU.MOREX.r3.6HG0592100</i>	29.042	1.69E-45	<i>AT3G42170</i>	<i>DAY-SLEEPER</i>	-	-
<i>HORVU.MOREX.r3.6HG0571480</i>	28.319	1.11E-13	<i>AT3G42170</i>	<i>DAY-SLEEPER</i>	-	-

Supplemental Table S6. SIFT results for *LWD1* haplotypes. The potential effect on protein function of non-synonymous SNPs identified in haplotypes VII and IX was calculated using SIFT (Sim et al., 2012).

Gene/Haplotype	SNP	SIFT result	SIFT score	Median sequence conservation	Sequences represented at this position
Haplotype VIII	T266M	Tolerated	0.13	3.38	3
Haplotype IX	G359S	Tolerated	0.59	3.38	3

Supplemental Table S7. RT-qPCR primer used in this study. The fragment size is based on genomic DNA.

Target gene	Primer	Sequence 5'-3'	Size (bp)
<i>ACT</i> (HORVU.MOREX.r3.5HG0457850)	ACT_591F	CGTGTTGGATTCTGGTGATG	208
	ACT_789R	AGCCACATATGCGAGCTTCT	
<i>CO1</i> (HORVU.MOREX.r3.7HG0671540)	CO1_2185F	CTGCTGGGGCTAGTGCTTAC	251
	CO1_3454R	CCTTGTTGCATAACGTGTGG	
<i>CO2</i> (HORVU.MOREX.r3.6HG0611630)	CO2_564F	AGTGGA CTCTTGGCTCCTCA	158
	CO2_721R	CATGCTGCTGTTCTTGCATT	
<i>ELF3</i> (HORVU.MOREX.r3.1HG0095050)	ELF3_DL_3060_F3	TGCTGTCCAAGTGTGGAGC	242
	ELF3_DL_4483_R3	CCTGGTTTCCTTCGGTGTTA	
<i>FT1</i> (HORVU.MOREX.r3.7HG0653910)	FT1_1955F	GGTAGACCCAGATGCTCCAA	120
	FT1_2183R	TCGTAGCACATCACCTCTG	
<i>GI</i> (HORVU.MOREX.r3.3HG0238250)	GI_6780F	TCAGTTAGAGCTCCTGGAAGT	263
	GI_7289R	GGTAGTTTGGGCTTTGGATG	
<i>LHY</i> (HORVU.MOREX.r3.7HG0699010)	HvLHY_672F	CCTGGAATTGGAGATGGAGA	210
	HvLHY_882R	TGAGCATGGCTTCTGATTTG	
<i>LUX1</i> (HORVU.MOREX.r3.3HG0328340)	LUX_1077F	AATTCAGTCCACGGATGCTC	222
	LUX_1298R	CTTCACTTCAGCTCCCCTTG	
<i>LWD1</i> (HORVU.MOREX.r3.6HG0583670)	LWD1_qPCR114F	CAGCTCATAGCCCATGACAA	114
	LWD1_qPCR114R	CTCCTTGTCCCGAAGATCAA	
<i>PHYB</i> (HORVU.MOREX.r3.4HG0381880)	HvPHYB-1151F	CCTGCGCACCAACTATCAGA	232
	HvPHYB-1383R	CTCCATGACACACCGTCAAC	
<i>PHYC</i> (HORVU.MOREX.r3.5HG0511090)	PHYC_0986F	ACTACCCGGCAACTGACATC	142
	PHYC_1127R	GAGCCACAGAGGCTGATAGG	
<i>Ppd-H1</i> (HORVU.MOREX.r3.2HG0107710)	PPD1_2165F	GATGGATTCAAAGGCAAGGA	172
	PPD1_2336R	GAACAATTGGCTCCTCCAAA	
<i>PRR1</i> (HORVU.MOREX.r3.6HG0595250)	HvPRR1_1056F	GAGCATAGCATGGCACTTCA	237
	HvPRR1_1292R	TGTCTTTCCTCGGAAATTGG	
<i>PRR59</i> (HORVU.MOREX.r3.4HG0350690)	PRR59_2064_F	GAAATTCCGCATGAAAAGGA	148
	PRR59_2212_R	TTCCGCATCTTCTGTTGTTG	
<i>PRR73</i> (HORVU.MOREX.r3.5HG0498830)	PRR73_441F	GCGCCGTAGAGAATCAG AAC	222
	RR73_662R	CATGTCGGGTACAGTCATCG	
<i>PRR95</i> (HORVU.MOREX.r3.5HG0498830)	PRR95_1467F	CAGAACTCCAGTGTGCGCAA	251
	PRR95_1717R	TGCTGTTGCCAGAGTTGTTC	
<i>VRN1</i> (HORVU.MOREX.r3.5HG0511210)	HVBM5a_292F	CTGAAGGCGAAGGTTGAGAC	203
	HVBM5a_494R	TTCTCCTCCTGCAGTGACCT	

Supplemental Table S8. PCR primer used in this study. The fragment size is based on genomic DNA, no fragment size is given for primers used exclusively for Sanger sequencing. Primer denoted as “full genomic sequence” were used to amplify candidate genes via PCR. These, and primers denoted as “Sanger” were used for Sanger sequencing to cover the full genomic sequence.

Target	Primer	Sequence 5'-3'	Size (bp)
Hygromycin on pMGE599	Hyg-156	ACGCACAATCCCCTATCC	603
	Hyg-047	GTGTCGTCCATCACAGTTTG	
<i>LWD1</i> (full genomic sequence)	<i>LWD1</i> 71us F	ATCAGACCCCTCCAACGACT	1362
	<i>LWD1</i> 21ds R	TTCCTCTTTCTACCCACCA	
<i>LWD1</i> (Sanger)	<i>LWD1</i> qPCR114F	CAGCTCATAGCCCATGACAA	-
<i>PRR1</i> (full genomic sequence)	<i>PRR1</i> 52us F	GTGGGGAGTCTCTGGTGATT	2351
	<i>PRR1</i> 17ds R	CCGCAACACCATTTACATA	
<i>PRR1</i> (Sanger)	<i>PRR1</i> 451 F	ACATTGGCAGGAACAAGGAG	-
	<i>PRR1</i> 1098 F	GTTGCCGCAAGTATGTGCT	-
<i>GR-RBP1</i> (full genomic sequence)	<i>GR-RBP1</i> 74us F	GCAGAGTGTGGTGGGTTGT	740
	<i>GR-RBP1</i> 81ds R	CACAAACGAGAAACCACAGAA	
<i>CRY1a</i> (full genomic sequence)	<i>CRY1a</i> 66us F	AACGAGCTTTTTCCTTGGGTAAT	2474
	<i>CRY1a</i> 35ds R	CTTCTCCATTCCATTCTCTATCTC	
<i>CRY1a</i> (Sanger)	<i>CRY1a</i> 740 F	AAACAACAAGTATGTAAGAACAGAAGA	-
	<i>CRY1a</i> 1533 F	TAACATGGAGCAACGAGAGC	-

Supplemental Table S9. guide RNAs for CRISPR-Cas9 used in this study. PAM sequences are underlined; the covered sequence is relative to the start codon of the CDS of *LWD1* (*HORVU.MOREX.r3.6HG0583670*).

Approach	sgRNA	Sequence	Covered sequence
1	sgRNA-7	GGCGGTGGCGCAGCCGCGGATGG	7-26
	sgRNA-97	GAGATCTATACCTACGAGGC CGG	97-116
2	sgRNA-1182	GGTCAGCTACCCAGCCTGACT TGG	1182-1201
	sgRNA-1222	TAATAAACTGCAGA TTCTCAGGG	1222-1241

Supplemental Table S10. NCBI GenBank accession numbers of genes.

Gene	NCBI Accession number
<i>CONSTANS-like 1 (CO1)</i>	AF490467
<i>CONSTANS-like 2 (CO2)</i>	AF490469
<i>EARLY FLOWERING 3 (ELF3)</i>	HQ850272
<i>FLOWERING LOCUS T1 (FT1)</i>	DQ100327
<i>FLOWERING LOCUS T2 (FT2)</i>	DQ297407
<i>FLOWERING LOCUS T3 (FT3)</i>	DQ411319
<i>GIGANTEA (GI)</i>	AY740524
<i>LATE ELONGATED HYPOCOTYL (LHY)</i>	JN603242
<i>LUX ARRHYTHMO (LUX1)</i>	BAJ88719
<i>LIGHT-REGULATED WD 1 (LWD1)</i>	XM_045095679.1
<i>PHYTOCHROME B (PHYB)</i>	DQ201143
<i>PHYTOCHROME C (PHYC)</i>	DQ238106
<i>PHOTOPERIOD 1 (Ppd-H1)</i>	AY970701
<i>PSEUDO-RESPONSE REGULATOR 1</i>	JN603243
<i>PSEUDO-RESPONSE REGULATOR 59 (PRR59)</i>	AK361360
<i>PSEUDO-RESPONSE REGULATOR 73 (PRR73)</i>	AK376549
<i>PSEUDO-RESPONSE REGULATOR 95 (PRR95)</i>	AK252005
<i>VERNALIZATION 1 (VRN1)</i>	AY785826

2 *FLOWERING LOCUS T1* is a pleiotropic regulator of reproductive development, plant architecture, and source-sink relations in barley

The following manuscript is in preparation for submission.

Authors:

Gesa Helmsorig¹, Einar B. Haraldsson¹, Jochen Kumlehn², Götz Hensel^{3,4}, Maria von Korff^{1,5}

Affiliations:

¹ Institute of Plant Genetics, Heinrich-Heine-Universität Düsseldorf, 40223 Düsseldorf, Germany

² Leibniz Institute of Plant Genetics and Crop Plant Research (IPK), Corrensstr. 3, OT9 Gatersleben, 06466 Seeland, Germany

³ Centre for Plant Genome Engineering, Institute of Plant Biochemistry, Heinrich-Heine-Universität Düsseldorf, 40223 Düsseldorf, Germany

⁴ Division of Molecular Biology, Centre of the Region Hana for Biotechnological and Agriculture Research, Faculty of Science, Palacký University, Olomouc, Czech

⁵ Cluster of Excellence on Plant Sciences "SMART Plants for Tomorrow's Needs", 40223 Düsseldorf, Germany

Contributions:

GH and MvK conceived and designed the experiments. GH genotyped and identified the *ft1* mutants, conducted plant phenotyping, sampled for RNA-seq, and did the analysis. EHB contributed to RNAseq analysis and provided the conversion between different gene identifiers. JK and GÖH designed and cloned CRISPR-Cas9 transformation vectors and performed the transformation and regeneration of *ft1* mutants. GH wrote the manuscript with the help of MvK.

Abstract

Flowering in the most favorable seasonal conditions is essential for the successful propagation of plants. To time the transition to floral development accordingly requires reliable mechanisms that enable plants to sense the correct season and transmit this information to reproductive tissues. Several external and internal cues, including photoperiod, are utilized to determine the time to flower. In the long-day plant barley (*Hordeum vulgare* L.), day lengths that exceed 12 hours strongly advance floral development. The central flowering time regulator in long days is *PHOTOPERIOD 1* (*Ppd-H1*), which induces the expression of *FLOWERING LOCUS T1* (*FT1*), orthologous to *Arabidopsis thaliana* florigen *FT*. While the role of *Ppd-H1* and *FT1* on reproductive development is well-understood in barley, details about the upstream regulation of *FT1* by *Ppd-H1* and the gene regulatory networks downstream of *FT1* remain scarce. Here, we present an in-depth phenotypic and transcriptomic study of the effect of *FT1* on barley development. By utilizing knock-out *ft1* mutants, we could show that *FT1* controls reproductive development, plant architecture, and plant fertility, and removing *FT1* changes the balance of vegetative to reproductive tissue. Allelic variation at *Ppd-H1* did not affect flowering of the *ft1* mutants, suggesting that *Ppd-H1* regulates flowering time exclusively through *FT1*. *FT1* affects the timing, the duration, and the end of flowering, which is linked to changes in meristem determinacy and plant longevity. In line with this, whole-transcriptome analysis revealed that *FT1* regulates the expression of numerous genes involved in floral development and meristem identity. *ft1* mutants were severely reduced in fertility, and the deregulation stress-response genes in the leaf and main shoot apex reflected this. Changes in expression patterns of photosynthesis components and carbohydrate metabolism indicate that *FT1* affects source-sink relationships on a whole-plant level.

Introduction

The domestication of our modern crops is regarded as one of the major transitions in human history, as stable food sources enabled populations to grow and civilization to advance (Brown et al., 2009). Subsequent domestication, selection, and improvement breeding have adapted the life cycle of crop plants to variations in photoperiod and temperature and gradually changed plant architecture (Doebley, 2004; Sang, 2009; Fernández-Calleja et al., 2021).

The architecture of a plant is mainly defined by plant height, leaf number and size, branch number, and inflorescence size. During vegetative growth, these traits are controlled by the activity of the shoot apical meristem (SAM), which produces leaf primordia and axillary meristems (AXMs) that grow out into leaves and branches, respectively (Wang et al., 2018). Reproductive growth is initiated by the irreversible transition of a vegetative SAM into a reproductive inflorescence meristem (IM), which ceases to produce leaf primordia and instead forms spikelet meristems (SMs). SMs are induced during the early stages of reproductive development and have the potential to develop into florets and, subsequently, into grains. Therefore, the number of initiated SMs on a shoot apex strongly affects the yield potential (Krieger et al., 2010; Bommert et al., 2013; Thirulogachandar and Schnurbusch, 2021).

The transition to reproductive development is regulated by external and internal factors, such as day length, temperature, vernalization, and plant age (Quiroz et al., 2021). Differences in temperature and photoperiod are important signals for plants to anticipate seasonal changes in the environment (Andrés and Coupland, 2012). Photoperiod greatly impacts flowering time and is a central target for improving plant performance (Haas et al., 2019; Fernández-Calleja et al., 2021). In the model species *Arabidopsis* (*Arabidopsis thaliana*) and rice (*Oryza sativa*), the small globular protein *FLOWERING LOCUS T* (*FT*) was identified as florigen, a mobile floral stimulus that transfers the information to induce flowering from leaves to the developing shoot apex in a photoperiod-dependent manner and was first described almost a century ago (Chailakhyan, 1936; Corbesier et al., 2007; Tamaki et al., 2007). In flowering-inducing conditions, the expression of *FT* or its rice ortholog, *HEADING DATE 3a* (*Hd3a*), is upregulated in phloem companion cells in the vascular tissue of the leaf, and the FT/Hd3a protein is transported through the phloem to the shoot apex (Kardailsky et al., 1999; Corbesier et al., 2007; Tamaki et al., 2007; Chen et al., 2018). In the shoot apex, the FT protein interacts with *FLOWERING LOCUS D* (*FD*), bridged by 14-3-3 proteins, to activate the expression of floral meristem identity genes that control the development of flowers (Abe et al., 2005; Wigge et al., 2005; Li and Dubcovsky, 2008; Taoka et al., 2011). These include MADS-box transcription factors that regulate the emergence of the different flower organs in a concerted effort of spatiotemporal gene expression and protein-protein interaction, as described by the ABCDE model (Coen and Meyerowitz, 1991; Fornara et al., 2003; Kuijjer et al., 2021). The role

of *FLOWERING LOCUS T* (*FT*)-like genes as integrators of several signals to induce the switch from vegetative to reproductive growth is highly conserved among angiosperm plants (Kardailsky et al., 1999; Kojima et al., 2002; Lifschitz et al., 2006; Faure et al., 2007).

While *FT* promotes flowering, a gene from the same family, *TERMINAL FLOWER 1* (*TFL1*), acts antagonistically as a flowering repressor and controls meristem determinacy (Shannon and Meeks-Wagner, 1991). Meristems can either be determinate, that is, completely consumed during development, or indeterminate, meaning that cells within the meristem remain active. Melzer et al. (2008) showed that central Arabidopsis flowering time genes are regulators of meristem determinacy in perennial plants, which are characterized by retaining indeterminate meristems to enable growth in the following season. In line with this, *ft* mutants are late flowering and show indeterminate growth, while *tfl* mutants flower early, and normally indeterminate inflorescences are converted to determinate flowers (Koornneef et al., 1991; Shannon and Meeks-Wagner, 1991). Thus, the *FT/TFL1* ratio modulates plant architecture by controlling meristem determinacy. Similarly, in tomato (*Solanum lycopersicum*), the ratio of *FT* and *TFL1* homologs, called *SINGLE FLOWER TRUSS* (*SFT*) and *SELF-PRUNING* (*SP*), respectively, controls determinate and indeterminate growth in the inflorescence (Shalit et al., 2009). *sft* mutants are late flowering and show altered plant architecture and strongly reduced fertility because only a few SMs are initiated before they revert to indeterminate vegetative branches (Lifschitz et al., 2006; Shalit et al., 2009; Krieger et al., 2010). Furthermore, the overexpression of *FT*-like genes from cotton (*Gossypium hirsutum*) and purging nut (*Jatropha curcas*) in tobacco affected diverse traits such as lateral shoot outgrowth, stem thickness, leaf morphology, leaf chlorophyll content, and the expression of genes involved in photosynthesis and carbohydrate biosynthesis (Li et al., 2015b; Wu et al., 2022). Overexpression of rice *Hd3a* in potato (*Solanum tuberosum*) induced tuberization in non-inductive photoperiods (Navarro et al., 2011). Consequently, the role of *FT*-like genes is not reduced to regulating flowering time; instead, they act as systemic regulators of plant growth.

The genomes of crops, such as cereal monocots, are characterized by a large number of *FT*-like genes (Peng et al., 2015; Halliwell et al., 2016). Wheat (*Triticum aestivum*) and barley (*Hordeum vulgare* L.) genomes each contain 12 *FT* paralogs due to gene duplication (Halliwell et al., 2016). Some of these *FT*-like genes were characterized and identified either as positive regulators of flowering or inflorescence development (*FT1*, *FT2*, and *FT3*) or as delaying floral development (*FT4*) (Kikuchi et al., 2009; Mulki et al., 2018; Shaw et al., 2019; Pieper et al., 2020). Because increased transcript levels of *FT1* are strongly associated with early flowering, *FT1* is presumed to be the primary gene controlling floral development and flowering time in barley and wheat (Yan et al., 2006; Faure et al., 2007; Lv et al., 2014). *FT1* controls the expression of related downstream genes, such as other *FT*-like genes, and changing *FT1* expression indirectly through variation at *Ppd-H1* revealed that *FT1* might additionally affect

source-sink relationships (Kikuchi et al., 2009; Lv et al., 2014; Digel et al., 2015). However, as several *FT*-like genes have been shown to promote or delay flowering, the specific role of *FT1* in flowering time regulation, developmental progression, plant architecture, and the genetic networks downstream of *FT1* remain elusive in barley.

QTL studies have identified *PHOTOPERIOD 1* (*Ppd-H1*) as a major gene controlling flowering time under long days (LDs) in barley and wheat (Laurie et al., 1995; Turner et al., 2005). *Ppd-H1* is a ortholog of the Arabidopsis *PSEUDO RESPONSE REGULATOR* (*PRR*) genes (Turner et al., 2005). Two major haplotypes have been described in natural barley populations, which differ for a non-synonymous mutation in the conserved CCT (CONSTANS, CO-like, and TOC1) domain (Turner et al., 2005). The ancestral wild-type (WT) allele, predominant in wild barley, landraces, and winter barley, is linked to rapid upregulation of *FT1*, floral development, and flowering under LDs. A mutation in the CCT domain of *Ppd-H1* is associated with delayed and reduced upregulation of *FT1* in the leaf and late flowering under LDs and was selected in spring barley, presumably as an adaptation to long growing seasons in northern cultivation areas (Turner et al., 2005; Jones et al., 2008). In Arabidopsis, *PRR* genes are central components of the circadian clock and peak sequentially during the progression of the day (McClung, 2021). A recent study showed that, additionally, *PRR* genes directly interact with *CONSTANS* (*CO*) to stabilize the protein, thus enhancing *FT* expression (Hayama et al., 2017). Activation of *CO* expression and the stabilization of the *CO* protein coincide only in flowering-promoting LD conditions, and *CO* directly activates *FT* expression in the leaf vasculature (Samach et al., 2000; An et al., 2004; Valverde et al., 2004; Sawa et al., 2007; Jang et al., 2008). In barley, the role of *Ppd-H1* has most likely diverged from the function of Arabidopsis *PRR* genes, as *Ppd-H1* affects the expression of flowering time genes but not of circadian clock genes (Campoli et al., 2012b). Furthermore, the closest barley *CO* ortholog, *CONSTANS 1* (*CO1*), appears to be less central in the induction of flowering (Campoli et al., 2012a; Shaw et al., 2020). Nonetheless, allelic differences at *Ppd-H1* correlate with changes in *FT1* expression levels in wheat and barley (Turner et al., 2005; Shaw et al., 2013; Digel et al., 2015). Thus, *Ppd-H1* most likely acts upstream of *FT1*. However, whether *Ppd-H1* affects flowering only through *FT1* or additional genes and networks remains elusive. Since allelic variation at *Ppd-H1* also affects the expression of *FT2* in the leaf and developing MSA (Kikuchi et al., 2009; Digel et al., 2015), other *FT*-like genes might be an alternative route for *Ppd-H1*-dependent photoperiodic flowering.

In this study, we aimed to unravel the detailed role of *FT1* in barley development. In particular, we wanted to focus on three specific aspects, which are a) to decipher whether the *Ppd-H1*-mediated photoperiodic response is transmitted exclusively through *FT1* or additional routes, b) to understand whether *FT1* is essential for floral induction in barley and if it affects plant

development and architecture, yield, flowering, and the end of flowering, as observed in other plant species; and c) to unravel what genetic networks are regulated by *FT1*, in particular whether *FT1* affects genes involved in carbohydrate metabolism and nutrient transport and, thus, source-sink relationships. For these purposes, we created *ft1* knock-out mutant plants using CRISPR-Cas9 in both wild-type and mutated *Ppd-H1* backgrounds. Phenotyping *ft1* mutants showed that *FT1* strongly promotes flowering in barley but is not essential, as the mutants were severely delayed in flowering but eventually produced spikes and grains. The effect of *Ppd-H1* seems to be conveyed only or primarily through *FT1*, as the mutants in different *Ppd-H1* backgrounds did not differ in flowering time. *ft1* plants were characterized by substantial changes in longevity, meristem determinacy, and plant and spike architecture. Plant fertility was decreased significantly regardless of the *Ppd-H1* allele. Transcriptomic profiling in leaves, stems, and shoot apices revealed that central regulators of flowering and spike development showed altered expression levels. Additionally, strong transcriptional reprogramming in physiological processes such as photosynthesis, carbohydrate distribution, and stress response seemed to be concerted by *FT1*. Thus, our results demonstrate that the role of *FT1* in barley is not restricted to the regulation of flowering time. Instead, *FT1* appears to be a highly pleiotropic regulator of plant growth and development, affecting plant and spike architecture, fertility, and source-sink relationships.

Results

***FT1* affects plant architecture and accelerates flowering under long days**

To investigate how *FT1* affects whole-plant development and interacts with other genes, we used CRISPR-Cas9 to target the coding sequence (CDS) of *FT1* in two different genetic backgrounds: the spring barley cultivar Golden Promise (GP) carrying the mutated *ppd-H1* allele and GP-fast, which carries a wild-type (WT) *Ppd-H1* allele introgressed from the winter barley Igri (Gol et al., 2021). We generated 17 M2 transformation lines, 14 in GP-fast and three in GP, that were genotyped by PCR and Sanger sequencing and assessed for differences in flowering time. Three late-flowering mutants were chosen for further experiments. These were characterized by a single base pair insertion at position 114 (+T, *ft1.a*), a deletion at position 113 (-C, *ft1.b*), and a deletion at position 88 (-G, *ft1.c*, Supplemental Figure S1 A). These indels resulted in frameshifts and premature stop codons, reducing protein length from 177 aa (WT) to 59 aa (*ft1.a*), 60 aa (*ft1.b*), and 29 aa (*ft1.c*, Figure 1 A, Supplemental Figure S1 B). *ft1.a* and *ft1.b* are in the background of GP-fast, and *ft1.c* in GP. Sister plants of the *ft1* lines without a mutation event within the *FT1* sequence were grown alongside as null segregant lines (*ft1.a-null*, *ft1.b-null*, *ft1.c-null*).

The parents GP-fast and GP, the *ft1* mutant lines *ft1.a*, *ft1.b*, and *ft1.c*, and the respective null segregant lines were grown under controlled long-day (LD) conditions to determine the effect of *FT1* on development and plant architecture in two genetic backgrounds differing for *Ppd-H1*. Flowering was scored on the main culm or the first flowering shoot in case the main culm had stopped development before this stage. In addition, plant height, tiller number, and leaf number were scored at flowering.

GP-fast flowered 41 days after emergence (DAE), followed by GP at 63 DAE (Figure 1 B, Supplemental Figure S2 A-E). The *ft1* lines were delayed significantly by an average of 48 days compared to GP and did not flower on the main culm. We did not observe significant differences between the *ft1* mutant lines differing at *Ppd-H1* (*ft1.a*: 114 DAE, *ft1.b*: 108 DAE, *ft1.c*: 112 DAE), suggesting that *Ppd-H1* acts only or primarily through *FT1* on flowering time. Plant height at flowering was significantly increased in GP and in the three *ft1* mutants compared to GP-fast, and no consistent differences between GP and the *ft1* mutants and amongst the three mutant lines were observed (Figure 1 C). GP plants produced 39 tillers and, therefore, significantly more than early flowering GP-fast, which produced, on average, only 13 tillers (Figure 1 D). *ft1* mutants, which flowered even later than GP, produced significantly more tillers than their respective parent (*ft1.a*: 29, *ft1.b*: 62, *ft1.c*: 87 tillers, Figure 1 D). While GP and GP-fast plants were fully senesced at grain maturity, *ft1* mutant plants continued producing new tillers until the plants were removed after more than two years. Consequently, the *ft1* mutant plants did not undergo whole-plant senescence, but senescence was restricted

to individual tillers. This resulted in plants with many tillers and a high amount of vegetative biomass (Supplemental Figure S2 F-K). Null segregant lines displayed no significant increase for all traits scored compared to their respective WT plants.

To investigate whether the extended development in the *ft1* mutants also affects leaf development, the leaf number, width, and length were scored on the main culm. In contrast to parents, all main culms of the *ft1* mutant lines were aborted prematurely and, therefore, did not develop a flag leaf. GP and the null segregant line in GP produced an average of 11 and 11.5 leaves on the main culm, thus significantly more than the eight leaves on the main culm of GP-fast and the null segregant lines in the GP-fast background (Figure 1 E). The *ft1* mutant lines produced significantly more leaves than GP and GP-fast; on average, 13 and 14 leaves were visible on the main culm until they stopped developing (Figure 1 E). Leaf length was significantly increased in the *ft1* mutants compared to the parents, particularly for the last leaves, which decreased in length in the parents but remained long in the *ft1* mutants (Supplemental Figure S3 A, B). Leaf width also differed between the *ft1* mutants and WT for the last leaves, which became successively slimmer in the parents but remained relatively wide in the *ft1* mutants (Supplemental Figure S3 C, D).

We repeated the experiment by growing GP-fast, GP, and the *ft1* mutants in smaller pots (75 cm³ instead of 1.5 L), which reduced the tiller number and increased the survival of the main culm in the *ft1* mutants. All lines flowered one to two weeks earlier in the small compared to the large pots (*ft1* mutants at 102 DAE, GP at 48 DAE, GP-fast at 34 DAE, Supplemental Figure S4 A), and tillering was strongly reduced, in particular in *ft1* mutants (to an average of 4.3, 6.6, and 5 tillers in *ft1.a*, *ft1.b* and *ft1.c*, Supplemental Figure S4 B). Main culm abortion was reduced from 100% in 1.5 L pots to 75% in *ft1.a* and *ft1.b* and 44% in *ft1.c* (Supplemental Figure S4 C). This allowed us to score the final leaf number on the main culm, which averaged 12.5 leaves for the *ft1* mutants compared to eight in GP-fast and ten in GP (Supplemental Figure S4 D).

In summary, *FT1* has pleiotropic effects on flowering time, tillering, leaf development, and plant longevity. *Ppd-H1* affected flowering only in the presence of a functional *FT1*, suggesting that *Ppd-H1* controls this trait only or mainly through *FT1*.

***FT1* accelerates the vegetative and reproductive development and increases fertility on whole-plant and single-spike level**

To dissect the effects of *FT1* on the development of the main shoot apex (MSA), the MSA of GP-fast, GP, and the three mutant lines *ft1.a*, *ft1.b*, and *ft1.c* were dissected during development and scored according to the scale by Waddington et al. (1983). This scale rates the progression of spikelet meristem (SM) initiation and the development of the most advanced floret meristem (FM) and pistil of the main inflorescence. During early development (W1.0),

the MSA remains vegetative, and only leaf primordia are initiated. The MSA transitions to a reproductive inflorescence at the double ridge stage (W1.5 - W2.0), when SMs become visible adjacent to the leaf primordia, forming the characteristic "double ridges". After spikelet initiation (W2.0), leaf primordia are suppressed, and instead, SMs are induced until approximately W5.0 (Thirulogachandar and Schnurbusch, 2021; Digel et al., 2015). Floral organ primordia start to differentiate at the stamen primordium stage (W3.5) when the central SM has differentiated into three stamen primordia. At W5.0, the last floral organ, the ovule, emerges. Floral organs grow and develop into florets until anthesis and pollination at W10.0. During the early reproductive development, the maximum number of SMs and, thus, the maximum number of flowers and grains are determined.

We scored the MSA development by dissecting three to four plants grown in 75 cm³ pots every few days and by determining the Waddington stage, the number of SMs and FMs, and the inflorescence size. The data was used to calculate the rate of SM initiation, FM development, and FM abortion (Supplemental Table S1).

The MSA of GP-fast plants developed significantly faster than that of GP; it transitioned from vegetative growth to a reproductive inflorescence (W2.0) at 10 DAE compared to 15.5 DAE in GP (Figure 2 A). The MSA development of GP-fast plants showed a linear development across all Waddington stages. At the same time, the developmental transition of the GP inflorescences was slightly slower at each Waddington stage, leading to gradually increasing differences between GP and GP-fast. Consequently, GP-fast plants reached pollination (W10.0) 14 days earlier than GP (GP-fast: 38 DAE, GP: 52 DAE). In contrast, the *ft1* mutants were characterized by a strongly extended vegetative growth period, as all three mutant lines transitioned to reproductive development at around 25 DAE, 10–15 days later than GP and GP-fast (Figure 2 A). Inflorescence development was further delayed during floral organ development, and plants reached pollination after an average of 101 days. No significant differences in developmental timing could be observed amongst the *ft1* mutants, regardless of their parental background. The average rate of SM induction (from W2.0 to the maximum SM stage) was 0.87 SMs/day in *ft1* mutants and, therefore, strongly reduced compared to the parents with 2.25 SMs/day in GP and 2.90 SMs/day in GP-fast (Supplemental Table S1). While SMs were induced until W4.5-W5.0 in both parents and *ft1* mutant lines, they were induced over a longer time period in the *ft1* mutants due to the delayed development compared to the parents. Consequently, this prolonged meristematic activity increased the SM number on the MSA of *ft1* mutants compared to GP-fast, even though SM induction rates were reduced (Figure 2 B, Supplemental Table S1). However, the higher number of SMs did not necessarily correlate with an increased inflorescence size, as the inflorescence density (measured in SMs/mm inflorescence) was significantly increased in *ft1* mutants and GP compared to GP-fast (Figure 2 C, Supplemental Figure S5).

After floral organ initiation, florets develop on a growing spike into flowers and grains. However, not all initiated SMs form FMs and mature into flowers, as some FMs are aborted during floral development. The rate of floret abortion was highest in GP-fast (3.5 FMs/day), followed by GP (2.8 FMs/day), and significantly lower in *ft1* plants (average rate 0.97 FMs/day, Supplemental Table S1) and therefore negatively correlated with the developmental timing. The total number of aborted florets was thus much lower in *ft1* plants compared to parents, with an average of 3.5 florets compared to 13 florets on GP-fast and GP plants. Consequently, *ft1* plants produced roughly ten more FMs than GP and 20 more than GP-fast (Figure 2 B, Table S1).

Besides differences in size and SM number, the MSA of GP-fast, GP, and *ft1* mutants were morphologically very similar during early reproductive developmental stages (W1.0-W3.0, Figure 2 D). However, at the stamen primordium stage (W3.5), secondary inflorescences started to emerge from the lowest central spikelet meristem (CSM) of the MSA in *ft1* plants (Figure 2 E-G). We observed this in 60–80% of the dissected main culms of *ft1* plants. This usually occurred only on one side of the inflorescences, in rarer cases (about 10%) on both. Compared to the MSA, the secondary inflorescences were delayed but appeared to develop normally. They resulted in branched spikes, of which some developed grains and others ectopic tillers at the base of the spike (Supplemental Figure S6).

Next, the effect of *FT1* on reproductive success was evaluated by scoring the number of spike-bearing tillers and the number of florets and grains on the main spike. Floret number and spike length were significantly higher in GP than in GP-fast, while grain number was not significantly different between both genotypes (Figure 3 A-C). Therefore, spike fertility, the number of grains per floret on the main spike was higher in GP-fast compared to GP (90% in GP-fast and 70% in GP, Figure 3 D). In *ft1* mutants, the floret number was increased compared to GP-fast but not to GP (Figure 3 A), whereas spike length was not significantly different from GP-fast spikes due to a higher density of florets on *ft1* spikes (Figure 3 C, E). Grain set and, thus, spike fertility was significantly reduced in all three *ft1* mutants compared to their parents (Figure 3 B, D). The average spike fertility in the *ft1* mutants ranged from 0% to 15% on the main culm. The tiller fertility, the ratio of spike-bearing tillers with at least one grain versus the total number of tillers, was close to 100% in GP-fast and GP. In contrast, tiller fertility of *ft1.a*, *ft1.b*, and *ft1.c* averaged only 20%, 29%, and 44%, respectively (Figure 3 F). *FT1* also affected grain morphology as thousand grain weight (TGW) and two-dimensional grain area were significantly reduced in *ft1* mutants compared to the parents, mainly due to reduced grain width (Supplemental Figure S7).

The phenotype of ovules and anthers of parental and *ft1* plants were compared to test possible causes for the reduced grain set and fertility. *ft1* mutant flowers exhibited substantial changes in anther morphology and size in many, but not all, florets, while the ovule did not show

noticeable differences compared to the parents (Figure 4 A). Anthers in GP-fast and GP were yellow and full of pollen grains easily spilling from the pollen sacs. In comparison, anthers in florets of *ft1* mutants looked paler and thinner and either lacked pollen grains or held a significantly reduced amount of pollen (Figure 4 A). Anthers of *ft1* mutant plants were also significantly shorter in length than their parents (Figure 4 C). We extracted pollen grains from central florets of parental and *ft1* spikes and quantified the proportion of viable pollen based on the differential staining of the pollen protoplasm and the cellulose contained in pollen walls and on pollen grain size variation. The staining of pollen from GP and GP-fast showed mostly round and viable pollen (Figure 4 B). By contrast, many pollen grains from *ft1* plants were significantly reduced in diameter (Figure 4 D). Electron microscopy pictures further demonstrated that parental pollen were round and full, while pollen from *ft1* mutants were shriveled, likely empty, and sometimes with a ruptured pollen wall (Supplemental Figure S8). Based on these measurements, pollen viability was reduced significantly from 96–97% in GP-fast and GP to an average of 81%, 78%, and 88% in *ft1.a*, *ft1.b*, and *ft1.c*, respectively (Figure 4 E). We thus concluded that the impaired anther and pollen development contributed to the reduction in floret fertility in the *ft1* mutant plants.

In conclusion, MSA development of *ft1* mutants was delayed compared to GP-fast and, to a lesser extent, to GP. This correlated with an increase in SM number and a reduction in FM abortion. Spike architecture in *ft1* plants was altered by the deregulated development of the lowest central spikelet primordium, which resulted in the outgrowth of secondary inflorescences and branched spikes. The floret number on the mature spike was increased in *ft1* plants compared to GP-fast. However, spike and tiller fertility were significantly reduced in *ft1* mutants compared to parents, likely resulting from reduced pollen number and viability. Furthermore, *FT1* affected grain filling and grain shape, as *ft1* mutants were characterized by a reduction in TGW and grain width.

***FT1* strongly affects the expression of genes involved in carbon metabolism and stress response in the leaf**

To identify genes and genetic networks underlying the *FT1*-controlled phenotypes, we conducted genome-wide transcriptome profiling in *ft1* mutants, GP, and GP-fast. For this purpose, we harvested leaves, MSAs, and the internode below the last node of the main spike at key reproductive stages: the start of spikelet initiation (W2.0), the onset of floral development (W3.5), and the stop of spikelet induction (W5.0).

To find genes regulated by *FT1*, we first performed pairwise comparisons between *ft1.a* and *ft1.b* mutants with GP-fast, carrying a WT *Ppd-H1* allele. We only selected genes significantly up- or downregulated (FDR \leq 0.01 in leaf and MSA, FDR \leq 0.05 in stem) in both mutant lines compared to GP-fast with a log fold change ($\log_2FC \geq 1$ or ≤ -1) in at least one developmental

stage. Subsequently, we identified differentially expressed genes (DEGs) using the pairwise comparison of *ft1.c* compared to GP, which carries the mutated allele of *ppd-H1* and is characterized by reduced levels of *FT1* expression. Since phenotypic differences of the *ft1* mutants to GP were smaller than to GP-fast, we expected fewer molecular changes and did not set a fold change threshold. Our final set of DEGs, therefore, contained all genes that were a) differentially regulated in *ft1.a* and *ft1.b* versus GP-fast in at least one developmental stage with a log fold change of at least 1, and b) differentially regulated between *ft1.c* and GP, albeit with a lower log fold change. This resulted in a total number of 545, 516, and 107 DEGs across all three *ft1* mutants in leaf, MSA, and stem, respectively. Lists with all DEGs can be found in Supplemental Datasets S1-S3.

In the leaf, of 545 DEGs, 248 DEGs were downregulated, and 297 DEGs were upregulated (Figure 5 A, Supplemental Figure S9 A). A PCA analysis of the leaf samples demonstrated that the genotype explained most variation (PC1, Supplemental Figure S10 A). Since the developmental stage did not clearly separate the samples, we discuss all DEGs across the stages together in the following.

FT1 was exclusively expressed in the leaf, and the expression was strongly downregulated in GP and all *ft1* mutants, regardless of the *Ppd-H1* background, compared to GP-fast (Supplemental Figure S11 A). Flowering promoters and known targets of *FT1*, such as *APETALA1*-like genes *BARLEY MAD5 BOX 3* (*BM3*, *HORVU.MOREX.r3.2HG0127410*) and *VERNALIZATION 1* (*VRN1*, *HORVU.MOREX.r3.5HG0511210*) (Turner et al., 2005; Digel et al., 2015) as well as *FLOWERING PROMOTING FACTOR* genes (e.g., *FPF1*, *HORVU.MOREX.r3.2HG0101810*) were downregulated (Supplemental Figure S11 B-D), while transcript levels of the flowering repressors *APETALA 2* (*AP2*, *HORVU.MOREX.r3.2HG0204770*), *MADS51* (*HORVU.MOREX.r3.3HG0310850*) and short vegetative phase (SVP)-like genes *BM1* (*HORVU.MOREX.r3.4HG0406150*), *BM10* (*HORVU.MOREX.r3.6HG0616500*), and *VEGETATIVE TO REPRODUCTIVE TRANSITION 2* (*VRT2*, *HORVU.MOREX.r3.7HG0664320*) were upregulated in *ft1* mutants (Hartmann et al., 2000; Trevaskis et al., 2007; Debernardi et al., 2022) (Supplemental Figure S11 E-I). In addition, transcript levels of the *FT1* paralog and flowering repressor *FT4* (*HORVU.MOREX.r3.2HG0117260*) were significantly increased in *ft1* plants compared to parents and in GP compared to GP-fast (Pieper et al., 2020, Supplemental Figure S11 J), while other *FT*-like genes, such as the flowering promoters *FT2* (*HORVU.MOREX.r3.3HG0244930*) and *FT3* (*HORVU.MOREX.r3.1HG0077250*), were not or only slightly reduced in *ft1* mutants compared to parents.

We observed that *ft1* mutants were characterized by more and larger leaves compared to GP and GP-fast and thus searched for DEGs with known roles in leaf development. Nuclear transcription factor Y (NF-Y) genes (e.g., *HORVU.MOREX.r3.4HG0335570*), which have been

described as positive regulators of leaf growth in *Arabidopsis* (Zhang et al., 2017), were upregulated in the *ft1* mutants compared to the parents (Supplemental Figure S11 K). A homolog of *ASYMMETRIC LEAVES* (*AS1*, *HORVU.MOREX.r3.5HG0441760*) with potential roles in cell division and differentiation and leaf patterning was strongly upregulated in the *ft1* mutants (Byrne et al., 2000) (Supplemental Figure S11 L). Further, we observed the upregulation of a *MYB HYPOCOTYL ELONGATION-RELATED* (*MYBH*) transcription factor (*HORVU.MOREX.r3.3HG0236900*) and SAUR-like genes (e.g., *HORVU.MOREX.r3.7HG0736410*), which control leaf expansion and auxin-promoted leaf senescence (Lu et al., 2014; Huang et al., 2015) (Supplemental Figure S11 M, N).

Accordingly, downregulated genes were enriched for genes involved in photosynthesis (Supplemental Figure S10 B), such as *LIGHT HARVESTING COMPLEX PHOTOSYSTEM II* (e.g., *LHCB4.2*, *HORVU.MOREX.r3.2HG0135600*), several photosystem subunits (e.g., *PSAO*, *HORVU.MOREX.r3.2HG0166730* and *PSAE-2*, *HORVU.MOREX.r3.5HG0526900*) and *CHLOROPHYLL A/B BINDING PROTEIN 1* (*CAB1*, *HORVU.MOREX.r3.5HG0522210*) (Figure 5 B-E). Amongst the downregulated genes were also RuBisCO subunits (e.g., *RBCS1A*, *HORVU.MOREX.r3.2HG0104740*), genes homologous to *Arabidopsis RUBISCO ACTIVASE* (e.g., *RCA*, *HORVU.MOREX.r3.4HG0357430*) and *D-RIBULOSE-5-PHOSPHATE-3-EPIMERASE* (*RPE*, *HORVU.MOREX.r3.4HG0403260*), a critical enzyme involved in the Calvin-Benson cycle (Figure 5 F-H). These molecular changes suggested that carbon assimilation was reduced in the *ft1* mutants. This was also supported by the observation that many genes involved in cell wall hydrolysis, sugar conversion, and carbohydrate metabolism were differentially expressed in *ft1* mutants. These included the upregulation of beta-glucosidases (*BGLU11*, *HORVU.MOREX.r3.5HG0495360*), glucanases (*PR2*, *HORVU.MOREX.r3.3HG0318590*), fructokinases (*FRK2*, *HORVU.MOREX.r3.3HG0306200*), and beta-amylases (*HORVU.MOREX.r3.4HG0355960*) (Figure 5 I-L).

The downregulation of genes involved in photosynthesis and upregulation of genes associated with catabolic processes resembles the molecular changes observed in barley plants subjected to biotic and abiotic stresses or plants undergoing senescence (Bilgin et al., 2010; Daszkowska-Golec et al., 2019; Mikołajczak et al., 2022). Indeed, DEGs in *ft1* leaves were enriched for genes related to biotic and abiotic defense mechanisms (Supplemental Figure S10 B). These included *EARLY-RESPONSIVE TO DEHYDRATION 9* (*ERD9*, *HORVU.MOREX.r3.2HG0139310*), *GLUTATHIONE S-TRANSFERASE F11* (*GSTF11*, *HORVU.MOREX.r3.4HG0409180*), disease resistance protein *RESISTANCE TO P. SYRINGAE PV MACULICOLA 1* (*RPM1*, *HORVU.MOREX.r3.1HG0003260*), and several kinases such as *MAP KINASE KINASE 2* (*MKK2*, *HORVU.MOREX.r3.7HG0650300*), and LRR transmembrane receptor kinase *HAESA-LIKE 3* (*HSL3*,

HORVU.MOREX.r3.7HG0718040) which are involved in signaling pathways in response to abiotic and biotic stress factors (Rodriguez et al., 2010; Rhodes et al., 2022) (Supplemental Figure S11 O-S).

Consequently, the leaves of *ft1* mutants were characterized by a molecular stress response, coupled with a downregulation of genes involved in carbon assimilation but an upregulation of genes associated with carbon metabolism or sugar break down.

***FT1* regulates chromatin accessibility and meristem maintenance in the developing MSA**

Since spike development was strongly altered in the *ft1* mutants, we also investigated the molecular changes in the developing MSA at spikelet initiation (W2.0), beginning of floral development (W3.5), and stop of spikelet induction (W5.0). As the stem is crucial for the transport between the vegetative and reproductive organs, we also probed the last stem internode directly under the at W3.5 and W5.0 to test whether source-sink relationships were affected.

In MSA tissue, we could identify 516 DEGs, of which the majority, 342, were upregulated in the *ft1* mutants while 174 DEGs were downregulated compared to the parents (Figure 6E, Supplemental Figure S9 B). A PCA showed that the samples clustered clearly by genotype and developmental stage (Supplemental Figure S12 A), and the number of DEGs increased with the developmental stage from 143 DEGs at W2.0 to 227 DEGs at W3.5 and 349 DEGs at W5.0 (Figure 6 E). In the stem, gene expression variation did not clearly separate either the genotypes or the stages (Supplemental Figure S13), and only 107 DEGs were identified across both stages (62 upregulated, 45 downregulated; Supplemental Figure S9 C).

In the MSA, the upregulated genes were enriched for functions in stress response and transcription and translation, while downregulated genes had functions in chromatin assembly and remodeling and DNA and nucleosome organization (Supplemental Figure S12 B). In line with the large number of genes upregulated in the *ft1* mutants, several genes involved in transcription and translation were upregulated, such as *HORVU.MOREX.r3.5HG0524690*, a homolog of Arabidopsis *TRANSCRIPTION ELONGATION FACTOR IIS (TFIIS)*, and *HORVU.MOREX.r3.2HG0107850*, homologous to the *ELONGATION FACTOR 1* alpha subunit (*EF1ALPHA*) (Figure 6 A, B). By contrast, genes encoding for histones (e.g., *H2A 2*, *HORVU.MOREX.r3.2HG0138300*, and *H2B*, *HORVU.MOREX.r3.7HG0739400*, Figure 6 C, D) involved in chromatin condensation and transcriptional activation, were downregulated in the *ft1* mutants. These transcriptional changes suggested that *ft1* mutants were characterized by chromatin de-condensation and higher DNA accessibility, resulting in altered transcriptional activity. The majority of upregulated genes had functions in stress response, which was in line with the observed stress phenotypes in *ft1* mutants, such as premature main culm abortion

and reduced grain set. In the MSA, upregulated stress-response genes included heat shock factors, chaperones, ABA-responsive genes, senescence and autophagy-associated genes, and genes involved in plant detoxification (Supplemental Figure S14 A-F). In addition, ABA, ethylene, and auxin-responsive genes were strongly upregulated in the *ft1* mutants compared to parents (Supplemental Figure S14 G-K). Similarly, in the stem, many stress-related genes were upregulated in *ft1* mutants compared to the parents, such as genes encoding heat shock factors, chaperones, and plant detoxification genes (Supplemental Figure S14 L-O).

In the MSA, genes involved in sugar metabolism were downregulated, including a cell wall invertase (*CINV2*, *HORVU.MOREX.r3.2HG0166450*, Figure 6 F) and *TREHALOSE-6-PHOSPHATE SYNTHASE 1* (*TPS1*, *HORVU.MOREX.r3.1HG0077190*, Figure 6 G) which catalyzes the synthesis of the sucrose-signaling trehalose, and the sugar transporter *SWEET 10* (*HORVU.MOREX.r3.7HG0684580*, Figure 6 H). Likewise, in the stem, sugar transporter *SWEET17* (*HORVU.MOREX.r3.5HG0428260*, Supplemental Figure S14 P) and sugar hydrolyzing acid beta-fructofuranosidases (e.g., *HORVU.MOREX.r3.7HG0635380*, Supplemental Figure S14 Q) were downregulated. At the same time, a beta-amylase (*HORVU.MOREX.r3.4HG0355960*), the key enzyme for starch degradation, was strongly upregulated in the MSA and stem where this enzyme is typically not expressed (Vinje et al., 2011, Figure 6 I). In the stem, we detected the upregulation of *NITRATE TRANSPORTER 1* (*NRT1*, *HORVU.MOREX.r3.6HG0605270*), *NITRATE REDUCTASE 1* (*NIA1*, *HORVU.MOREX.r3.6HG0541410*), and *NITRITE REDUCTASE 1* (*NIR1*, *HORVU.MOREX.r3.6HG0619730*), controlling the transport of nitrate and its conversion to nitrite and then to ammonium (Supplemental Figure S14 R-T). These molecular changes suggested that the MSAs of *ft1* plants were characterized by limited sugar availability, possibly due to the downregulation of the photosynthetic apparatus in the leaf. The upregulation of nitrate metabolism and -transport suggests the remobilization of nitrogen from the leaves to the stem and MSA. The overall transcriptional changes in the MSA and stem of the *ft1* mutants were thus reminiscent of those observed under stress and indicated changes in carbon and nitrogen availability and distribution (Perrella et al., 2022).

We focused our further analysis on developmental genes putatively regulated by *FT1* that might be linked to the impaired spike development in the *ft1* mutants. In barley, *FT1* is only expressed in the leaf, and *FT1* expression correlates positively with inflorescence development, specifically with floral development (Digel et al., 2015). The expression level of the *FT1* paralog *FT2* with putative roles in floral development (Shaw et al., 2019) was strongly downregulated in the MSA and stem of *ft1* mutants and GP compared to GP-fast (Figure 6 J). In addition, several MADS-box transcription factors specifying floral organ and meristem identity such as *AGAMOUS-LIKE 6* (*AGL6*, *MADS6*, *HORVU.MOREX.r3.6HG0604360*), the *APETALA1*-like genes *BM3* (*HORVU.MOREX.r3.2HG0127410*) and *BM8*

(*HORVU.MOREX.r3.2HG0156870*), the barley *TFL1*-homolog *CENTRORADIALIS* (*CEN*, *HORVU.MOREX.r3.2HG0166090*) and a *SEPALLATA1*-like gene (*MADS34*, *HORVU.MOREX.r3.5HG0511250*) were downregulated in the *ft1* mutants (Figure 6 K-O). At the same time, an *AP2*-like gene (*HORVU.MOREX.r3.3HG0294880*) and an *AGL14*-like gene (*HORVU.MOREX.r3.3HG0311250*), putatively involved in meristem maintenance, and the floral repressor *MADS51* (*HORVU.MOREX.r3.3HG0310850*) were strongly upregulated in the *ft1* mutants, the latter also in the stem (Figure 6 P-R). Similarly, in the stem, several putative repressors of floral development, such as the MADS-box transcription factors *AGL14*-like (*HORVU.MOREX.r3.3HG0310820*), *AGL20*-like (*HORVU.MOREX.r3.4HG0412460*) and *SHATTERPROOF 2* (*SHP2*, *HORVU.MOREX.r3.4HG0413180*) involved in dehiscence zone differentiation during fruit development, were upregulated while *BM3*, *CEN* and a *CEN*-like gene (*HORVU.MOREX.r3.4HG0407080*) were downregulated in the *ft1* mutants compared to WTs (Supplemental Figure S15 A-F).

The *ft1* mutants were thus characterized by an altered expression of meristem maintenance genes and floral homeotic genes in the MSA and stem below the MSA, which is presumably linked to the prolonged meristematic activity of the inflorescence meristem and increased SM number, as well as to the delay in floral development and the high rates of floral abortion in the *ft1* mutants.

In summary, *FT1* has pleiotropic effects on different shoot traits, correlating with profound transcriptional reprogramming in leaf, stem, and MSA in the *ft1* mutants. The *ft1* mutants are characterized by a stronger vegetative program at the expense of reproductive growth, as demonstrated by prolonged and increased leaf and tiller development, increased spike branching, and floret and spike abortion. The upregulation of senescence-associated genes and downregulation of photosynthesis genes in the *ft1* leaves, coupled with altered expression of genes involved in carbon metabolism and nitrogen transport in the MSA and stem, suggest changes in source and sink functioning. The upregulation of stress-response genes in all tissues indicates that the knock-out of *FT1* and, thus, the removal of LD signaling represents a stress condition.

Discussion

***FT1* has a pleiotropic effect on plant development**

FT-like genes are central regulators of reproductive development in flowering plants. Besides flowering, *FT*-like genes are major factors in a wide range of developmental processes, including fruit and grain set, vegetative growth, stomatal control, and tuberization (Lifschitz et al., 2006; Kinoshita et al., 2011; Navarro et al., 2011; Li et al., 2015b). These multifaceted roles of *FT*-like genes have resulted from extensive gene duplication events, which occurred independently in nearly all modern angiosperm lineages and were followed by sub- or neo-functionalization (Pin and Nilsson, 2012). Barley carries 12 *FT* paralog, of which *FT1* is central to reproductive development (Faure et al., 2007; Digel et al., 2015). With this study, we aimed to a) understand if natural variation at *Ppd-H1* affects plant development only through modifying *FT1* expression, b) characterize the effects of *FT1* on whole-plant development, and c) identify the molecular networks controlled by *FT1* in the leaf and developing shoot apex.

We generated *ft1* mutants in the background of a wild-type and a mutated *Ppd-H1* allele. The *FT1* proteins in all mutants were truncated ahead of residues R62, T66, P94, F101, and R130 that were identified as critical for the interaction of *FT1* with 14-3-3 proteins in wheat and rice (Taoka et al., 2011; Li et al., 2015a). Thus, all proteins were therefore most likely not able to function in their role as flowering inducers. Loss of a functional *FT1* protein had pleiotropic effects on plant growth and architecture, as it strongly delayed all phases of plant development (Figure 1). Development was delayed regardless of the variation at *Ppd-H1*, indicating that the regulation of developmental progression by *Ppd-H1* occurs exclusively through *FT1*. Longer vegetative growth resulted in more and bigger leaves, taller plants, and more tillers. Decelerated reproductive development increased the number of SMs initiated on the developing spike and delayed floral development and flowering (Figure 2). Impaired floral development significantly reduced plant fertility (Figure 3, Figure 4). Previous studies showed that reduced *FT1* and *FT2* expression coincides with increased SM number but reduced grain set and, thus, fertility (Shaw et al., 2013; Shaw et al., 2019). RNA Sequencing revealed that *FT2* expression in the MSA was co-regulated with *FT1* expression in the leaf and, thus, strongly reduced in *ft1* mutants. *FT1*, therefore, has a strong effect on developmental progression, which decreases the duration of vegetative growth and leaf and tiller number. On the other hand, *FT1* promotes, presumably through *FT2* expression in the MSA, reproductive development, spike fertility, and reproductive biomass. Therefore, the loss of *FT1* function resulted in an imbalance in the ratio of vegetative to reproductive biomass and, consequently, in the source-sink homeostasis of the plant. These phenotypic effects of *FT1* were quantitative, as the phenotypic changes were strongest in the *ft1* mutant lines and intermediate in GP with

reduced *FT1* expression in the leaf compared to GP-fast with high expression levels of *FT1* in the leaf.

ft1 plants initiated more leaf and spikelet meristems and thus produced more leaves and more spikelets on the developing inflorescence. In addition, the differentiation of FMs in *ft1* mutants was impaired as SMs at the base of the MSA developed into IMs, resulting in a branch-like spike architecture (Figure 2). Hence, *FT1* promotes meristem identity in barley, as observed in other plant species (Koornneef et al., 1991; Krieger et al., 2010). The expression of *TFL1* homolog *CEN* was strongly downregulated in the MSA and stem of *ft1* mutants. Reduced *CEN* expression is usually correlated with early flowering and a reduction in spikelet number in barley (Bi et al., 2019). However, *FT1* and *CEN* are proposed to interact, and low *CEN* expression levels in the background of low *FT1* expression delay flowering and increase the number of SMs (Bi et al., 2019). This was also observed in *ft1* mutants and thus confirms that the effect of *CEN* in regulating spikelet development is dependent on *FT1* expression. Furthermore, *ft1* plants continuously initiated tillers and showed no whole-plant senescence but only senescence of individual tillers. This is reminiscent of perennial plants, which do not undergo whole-plant senescence but maintain undifferentiated meristems (Albani and Coupland, 2010). The downregulation of flowering time inducers and consequent reduction in meristem determinacy in annual *Arabidopsis* resulted in plants with markedly increased longevity, suggesting their involvement in longevity in annual life (Melzer et al., 2008). We could also observe that *ft1* plants produced grains for several months due to continuous tillering. This is significantly longer than GP-fast and GP plants that only flower for a few weeks. Therefore, *FT1* appears to affect end-of-flowering and whole-plant senescence. Recent studies have shown that regulators of flowering time also affect the end or duration of flowering (Balanzà et al., 2018; Miryeganeh, 2018). González-Suárez et al. (2023) correlated *FT1* expression to flowering duration and showed that *FT1* levels do not only have to reach a certain threshold to induce flowering but also to conclude it. As *ft1* plants showed significantly increased longevity, we conclude that *FT1* controls the beginning and duration of flowering in barley.

***FT1* changes the expression of genes involved in stress response and source-sink relationships**

As the effect of *FT1* was highly pleiotropic, and the development and morphology of multiple above-ground organs were altered in *ft1* mutants, we decided to investigate the molecular effect of *FT1* via RNA sequencing in the leaf, stem, and developing inflorescence. In the leaf, we could observe a strong downregulation of genes involved in the light- and dark reaction of photosynthesis and an upregulation of genes linked to sugar breakdown and stress response (Figure 5). The downregulation of photosystem components and RuBisCO subunits might

reduce carbon assimilation and sugar availability in *ft1* plants. This hypothesis is supported by the upregulation of genes involved in the breakdown of sugars from cell walls or starch and the downregulation of genes associated with Trehalose 6-phosphate (T6P) signaling (Figure 6). In Arabidopsis, T6P is a signal of sucrose availability that regulates diverse plant development processes (Fichtner and Lunn, 2021). This includes flowering, as the expression of *FT1* depends on *T6P SYNTHASE (TPS1)* activity (Wahl et al., 2013). The downregulation of a *TPS1*-like gene in *ft1* mutants could either be a response to reduced sugar availability or indicate that this signaling is, in fact, bidirectional and that changes in *FT1* expression levels can also affect T6P levels and, thus, plant metabolism.

In the MSA, we observed the differential expression of genes linked to stress response, chromatin remodeling, and floral development (Figure 6). The latter included the downregulation of several MADS-box genes and the upregulation of an *AP2*-like gene in the MSA. MADS-box genes are involved in the maintenance of meristems (Melzer et al., 2008; Yasui et al., 2017), and *AP2* has been hypothesized to promote the activity of the meristem maintenance gene *WUSCHEL* to positively control the duration of IM activity in Arabidopsis (Balanzà et al., 2018). Thus, the differential expression of MADS-box and *AP2*-like genes might be causative for the prolonged IM activity we observed in *ft1* mutants and GP. While the prolonged activity of the IM in *ft1* plants resulted in more spikelet meristems, further floral development was impaired, resulting in an overall strong reduction in grain number per spike. Accordingly, developing inflorescences of *ft1* plants were characterized by the deregulation of floral homeotic genes such as *AGL6*, *BM3*, *BM8*, *MADS34*, and *AP2-like*, which have been linked to floral development in wheat and barley (Trevaskis et al., 2007; Li et al., 2021; Debernardi et al., 2022; Kong et al., 2022). *FT1*, therefore, regulates the expression of genes controlling the maintenance and differentiation of the IM.

We also observed that the *ft1* knock-out mutants were characterized by profound changes in the expression of histone subunits, indicating that developmental transitions are linked to epigenetic modifications in the barley MSA. Changes in DNA methylation patterns have also been shown to accompany the transition from vegetative to reproductive growth in rice MSAs (Higo et al., 2020). The downregulation of histones in *ft1* mutants indicates that *FT1*, or the delay in development caused by loss of *FT1*, affects epigenetic regulation and chromatin remodeling. We could also observe extensive changes in transcription levels and the transcription and translation machinery, which could also be linked to changes in chromatin accessibility (You et al., 2017).

Among the most striking molecular changes in the *ft1* mutants were the strong upregulation of stress-response genes in the leaf, stem, and MSA. This was linked to stress phenotypes such as premature tiller abortion, reduced fertility, and reduced pollen viability in *ft1* mutants, which is typically only observed in plants grown under abiotic stress conditions (Ejaz and von Korff,

2017; Gol et al., 2021). Abiotic stress is also known to cause epigenetic changes (Miryeganeh, 2021; John et al., 2023). Thus, the differential expression of histones might be consequential to the stress in *ft1* plants, as revealed by the upregulation of stress-related genes.

While we cannot conclusively resolve what triggers the stress response, we speculate that *ft1* mutants were characterized by impaired homeostasis. *FT1* is the major molecular component for photoperiod signaling. Plants were grown under LDs, but the observed phenotypes strongly resemble plants cultivated under non-inducible short-day (SD) conditions (Digel et al., 2015). Photosynthesis and plant metabolism are not synchronized with developmental decisions if plants are grown under LD but are developmentally controlled as under SD. The distribution and partitioning of carbohydrates are part of a delicate system where metabolic needs in the sink are balanced to primary assimilates in the source leaf. Environmental conditions, including photoperiod, strongly affect this system (Mengin et al., 2017; Jeandet et al., 2022). An imbalance in the source-sink relationship, as implied by the differential expression of several genes involved in carbohydrate metabolism, might create a metabolic state that triggers a stress response in the plant. Consequently, this suggests a direct link between flowering time regulation and metabolism, and *FT1* as a central component of this connection. However, additional data on photosynthesis and carbon content in *ft1* plants is required to enlighten this relationship further.

All in all, we could identify the flowering time gene *FT1* as a pleiotropic regulator of plant development, affecting developmental progression but also meristem determinacy and the carbohydrate status of a plant. Loss of *FT1* function strongly impedes development, presumably due to a loss of synchronization between plant growth and environmental conditions, resulting in carbohydrate imbalances that strongly reduce plant yield.

Materials and Methods

Plant material

Spring cultivar Golden Promise (GP, carrying a mutated *ppd-H1* allele) and its derived introgression line GP-fast (wild-type *Ppd-H1* introgressed into GP from Igri, Gol et al., 2021) were transformed with a CRISPR-Cas9 construct (pGH465, Supplemental Figure S16) to create plants with a nonfunctional *FT1* (*HORVU.MOREX.r3.7HG0653910*) gene. The sgRNA targeted a sequence within the first exon of *FT1* (position 97-116 relative to the start codon, 5'→3': TGACCTTCGGGAACAGGGCCGTGTCCAA). M1 grains were grown in the greenhouse for single-seed propagation.

From 17 different M1 lines, 2-3 grains were grown in a plant growth chamber under controlled LD conditions as described below. DNA was extracted from leaf material using the KingFisher Flex (ThermoFisher) and the BioSprint 96 DNA Plant Kit (QIAGEN) according to the manufacturer's instructions. To identify mutations within the CDS of *FT1*, the complete genomic sequence of *FT1* was amplified with flanking primers (fwd 5'→3': GAAGGAAGGAGAAATGGCCG, rev 5'→3': GATCGAGCGAGCATTAGTCA). PCR products were cleaned using the ExoSAP-IT PCR Product Cleanup Kit (ThermoFisher) and sequenced with Sanger Sequencing. Sequences were compared using MEGA-11 (Version 11.0.10, Tamura et al., 2021).

Three lines with single nucleotide polymorphisms (SNPs) were chosen for further experiments and termed *ft1.a*, *ft1.b* (in the background of GP-fast), and *ft1.c* (in the background of GP). Sister plants from the three mutant lines that did not show a mutation event within the *FT1* sequence were chosen as null segregant lines.

Growth conditions and plant phenotyping

All plants were grown in soil in controlled growth chambers under long days (LD, 16 h light, 20 °C, PAR ~250 μmol/m²s; 8 h dark, 16 °C). Plants were grown in Einheitserde ED73 (Einheitserde Werkverband e.V.) with 7% sand and 4 g/L Osmocote Exact Hi.End 3-4M, 4th generation (ICL Group Ltd.). All plants were stratified for 3–4 days at 4 °C and darkness after sowing.

WT plants, mutant lines, and null segregant lines were sown in QuickPot 96T trays (HerkuPlast Kubern GmbH, pot volume 75 cm³). At ten days after emergence (DAE), at least four (null segregant lines) or eight (*ft1* lines) plants per genotype were repotted to single 1.5 L pots, and plants were cultivated under LD conditions for phenotyping. Flowering was scored as the days between the emergence of the seedling from the soil and plants reaching Zadoks' stage 49 when the awns exited the leaf sheath (Zadoks et al., 1974). Plant height was measured at flowering as the distance between soil and flag leaf ligule of the main culm. Tiller number was

counted as all secondary tillers that had emerged after the main culm at flowering, and the leaf number was determined on the main culm. When the main culm of *ft1* mutant plants was aborted prematurely, leaf number was scored until abortion. Leaf width and length were measured on fully elongated leaves on the main culm as the leaf blade length (from the ligule to the leaf tip) and the maximum width of the blade. If available, floret and grain number and spike length were determined on the main culm. Tiller fertility was determined by dividing the number of tillers with a spike that held at least one grain by the total tiller number.

As the main culm of *ft1* mutants was aborted prematurely, GP, GP-fast, *ft1.a*, *ft1.b*, and *ft1.c* plants were cultivated in a consecutive experiment in QuickPot 96T trays (HerkuPlast Kubern GmbH, pot volume 75 cm³) until maturity to reduce tillering and main culm abortion. At least seven plants were scored per genotype. Flowering, plant height, tiller number, tiller fertility, and number of leaves at flowering were scored as described above. The main culm abortion rate was determined by scoring whether the main culm produced a spike or not. If the main culm was not aborted, spike length, floret number, and grain number were determined on the main culm. This was used to calculate the spike density (as florets per cm spike length) and spike fertility (as grains per florets).

Main shoot apex (MSA) development of GP, GP-fast, *ft1.a*, *ft1.b*, and *ft1.c* was monitored under LD. Every 4–13 days, the main culm of 3–4 individual plants was dissected, starting 4 DAE for GP-fast and 7 DAE for the other genotypes. Parent plants were dissected more frequently than *ft1* mutants due to the faster development. The stage of the MSA was documented using the stereo microscope Nikon SMZ18 with a Nikon DS-Fi2 camera, analyzed with the NIS-Elements Software (version 5.21.03, Nikon Instruments Europe BV), and quantified according to the Waddington scale (Waddington et al., 1983). Inflorescence size was scored as the distance between the lowest spikelet meristem (SM) and the tip of the inflorescence meristem (IM). The number of developing SMs, including those that had initiated floret meristems (FMs) or developed into florets, was determined from Waddington stage W2.0 to W10.0. This data was used to calculate the inflorescence density (SMs per mm inflorescence length). SM initiation and FM abortion rate were calculated using the R package *segmented* (version 1.6-2, Muggeo, 2003, 2008) in R Studio (2022.2.0.443, RStudio Team, 2022). The SM number was plotted against days after emergence, and one break-point was calculated automatically to separate initiation from abortion. The slope of segment 1 equals the SM initiation rate (SMs/day), and the slope of segment 2 equals the FM abortion rate (FMs/day). The break-point was set as the maximum SM stage, and the corresponding maximum SM number and the final number of FMs at W10.0 were calculated with the linear regressions provided by *segmented*. The number of aborted FMs was determined by subtracting the maximum SM number from the final number of FMs.

Pollen, anther, and grain measurements

Spikes with the central florets at approximately Waddington stage W10.0 were used to test the pollen viability according to a modified protocol from Peterson et al. (2010). Main culm spikes were harvested from at least three individual plants per genotype. Six central florets (from both sides of the two-rowed spike) were opened from each spike, and stamen size was determined by measuring the size of the three stamens per floret using the software Fiji (Schindelin et al., 2012). From 2–3 of these florets, the stamens were transferred into the staining solution (as described in Peterson et al., 2010) without prior fixing. Samples were incubated for 40 min at 100 °C. Then, free pollen in the staining solution were transferred to a microscope slide. The examination was performed using a Nikon stereo microscope (Nikon SMZ18), and the pictures were taken with a Nikon DS-Fi2 digital camera connected to the microscope. Pollen viability was determined by visually inspecting whether pollen were stained purple (classified as viable) or stained light blue (classified as non-viable). For each floret, 60–400 pollen were classified. The viability (ratio of viable to non-viable) was averaged per floret. To determine the average pollen diameter, ten randomly chosen fertile pollen were measured per floret, using Fiji. Numbers were averaged for each floret.

For SEM imaging, pollen were collected from anthers of GP-fast and *ft1.a* plants and transferred into a 2 ml tube with 1 ml of 1x PBS (pH 7.4). The PBS was discarded, and 1 ml fixative solution (1% Glutaraldehyde, 4% Paraformaldehyde, 0.03% Triton-X100, 1x PBS pH 7.4) was added under the fume hood. A vacuum was applied for 1–2 h at room temperature (RT) until the pollen had sunk to the bottom of the tube. The fixative was discarded and followed by three 15-minute washing steps with 1 ml of 1x PBS. The pollen were dehydrated by incubating them step-by-step in an increasing percentage of ethanol for 30 min each: Pollen were transferred to 10% EtOH first, followed by 20%, 30%, 50%, 70%, 90%, and final 100%. Next, pollen were transferred to a 1:2 hexamethyldisilazane (HMDS) solution in 100% EtOH and incubated for 20 min at RT. Subsequently, pollen were transferred to a 2:1 solution of HMDS in 100% EtOH and incubated for 20 min. Finally, pollen were transferred to 100% HMDS and left overnight in the fume hood to dry. Until imaging, pollen were stored dry. SEM images were taken at the Forschungszentrum Jülich.

Different yield parameters were measured using a MARViN ProLine (MARViTECH GmbH) and an external scale on grains from GP, GP-fast, *ft1.a*, *ft1.b*, and *ft1.c*. Per genotype, five replicates, each containing two grains from three individual plants (thus, six grains in total), were measured with the palea facing upwards. Thousand grain weight (TGW), grain area, length, and width were determined. Two randomly selected grains per genotype were photographed with the palea and with the lemma facing upwards.

RNA sample preparation and RNA Sequencing

GP, GP-fast, *ft1.a*, *ft1.b*, and *ft1.c* plants were sown in QuickPot 96T trays (HerkuPlast Kubern GmbH, pot volume 75 cm³) and transferred to a plant growth chamber after stratification and cultivated under LD conditions as described above.

For RNA Sequencing, plants were sampled at three developmental stages (W2.0, W3.5, and W5.0). Samples were taken at Zeitgeber Time (ZT) 14–15, shortly before the onset of the night when *FT1* and *Ppd-H1* expression was high. Three replicates were obtained for each developmental stage and each tissue. MSAs were collected under a stereo microscope to ensure the correct developmental stage, and the MSA of multiple plants (W2.0: 15 plants, W3.5: 5 plants, W5.0: 4 plants) were pooled for one replicate. Leaves were sampled at the same developmental stages, and the material of two different plants was pooled for one replicate. The middle section of the youngest, fully elongated leaf was sampled, which resulted in some variation in leaf number across the genotypes due to the differences in development (see Supplemental Table S2). Once stem elongation had started (at W3.5 and W5.0), the first internode below the MSA was sampled. For each replicate, the internodes from two plants were pooled. All samples were frozen immediately in liquid nitrogen and stored at -80 °C.

RNA extraction was performed with the RNeasy Plant Mini Kit (QIAGEN) according to the manufacturer's instructions. Remaining DNA was removed using the RNase-Free DNase Set (QIAGEN). The quantity and quality of the RNA was determined with a Nanophotometer (Implen) and on a 1% agarose gel. Paired-end sequencing was performed by Novogene Co, Ltd. using a NovaSeq PE150 platform (Illumina), resulting in 33–69 million reads (5–10.5 Gbp) per sample.

RNA Sequencing analysis

The initial quality control of the raw reads was performed with FastQC and then summarized with MultiQC (version 1.7, Ewels et al., 2016). No trimming of the reads was required. Reads were mapped against the most recent reference transcriptome BaRTv2 (Coulter et al., 2022). Mapping was performed using Salmon (version 1.9.0, Patro et al., 2017), and the mapping rate averaged 90.3% across samples. Genes with at least five counts per million in at least three samples across all genotypes were considered as expressed. Out of a total number of 39434 annotated genes in the BaRT2 transcriptome reference, we identified 17459 (44%), 16930 (43%), and 18508 (47%) genes expressed in MSA, leaf, and stem, respectively. The 3D RNA-seq pipeline was used to calculate Transcripts per million (TPM) to generate PCAs (Guo et al., 2021). The false discovery rate (FDR, BH adjusted) was calculated using the R package *edgeR* (Robinson et al., 2010). The log₂ fold change (log₂FC) was calculated with a pseudo count of 1 and by pairwise comparison of each *ft1* mutant to their respective parent (*ft1.a* and *ft1.b* against GP-fast, *ft1.c* against GP). This was done individually for each tissue

and developmental stage. The raw data, including all FDR values, can be found in Supplemental Datasets S4-S6.

Differentially expressed genes (DEGs) were defined for each tissue as those genes that showed significant differences in expression ($FDR \leq 0.01$ in leaf and MSA, $FDR \leq 0.05$ in stem) in all pairwise comparisons (*ft1.a* vs. GP-fast, *ft1.b* vs. GP-fast and *ft1.c* vs. GP) and a $\log_2FC > 1$ or < -1 in *ft1.a* vs. GP-fast and *ft1.b* vs. GP-fast. No \log_2FC was set for the comparison of *ft1.c* vs. GP. Genes were considered as differentially expressed if they met these criteria in at least one developmental stage.

For additional annotation, a strict one-to-one conversion between BaRTv2 and MorexV3 gene models (Mascher et al., 2021) was created for all BaRTv2 identifiers. First, the longest CDS of each gene model was selected, and the respective datasets were aligned against each other in both directions, using BLASTN (version 2.13.0+), default parameters with "-outfmt 6". The respective outputs were ordered by seqid, bitscore, evalue, and pident. A one-to-one conversion was reported when there was a reciprocal best hit between a gene model in both directions. If there was no one-to-one conversion for the remaining DEGs, they were manually curated from the remaining best-hit alignments in both directions. In addition, the MorexV3 protein sequences (Hv_Morex.pgsb.Jul2020.aa.fa) were aligned with BLASTP (version 2.13.0+) "-outfmt 6 -max_target_seqs 1" against a local BLASTP database of Araport11 (Araport11_pep_20220914_representative_gene_model, Cheng et al., 2017) and the functional annotations were retrieved from Araport11_GFF3_genes_transposons.current.gff (release 2023-01-02 by TAIR).

GO term enrichment was performed using ShinyGO 0.80 (Ge et al., 2020) on DEGs, separated into upregulated and downregulated genes. For this, MorexV3 identifiers were used as input data. Not all BaRTv2 IDs could be annotated with a MorexV3 ID, so the number of genes used for GO term enrichment was reduced by approximately 2-5% as the BaRTv2 annotation is more complete (see Supplemental Table S3 for detailed numbers). The FDR cut-off for the GO term enrichment was set at 0.05. Top GO terms, including fold enrichment and FDR values, can be found in Supplemental Datasets S7 and S8.

Statistical analyses

All statistical tests were performed using R Studio (RStudio Team, 2022). A 2-tailed, unpaired Student's t-test (function *t_test* from the package *rstatix*, v0.7.2) was used to determine the significance between two group means, with a *p*-value cutoff at ≤ 0.05 . Significance between more than two groups was determined using a one-way ANOVA (function *aov*) and a subsequent Tukey test (function *HSD.test* from package *agricolae*, v1.3-5), *p*-value cutoff at ≤ 0.05 . Polynomial regressions (Loess smooth line) were calculated with a 95% confidence interval.

References

- Abe M, Kobayashi Y, Yamamoto S, Daimon Y, Yamaguchi A, Ikeda Y, Ichinoki H, Notaguchi M, Goto K, Araki T** (2005) Fd, a bZIP protein mediating signals from the floral pathway integrator FT at the shoot apex. *Science (New York, N.Y.)*, **309**(5737): 1052–1056.
- Albani MC, Coupland G** (2010) Comparative analysis of flowering in annual and perennial plants. *Current Topics in Developmental Biology*, **91**: 323–348.
- An H, Roussot C, Suárez-López P, Corbesier L, Vincent C, Piñeiro M, Hepworth S, Mouradov A, Justin S, Turnbull C, et al.** (2004) CONSTANS acts in the phloem to regulate a systemic signal that induces photoperiodic flowering of *Arabidopsis*. *Development (Cambridge, England)*, **131**(15): 3615–3626.
- Andrés F, Coupland G** (2012) The genetic basis of flowering responses to seasonal cues. *Nature Reviews. Genetics*, **13**(9): 627–639.
- Balanzà V, Martínez-Fernández I, Sato S, Yanofsky MF, Kaufmann K, Angenent GC, Bemer M, Ferrándiz C** (2018) Genetic control of meristem arrest and life span in *Arabidopsis* by a *FRUITFULL-APETALA2* pathway. *Nature Communications*, **9**(1): 565.
- Bi X, van Esse W, Mulki MA, Kirschner G, Zhong J, Simon R, von Korff M** (2019) *CENTRORADIALIS* Interacts with *FLOWERING LOCUS T*-Like Genes to Control Floret Development and Grain Number. *Plant Physiology*, **180**(2): 1013–1030.
- Bilgin DD, Zavala JA, Zhu J, Clough SJ, Ort DR, DeLucia EH** (2010) Biotic stress globally downregulates photosynthesis genes. *Plant, Cell & Environment*, **33**(10): 1597–1613.
- Bommert P, Nagasawa NS, Jackson D** (2013) Quantitative variation in maize kernel row number is controlled by the *FASCIATED EAR2* locus. *Nature Genetics*, **45**(3): 334–337.
- Brown TA, Jones MK, Powell W, Allaby RG** (2009) The complex origins of domesticated crops in the Fertile Crescent. *Trends in Ecology & Evolution*, **24**(2): 103–109.
- Byrne ME, Barley R, Curtis M, Arroyo JM, Dunham M, Hudson A, Martienssen RA** (2000) *Asymmetric leaves1* mediates leaf patterning and stem cell function in *Arabidopsis*. *Nature*, **408**(6815): 967–971.
- Campoli C, Drosse B, Searle I, Coupland G, von Korff M** (2012a) Functional characterisation of *HvCO1*, the barley (*Hordeum vulgare*) flowering time ortholog of *CONSTANS*. *The Plant Journal : For Cell and Molecular Biology*, **69**(5): 868–880.
- Campoli C, Shtaya M, Davis SJ, von Korff M** (2012b) Expression conservation within the circadian clock of a monocot: Natural variation at barley *Ppd-H1* affects circadian expression of flowering time genes, but not clock orthologs. *BMC Plant Biology*, **12**: 97.
- Chailakhyan M** (1936) New facts in support of the hormonal theory of plant development. *C.R. (Dokl.) Acad. Sci. USSR* **13**: 79–83.

- Chen Q, Payyavula RS, Chen L, Zhang J, Zhang C, Turgeon R** (2018) *Flowering LOCUS T* mRNA is synthesized in specialized companion cells in *Arabidopsis* and Maryland Mammoth tobacco leaf veins. Proceedings of the National Academy of Sciences of the United States of America, **115**(11): 2830–2835.
- Cheng C-Y, Krishnakumar V, Chan AP, Thibaud-Nissen F, Schobel S, Town CD** (2017) Araport11: A complete reannotation of the *Arabidopsis thaliana* reference genome. The Plant Journal, **89**(4): 789–804.
- Coen ES, Meyerowitz EM** (1991) The war of the whorls: Genetic interactions controlling flower development. Nature, **353**(6339): 31–37.
- Corbesier L, Vincent C, Jang S, Fornara F, Fan Q, Searle I, Giakountis A, Farrona S, Gissot L, Turnbull C, et al.** (2007) FT protein movement contributes to long-distance signaling in floral induction of *Arabidopsis*. Science (New York, N.Y.), **316**(5827): 1030–1033.
- Coulter M, Entizne JC, Guo W, Bayer M, Wonneberger R, Milne L, Schreiber M, Haaning A, Muehlbauer GJ, McCallum N, et al.** (2022) BaRTv2: A highly resolved barley reference transcriptome for accurate transcript-specific RNA-seq quantification. The Plant Journal : For Cell and Molecular Biology, **111**(4): 1183–1202.
- Daszkowska-Golec A, Collin A, Sitko K, Janiak A, Kalaji HM, Szarejko I** (2019) Genetic and Physiological Dissection of Photosynthesis in Barley Exposed to Drought Stress. International Journal of Molecular Sciences, **20**(24).
- Debernardi JM, Woods DP, Li K, Li C, Dubcovsky J** (2022) MiR172-*APETALA2*-like genes integrate vernalization and plant age to control flowering time in wheat. PLoS Genetics, **18**(4): e1010157.
- Digel B, Pankin A, von Korff M** (2015) Global Transcriptome Profiling of Developing Leaf and Shoot Apices Reveals Distinct Genetic and Environmental Control of Floral Transition and Inflorescence Development in Barley. The Plant Cell, **27**(9): 2318–2334.
- Doebley J** (2004) The genetics of maize evolution. Annual Review of Genetics, **38**: 37–59.
- Ejaz M, von Korff M** (2017) The Genetic Control of Reproductive Development under High Ambient Temperature. Plant Physiology, **173**(1): 294–306.
- Ewels P, Magnusson M, Lundin S, Källér M** (2016) MultiQC: Summarize analysis results for multiple tools and samples in a single report. Bioinformatics (Oxford, England), **32**(19): 3047–3048.
- Faure S, Higgins J, Turner A, Laurie DA** (2007) The *FLOWERING LOCUS T*-like gene family in barley (*Hordeum vulgare*). Genetics, **176**(1): 599–609.
- Fernández-Calleja M, Casas AM, Igartua E** (2021) Major flowering time genes of barley: Allelic diversity, effects, and comparison with wheat. Theoretical and Applied Genetics, **134**(7): 1867–1897.
- Fichtner F, Lunn JE** (2021) The Role of Trehalose 6-Phosphate (Tre6P) in Plant Metabolism and Development. Annual Review of Plant Biology, **72**: 737–760.

- Fornara F, Marziani G, Mizzi L, Kater M, Colombo L** (2003) MADS-Box Genes Controlling Flower Development in Rice. *Plant Biology*, **5**(1): 16–22.
- Ge SX, Jung D, Yao R** (2020) Shinygo: A graphical gene-set enrichment tool for animals and plants. *Bioinformatics* (Oxford, England), **36**(8): 2628–2629.
- Gol L, Haraldsson EB, von Korff M** (2021) *Ppd-H1* integrates drought stress signals to control spike development and flowering time in barley. *Journal of Experimental Botany*, **72**(1): 122–136.
- González-Suárez P, Walker CH, Bennett T** (2023) *FLOWERING LOCUS T* mediates photo-thermal timing of inflorescence meristem arrest in *Arabidopsis thaliana*. *Plant Physiology*, **192**(3): 2276–2289.
- Guo W, Tzioutziou NA, Stephen G, Milne I, Calixto CP, Waugh R, Brown JWS, Zhang R** (2021) 3D RNA-seq: A powerful and flexible tool for rapid and accurate differential expression and alternative splicing analysis of RNA-seq data for biologists. *RNA Biology*, **18**(11): 1574–1587.
- Haas M, Schreiber M, Mascher M** (2019) Domestication and crop evolution of wheat and barley: Genes, genomics, and future directions. *Journal of Integrative Plant Biology*, **61**(3): 204–225.
- Halliwel J, Borrill P, Gordon A, Kowalczyk R, Pagano ML, Saccomanno B, Bentley AR, Uauy C, Cockram J** (2016) Systematic Investigation of *FLOWERING LOCUS T*-Like Poaceae Gene Families Identifies the Short-Day Expressed Flowering Pathway Gene, *TaFT3* in Wheat (*Triticum aestivum* L.). *Frontiers in Plant Science*, **7**: 857.
- Hartmann U, Höhmann S, Nettesheim K, Wisman E, Saedler H, Huijser P** (2000) Molecular cloning of SVP: A negative regulator of the floral transition in *Arabidopsis*. *The Plant Journal : For Cell and Molecular Biology*, **21**(4): 351–360.
- Hayama R, Sarid-Krebs L, Richter R, Fernández V, Jang S, Coupland G** (2017) Pseudo RESPONSE REGULATORS stabilize CONSTANS protein to promote flowering in response to day length. *The EMBO Journal*, **36**(7): 904–918.
- Higo A, Saihara N, Miura F, Higashi Y, Yamada M, Tamaki S, Ito T, Tarutani Y, Sakamoto T, Fujiwara M, et al.** (2020) DNA methylation is reconfigured at the onset of reproduction in rice shoot apical meristem. *Nature Communications*, **11**(1): 4079.
- Huang C-K, Lo P-C, Huang L-F, Wu S-J, Yeh C-H, Lu C-A** (2015) A single-repeat MYB transcription repressor, MYBH, participates in regulation of leaf senescence in *Arabidopsis*. *Plant Molecular Biology*, **88**(3): 269–286.
- Jang S, Marchal V, Panigrahi KCS, Wenkel S, Soppe W, Deng X-W, Valverde F, Coupland G** (2008) *Arabidopsis* COP1 shapes the temporal pattern of CO accumulation conferring a photoperiodic flowering response. *The EMBO Journal*, **27**(8): 1277–1288.
- Jeandet P, Formela-Luboińska M, Labudda M, Morkunas I** (2022) The Role of Sugars in Plant Responses to Stress and Their Regulatory Function during Development. *International Journal of Molecular Sciences*, **23**(9).

- John S, Apelt F, Kumar A, Acosta IF, Bents D, Annunziata MG, Fichtner F, Gutjahr C, Mueller-Roeber B, Olas JJ (2023)** Transcription factor HSFA7b controls thermomemory at the shoot apical meristem by regulating ethylene biosynthesis and signaling in *Arabidopsis*. *Plant Communications*: 100743.
- Jones H, Leigh FJ, Mackay I, Bower MA, Smith LMJ, Charles MP, Jones G, Jones MK, Brown TA, Powell W (2008)** Population-based resequencing reveals that the flowering time adaptation of cultivated barley originated east of the Fertile Crescent. *Molecular Biology and Evolution*, **25**(10): 2211–2219.
- Kardailsky I, Shukla VK, Ahn JH, Dagenais N, Christensen SK, Nguyen JT, Chory J, Harrison MJ, Weigel D (1999)** Activation tagging of the floral inducer *FT*. *Science (New York, N.Y.)*, **286**(5446): 1962–1965.
- Kikuchi R, Kawahigashi H, Ando T, Tonooka T, Handa H (2009)** Molecular and functional characterization of PEBP genes in barley reveal the diversification of their roles in flowering. *Plant Physiology*, **149**(3): 1341–1353.
- Kinoshita T, Ono N, Hayashi Y, Morimoto S, Nakamura S, Soda M, Kato Y, Ohnishi M, Nakano T, Inoue S, et al. (2011)** *FLOWERING LOCUS T* regulates stomatal opening. *Current Biology : CB*, **21**(14): 1232–1238.
- Kojima S, Takahashi Y, Kobayashi Y, Monna L, Sasaki T, Araki T, Yano M (2002)** *Hd3a*, a rice ortholog of the *Arabidopsis FT* gene, promotes transition to flowering downstream of *Hd1* under short-day conditions. *Plant & Cell Physiology*, **43**(10): 1096–1105.
- Kong X, Wang F, Geng S, Guan J, Tao S, Jia M, Sun G, Wang Z, Wang K, Ye X, et al. (2022)** The wheat *AGL6*-like MADS-box gene is a master regulator for floral organ identity and a target for spikelet meristem development manipulation. *Plant Biotechnology Journal*, **20**(1): 75–88.
- Koornneef M, Hanhart CJ, van der Veen JH (1991)** A genetic and physiological analysis of late flowering mutants in *Arabidopsis thaliana*. *Molecular & General Genetics : MGG*, **229**(1): 57–66.
- Krieger U, Lippman ZB, Zamir D (2010)** The flowering gene *SINGLE FLOWER TRUSS* drives heterosis for yield in tomato. *Nature Genetics*, **42**(5): 459–463.
- Kuijter HN, Shirley NJ, Khor SF, Shi J, Schwerdt J, Zhang D, Li G, Burton RA (2021)** Transcript Profiling of MIKCC MADS-Box Genes Reveals Conserved and Novel Roles in Barley Inflorescence Development. *Frontiers in Plant Science*, **12**: 705286.
- Laurie DA, Pratchett N, Snape JW, Bezant JH (1995)** RFLP mapping of five major genes and eight quantitative trait loci controlling flowering time in a winter × spring barley (*Hordeum vulgare L.*) cross. *Genome*, **38**(3): 575–585.
- Li C, Dubcovsky J (2008)** Wheat FT protein regulates *VRN1* transcription through interactions with FDL2. *The Plant Journal : For Cell and Molecular Biology*, **55**(4): 543–554.
- Li C, Lin H, Dubcovsky J (2015a)** Factorial combinations of protein interactions generate a multiplicity of florigen activation complexes in wheat and barley. *The Plant Journal*, **84**(1): 70–82.

- Li C, Zhang Y, Zhang K, Guo D, Cui B, Wang X, Huang X** (2015b) Promoting flowering, lateral shoot outgrowth, leaf development, and flower abscission in tobacco plants overexpressing cotton *FLOWERING LOCUS T (FT)*-like gene *GhFT1*. *Frontiers in Plant Science*, **6**: 454.
- Li G, Kuijter HNJ, Yang X, Liu H, Shen C, Shi J, Betts N, Tucker MR, Liang W, Waugh R, et al.** (2021) *MADS1* maintains barley spike morphology at high ambient temperatures. *Nature Plants*, **7**(8): 1093–1107.
- Lifschitz E, Eviatar T, Rozman A, Shalit A, Goldshmidt A, Amsellem Z, Alvarez JP, Eshed Y** (2006) The tomato *FT* ortholog triggers systemic signals that regulate growth and flowering and substitute for diverse environmental stimuli. *Proceedings of the National Academy of Sciences of the United States of America*, **103**(16): 6398–6403.
- Lu D, Wang T, Persson S, Mueller-Roeber B, Schippers JHM** (2014) Transcriptional control of ROS homeostasis by *KUODA1* regulates cell expansion during leaf development. *Nature Communications*, **5**: 3767.
- Lv B, Nitcher R, Han X, Wang S, Ni F, Li K, Pearce S, Wu J, Dubcovsky J, Fu D** (2014) Characterization of *FLOWERING LOCUS T1 (FT1)* gene in *Brachypodium* and wheat. *PloS One*, **9**(4): e94171.
- Mascher M, Wicker T, Jenkins J, Plott C, Lux T, Koh CS, Ens J, Gundlach H, Boston LB, Tulpová Z, et al.** (2021) Long-read sequence assembly: A technical evaluation in barley. *The Plant Cell*, **33**(6): 1888–1906.
- McClung CR** (2021) Circadian Clock Components Offer Targets for Crop Domestication and Improvement. *Genes*, **12**(3).
- Melzer S, Lens F, Gennen J, Vanneste S, Rohde A, Beeckman T** (2008) Flowering-time genes modulate meristem determinacy and growth form in *Arabidopsis thaliana*. *Nature Genetics*, **40**(12): 1489–1492.
- Mengin V, Pyl E-T, Alexandre Moraes T, Sulpice R, Krohn N, Encke B, Stitt M** (2017) Photosynthate partitioning to starch in *Arabidopsis thaliana* is insensitive to light intensity but sensitive to photoperiod due to a restriction on growth in the light in short photoperiods. *Plant, Cell & Environment*, **40**(11): 2608–2627.
- Mikołajczak K, Kuczyńska A, Krajewski P, Kempa M, Nuc M** (2022) Transcriptome profiling disclosed the effect of single and combined drought and heat stress on reprogramming of genes expression in barley flag leaf. *Frontiers in Plant Science*, **13**: 1096685.
- Miryeganeh M, Yamaguchi M, Kudoh H** (2018) Synchronisation of *Arabidopsis* flowering time and whole-plant senescence in seasonal environments. *Scientific Reports*, **8**(1): 10282.
- Miryeganeh M** (2021) Plants' Epigenetic Mechanisms and Abiotic Stress. *Genes*, **12**(8).
- Muggeo VMR** (2003) Estimating regression models with unknown break-points. *Statistics in Medicine*, **22**(19): 3055–3071.
- Muggeo VMR** (2008) segmented: An R Package to Fit Regression Models with Broken-Line Relationships. *R News*. (8/1): 20–25.

- Mulki MA, Bi X, von Korff M** (2018) *Flowering LOCUS T3* Controls Spikelet Initiation But Not Floral Development. *Plant Physiology*, **178**(3): 1170–1186.
- Navarro C, Abelenda JA, Cruz-Oró E, Cuéllar CA, Tamaki S, Silva J, Shimamoto K, Prat S** (2011) Control of flowering and storage organ formation in potato by *FLOWERING LOCUS T*. *Nature*, **478**(7367): 119–122.
- Patro R, Duggal G, Love MI, Irizarry RA, Kingsford C** (2017) Salmon provides fast and bias-aware quantification of transcript expression. *Nature Methods*, **14**(4): 417–419.
- Peng FY, Hu Z, Yang R-C** (2015) Genome-Wide Comparative Analysis of Flowering-Related Genes in Arabidopsis, Wheat, and Barley. *International Journal of Plant Genomics*, **2015**: 874361.
- Perrella G, Bäurle I, van Zanten M** (2022) Epigenetic regulation of thermomorphogenesis and heat stress tolerance. *The New Phytologist*, **234**(4): 1144–1160.
- Peterson R, Slovin JP, Chen C** (2010) A simplified method for differential staining of aborted and non-aborted pollen grains. *International Journal of Plant Biology*, **1**(2): 13.
- Pieper R, Tomé F, Pankin A, von Korff M** (2021) *FLOWERING LOCUS T4* delays flowering and decreases floret fertility in barley. *Journal of Experimental Botany*, **72**(1): 107–121.
- Pin PA, Nilsson O** (2012) The multifaceted roles of *FLOWERING LOCUS T* in plant development. *Plant, Cell & Environment*, **35**(10): 1742–1755.
- Quiroz S, Yustis JC, Chávez-Hernández EC, Martínez T, La Sanchez MdP, Garay-Arroyo A, Álvarez-Buylla ER, García-Ponce B** (2021) Beyond the Genetic Pathways, Flowering Regulation Complexity in Arabidopsis thaliana. *International Journal of Molecular Sciences*, **22**(11).
- Rhodes J, Roman A-O, Bjornson M, Brandt B, Derbyshire P, Wyler M, Schmid MW, Menke FLH, Santiago J, Zipfel C** (2022) Perception of a conserved family of plant signalling peptides by the receptor kinase HSL3. *ELife*, **11**.
- Robinson MD, McCarthy DJ, Smyth GK** (2010) edgeR: A Bioconductor package for differential expression analysis of digital gene expression data. *Bioinformatics* (Oxford, England), **26**(1): 139–140.
- Rodriguez MCS, Petersen M, Mundy J** (2010) Mitogen-activated protein kinase signaling in plants. *Annual Review of Plant Biology*, **61**: 621–649.
- RStudio Team** (2022). RStudio: Integrated Development for R. RStudio [Computer software]. Boston, MA: PBC: PBC. Retrieved from <http://www.rstudio.com/>.
- Samach A, Onouchi H, Gold SE, Ditta GS, Schwarz-Sommer Z, Yanofsky MF, Coupland G** (2000) Distinct roles of *CONSTANS* target genes in reproductive development of *Arabidopsis*. *Science* (New York, N.Y.), **288**(5471): 1613–1616.
- Sang T** (2009) Genes and mutations underlying domestication transitions in grasses. *Plant Physiology*, **149**(1): 63–70.

- Sawa M, Nusinow DA, Kay SA, Imaizumi T** (2007) FKF1 and GIGANTEA complex formation is required for day-length measurement in *Arabidopsis*. *Science*, **318**(5848): 261–265.
- Schindelin J, Arganda-Carreras I, Frise E, Kaynig V, Longair M, Pietzsch T, Preibisch S, Rueden C, Saalfeld S, Schmid B, et al.** (2012) Fiji: An open-source platform for biological-image analysis. *Nature Methods*, **9**(7): 676–682.
- Shalit A, Rozman A, Goldshmidt A, Alvarez JP, Bowman JL, Eshed Y, Lifschitz E** (2009) The flowering hormone florigen functions as a general systemic regulator of growth and termination. *Proceedings of the National Academy of Sciences of the United States of America*, **106**(20): 8392–8397.
- Shannon S, Meeks-Wagner DR** (1991) A Mutation in the *Arabidopsis TFL1* Gene Affects Inflorescence Meristem Development. *The Plant Cell*, **3**(9): 877.
- Shaw LM, Li C, Woods DP, Alvarez MA, Lin H, Lau MY, Chen A, Dubcovsky J** (2020) Epistatic interactions between *PHOTOPERIOD1*, *CONSTANS1* and *CONSTANS2* modulate the photoperiodic response in wheat. *PLoS Genetics*, **16**(7): e1008812.
- Shaw LM, Lyu B, Turner R, Li C, Chen F, Han X, Fu D, Dubcovsky J** (2019) *Flowering LOCUS T2* regulates spike development and fertility in temperate cereals. *Journal of Experimental Botany*, **70**(1): 193–204.
- Shaw LM, Turner AS, Herry L, Griffiths S, Laurie DA** (2013) Mutant alleles of *Photoperiod-1* in wheat (*Triticum aestivum* L.) that confer a late flowering phenotype in long days. *PLoS One*, **8**(11): e79459.
- Sievers F, Wilm A, Dineen D, Gibson TJ, Karplus K, Li W, Lopez R, McWilliam H, Remmert M, Söding J, et al.** (2011) Fast, scalable generation of high-quality protein multiple sequence alignments using Clustal Omega. *Molecular Systems Biology*, **7**: 539.
- Tamaki S, Matsuo S, Wong HL, Yokoi S, Shimamoto K** (2007) Hd3a protein is a mobile flowering signal in rice. *Science (New York, N.Y.)*, **316**(5827): 1033–1036.
- Tamura K, Stecher G, Kumar S** (2021) MEGA11: Molecular Evolutionary Genetics Analysis Version 11. *Molecular Biology and Evolution*, **38**(7): 3022–3027.
- Taoka K, Ohki I, Tsuji H, Furuita K, Hayashi K, Yanase T, Yamaguchi M, Nakashima C, Purwestri YA, Tamaki S, et al.** (2011) 14-3-3 proteins act as intracellular receptors for rice Hd3a florigen. *Nature*, **476**(7360): 332–335.
- Thirulogachandar V, Schnurbusch T** (2021) ‘spikelet stop’ determines the maximum yield potential stage in barley. *Journal of Experimental Botany*, **72**(22): 7743–7753.
- Trevaskis B, Tadege M, Hemming MN, Peacock WJ, Dennis ES, Sheldon C** (2007) *Short Vegetative Phase-Like* MADS-Box Genes Inhibit Floral Meristem Identity in Barley. *Plant Physiology*, **143**(1): 225–235.
- Turner A, Beales J, Faure S, Dunford RP, Laurie DA** (2005) The pseudo-response regulator *Ppd-H1* provides adaptation to photoperiod in barley. *Science (New York, N.Y.)*, **310**(5750): 1031–1034.

- Valverde F, Mouradov A, Soppe W, Ravenscroft D, Samach A, Coupland G** (2004) Photoreceptor regulation of CONSTANS protein in photoperiodic flowering. *Science*, **303**(5660): 1003–1006.
- Vinje MA, Willis DK, Duke SH, Henson CA** (2011) Differential expression of two β -amylase genes (*Bmy1* and *Bmy2*) in developing and mature barley grain. *Planta*, **233**(5): 1001–1010.
- Waddington SR, Cartwright PM, Wall PC** (1983) A Quantitative Scale of Spike Initial and Pistil Development in Barley and Wheat. *Annals of Botany*, **51**(1): 119–130.
- Wahl V, Ponnu J, Schlereth A, Arrivault S, Langenecker T, Franke A, Feil R, Lunn JE, Stitt M, Schmid M** (2013) Regulation of flowering by Trehalose-6-Phosphate signaling in *Arabidopsis thaliana*. *Science*, **339**(6120): 704–707.
- Wang B, Smith SM, Li J** (2018) Genetic Regulation of Shoot Architecture. *Annual Review of Plant Biology*, **69**: 437–468.
- Wigge PA, Kim MC, Jaeger KE, Busch W, Schmid M, Lohmann JU, Weigel D** (2005) Integration of spatial and temporal information during floral induction in *Arabidopsis*. *Science (New York, N.Y.)*, **309**(5737): 1056–1059.
- Wu J, Wu Q, Bo Z, Zhu X, Zhang J, Li Q, Kong W** (2022) Comprehensive Effects of *Flowering Locus T*-Mediated Stem Growth in Tobacco. *Frontiers in Plant Science*, **13**: 922919.
- Yan L, Fu D, Li C, Blechl A, Tranquilli G, Bonafede M, Sanchez A, Valarik M, Yasuda S, Dubcovsky J** (2006) The wheat and barley vernalization gene *VRN3* is an orthologue of *FT*. *Proceedings of the National Academy of Sciences of the United States of America*, **103**(51): 19581–19586.
- Yasui Y, Tanaka W, Sakamoto T, Kurata T, Hirano H-Y** (2017) Genetic Enhancer Analysis Reveals that *FLORAL ORGAN NUMBER2* and *OsmADS3* Co-operatively Regulate Maintenance and Determinacy of the Flower Meristem in Rice. *Plant & Cell Physiology*, **58**(5): 893–903.
- You Y, Sawikowska A, Neumann M, Posé D, Capovilla G, Langenecker T, Neher RA, Krajewski P, Schmid M** (2017) Temporal dynamics of gene expression and histone marks at the *Arabidopsis* shoot meristem during flowering. *Nature Communications*, **8**: 15120.
- Zadoks JC, Chang TT, Konzak CF** (1974) A decimal code for the growth stages of cereals. *Weed Research*, **14**(6): 415–421.
- Zhang M, Hu X, Zhu M, Xu M, Wang L** (2017) Transcription factors NF-YA2 and NF-YA10 regulate leaf growth via auxin signaling in *Arabidopsis*. *Scientific Reports*, **7**(1): 1395.

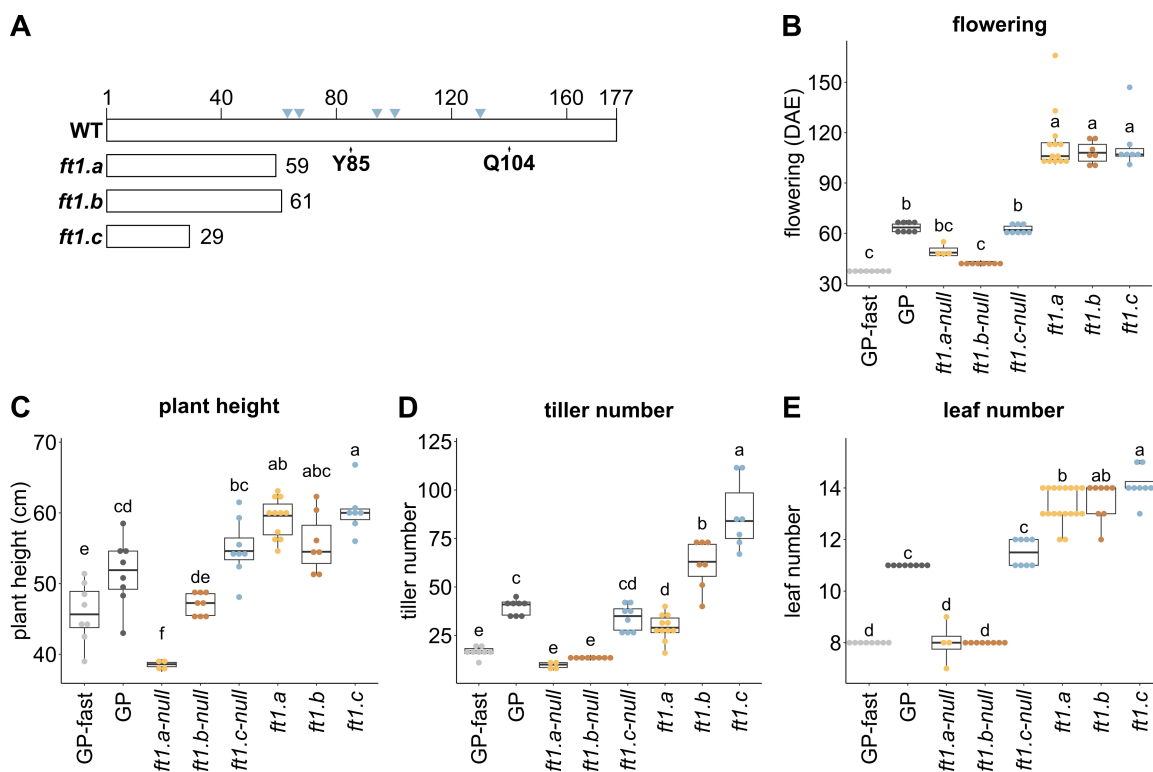


Figure 1. Phenotype of *ft1* mutants. **A** Schematic overview of the FT1 protein sequence in *ft1.a*, *ft1.b*, and *ft1.c* compared to wild-type (WT). Residues Y85 and Q104, important for flowering-activating function, are marked (Hanzawa et al., 2005; Ahn et al., 2006). Blue triangles indicate the amino acid residues R62, T66, P94, F101, and R130, critical for FT-14-3-3 interactions in wheat and rice (Taoka et al. 2011; Li et al. 2015). The numbers on the right indicate the protein length of the mutated FT1 proteins. **B-E** GP-fast, GP, *ft1* mutants, and respective null segregant lines *ft1.a-null*, *ft1.b-null*, and *ft1.c-null* were grown under controlled long-day (LD) conditions in 1.5 L pots and different traits related to the development and plant architecture were scored at heading (B, C, D) or the end of stem elongation (E). **B** Flowering was scored in days after emergence (DAE) as tipping of the awns on the main culm of the plants, or in case it did not mature fully, the first tiller tipping. **C, D** Plant height (from soil to flag leaf ligule) and tiller number were scored when plants flowered. **E** Leaf number was counted at the end of stem elongation on the main culm. At least four (null segregant lines) or eight (*ft1* lines) different plants were scored for each genotype. Significance levels were determined by one-way ANOVA and subsequent Tukey's test ($p \leq 0.05$), $n = 4-13$ plants.

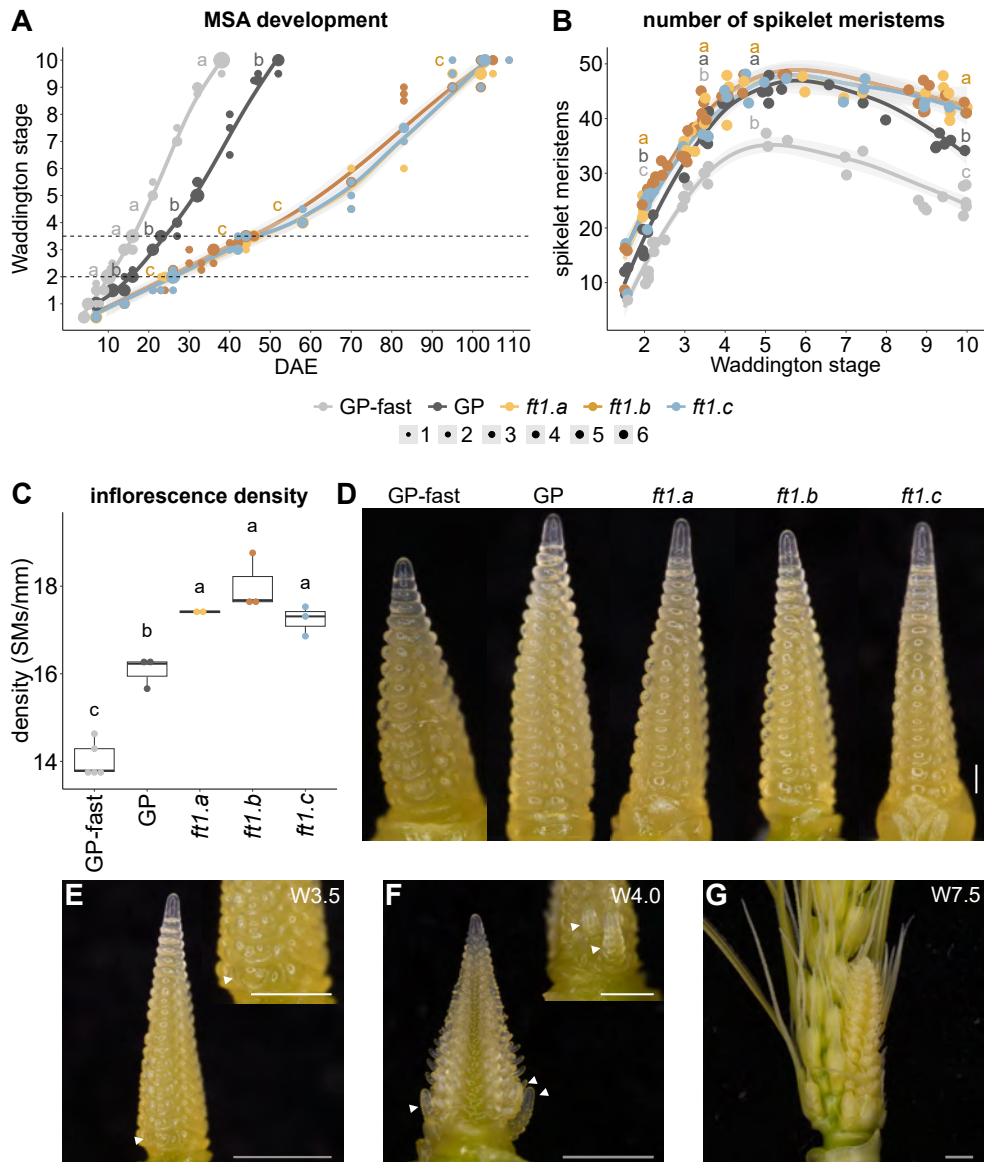


Figure 2. Effects of *FT1* on reproductive development. **A-D** The main shoot apex (MSA) development was monitored from 4 days after emergence (DAE) to flowering on the main culm of GP-fast, GP, and *ft1* mutants. Plants were grown under controlled long-day (LD) conditions in 75 cm³ pots, and 3-4 plants were dissected per genotype and time point. **A** Development of the MSA according to the scale by Waddington et al. (1983). Dot sizes indicate the number of plants per data point (1-6), and grey areas show the 95% confidence interval of a polynomial regression (Loess smooth line). The dotted lines indicate the transition from vegetative to reproductive growth (W2.0) and early to late reproductive development (W3.5). **B** Number of spikelet meristems (SM) on the MSA. Significance levels in (A) and (B) were determined by one-way ANOVA and subsequent Tukey's test ($p \leq 0.05$, $n = 2-15$) at developmental stages W2.0, W3.5, W4.5/W5.0, and W10.0. Values from W4.5 and W5.0 were combined. Values from mutants were combined and compared against GP-fast and GP. The colors of the characters indicate the respective group (light grey: GP-fast, dark grey: GP, orange: mutants). **C** Inflorescence density at W3.0. The density was calculated by dividing the number of SMs by inflorescence size. Significance levels were determined by one-way ANOVA and subsequent Tukey's test ($p \leq 0.05$, $n = 2-4$ plants). **D** Representative images of GP-fast, GP, and *ft1* mutant MSAs at Waddington stage W3.0; scale equals 100 μ m. **E-G** Inflorescences of *ft1.a* plants from reproductive (W3.5 and W4.5) to floral development (W7.5). White arrows indicate secondary inflorescences at the base of the primary inflorescence. Small and big images of each panel show the same MSA from a different angle. White scale bars equal 500 μ m, grey scale bars 1000 μ m.

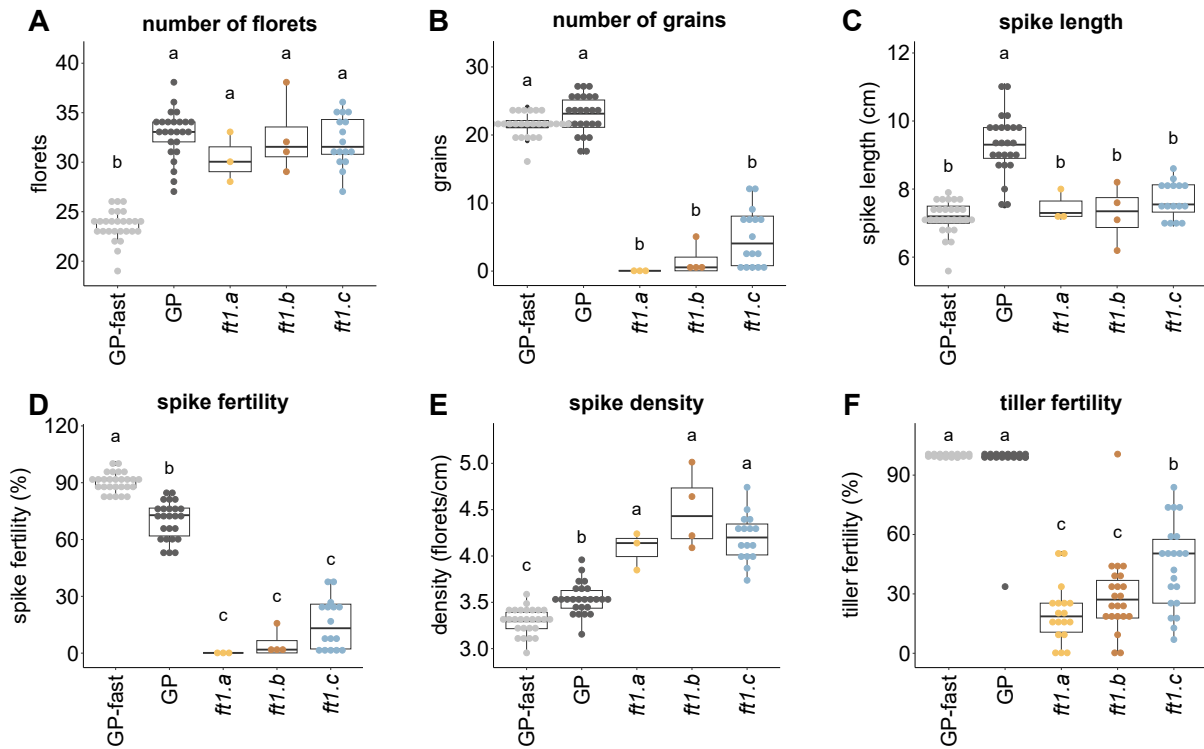


Figure 3: Reproductive traits in *ft1* plants. GP-fast, GP, and *ft1* mutants were grown under controlled long-day (LD) conditions in 75 cm³ pots. Floret number (A), grain number (B), and spike length (C) were scored on the main culm. Spike fertility (D) was calculated by dividing the number of grains by the number of florets and spike density (E) by dividing the number of florets by spike length (in cm). Tiller fertility (F) was determined by dividing the number of tillers with a spike that holds at least one seed by the final tiller number. Significance levels were determined by one-way ANOVA and subsequent Tukey's test ($p \leq 0.05$, $n = 3-27$).

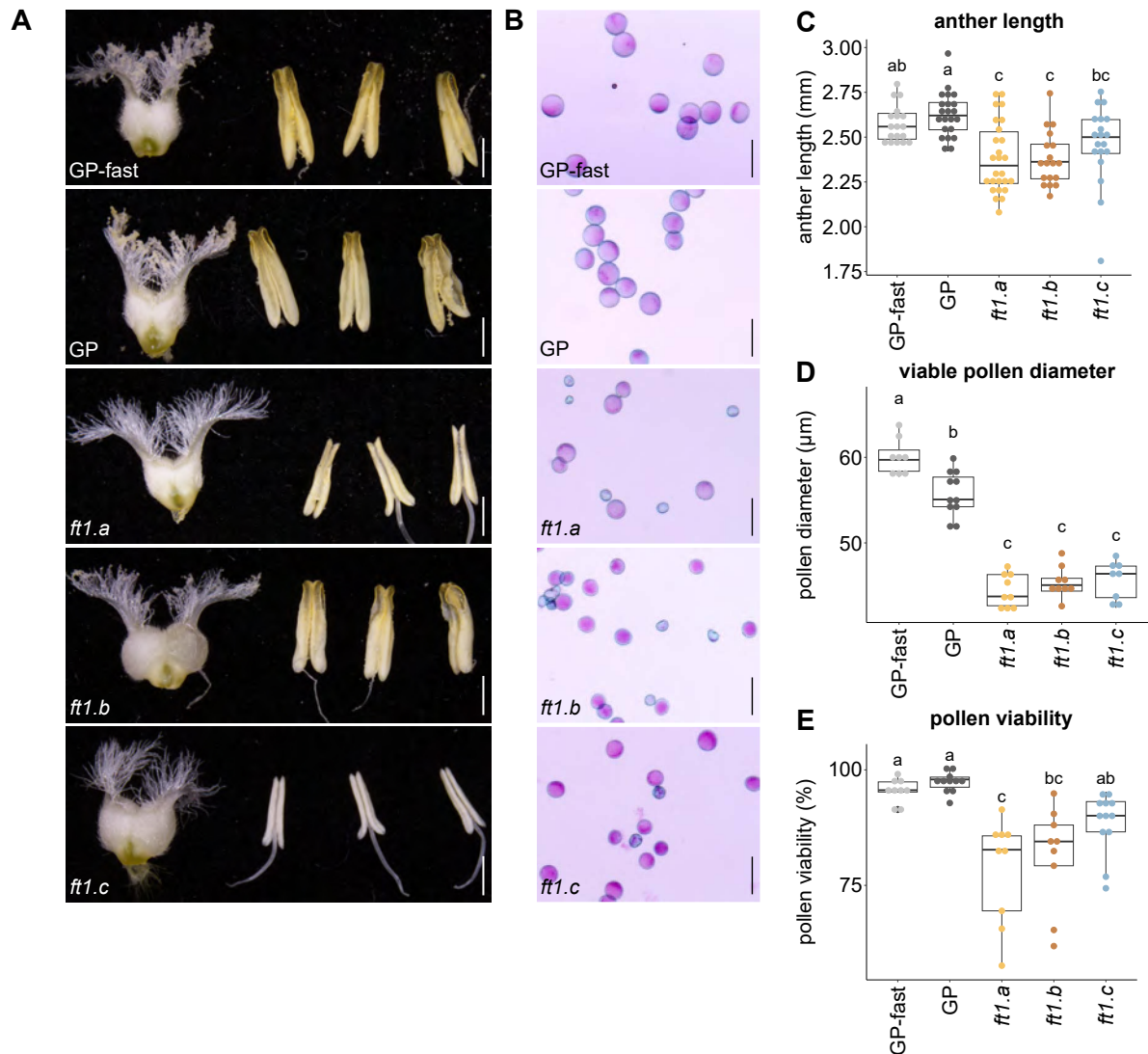


Figure 4: *FT1* affects pollen fertility. GP-fast, GP, and *ft1* mutants were grown under controlled long-day (LD) conditions in 75 cm³ pots. **A** Representative images of GP-fast, GP, *ft1.a*, *ft1.b*, and *ft1.c* ovules and anthers; scales equal 1000 μm . **B** Representative images of stained pollen from the same genotypes; scales equal 100 μm . **C** Anther length (in mm) was determined by measuring the length of anthers from 6 central florets, each from 3-4 plants per genotype. **D** Pollen diameter (in μm) was determined by measuring the diameter of 10 viable (stained purple) pollen from 2-3 central florets of 3-4 plants per genotype. Values were averaged for each floret. **E** Pollen viability (in %) was determined by counting viable and non-viable pollen from 2-3 central florets of 3-4 plants per genotype. Values were averaged for each floret. Significance levels were determined by one-way ANOVA and subsequent Tukey's test ($p \leq 0.05$, $n = 8-23$).

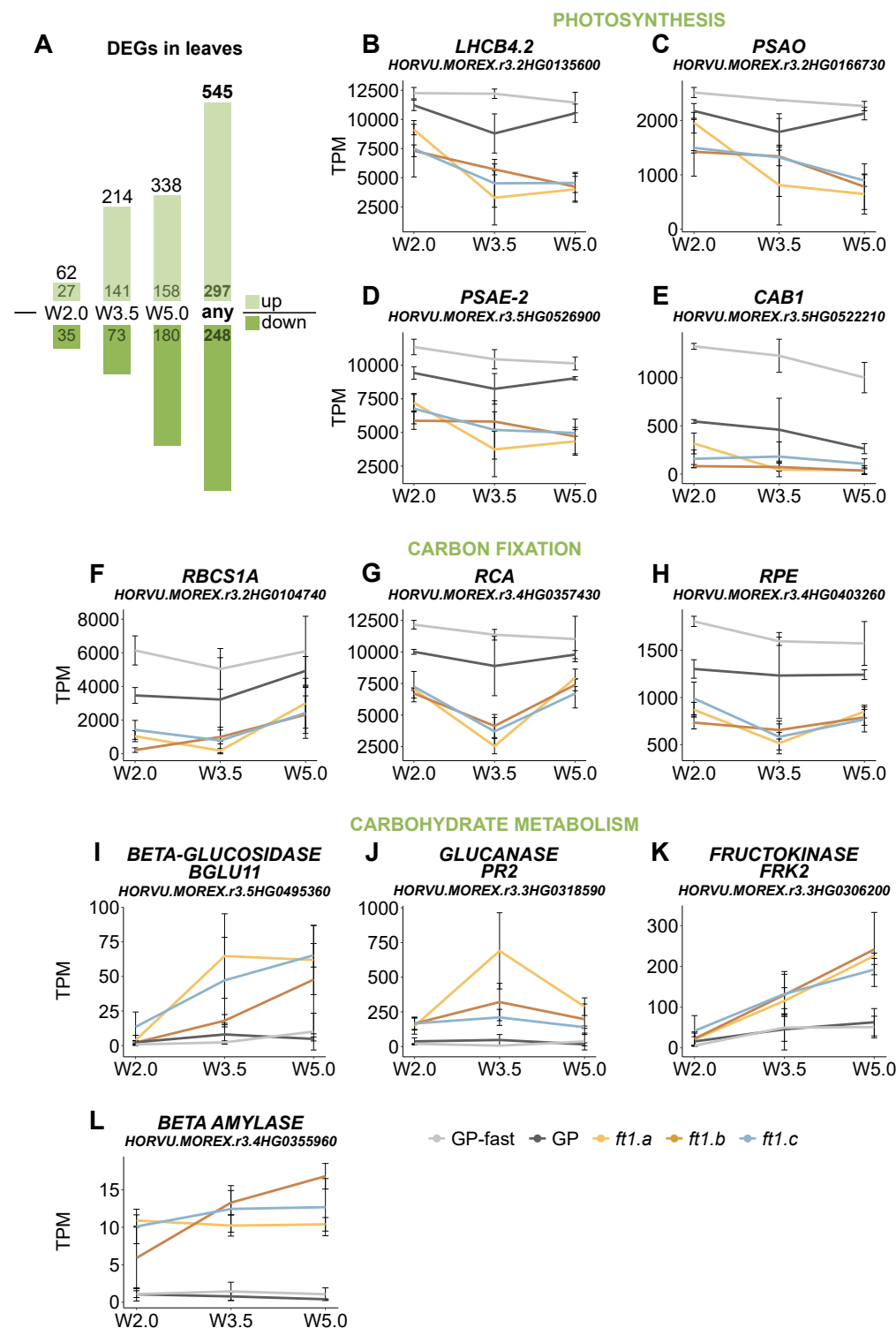


Figure 5. Differential gene expression in leaves. **A** The number of differentially expressed genes (DEGs). Shown are the overlap of DEGs in *ft1.a* and *ft1.b* compared to GP-fast and *ft1.c* compared to GP. DEGs are either counted separately by developmental stage (W2.0, W3.5, W5.0) or combined as DEGs at any of these stages (“any”). The latter are considered as the core set of 545 DEGs. Numbers are separated into upregulated (light green) and downregulated (dark green) genes. The numbers on top equal the total number of genes for each stage. **B-L** Gene expression in GP-fast (light grey), GP (dark grey), *ft1.a* (yellow), *ft1.b* (orange), and *ft1.c* (blue). Expression patterns of exemplary genes are shown in transcripts per million (TPM) by developmental stage. Shown are genes related to photosynthesis (**B-E**), carbon fixation (**F-H**), and carbohydrate metabolism (**I-L**). Each value represents the mean of three independent biological replicates; error bars indicate the standard deviation of the mean.

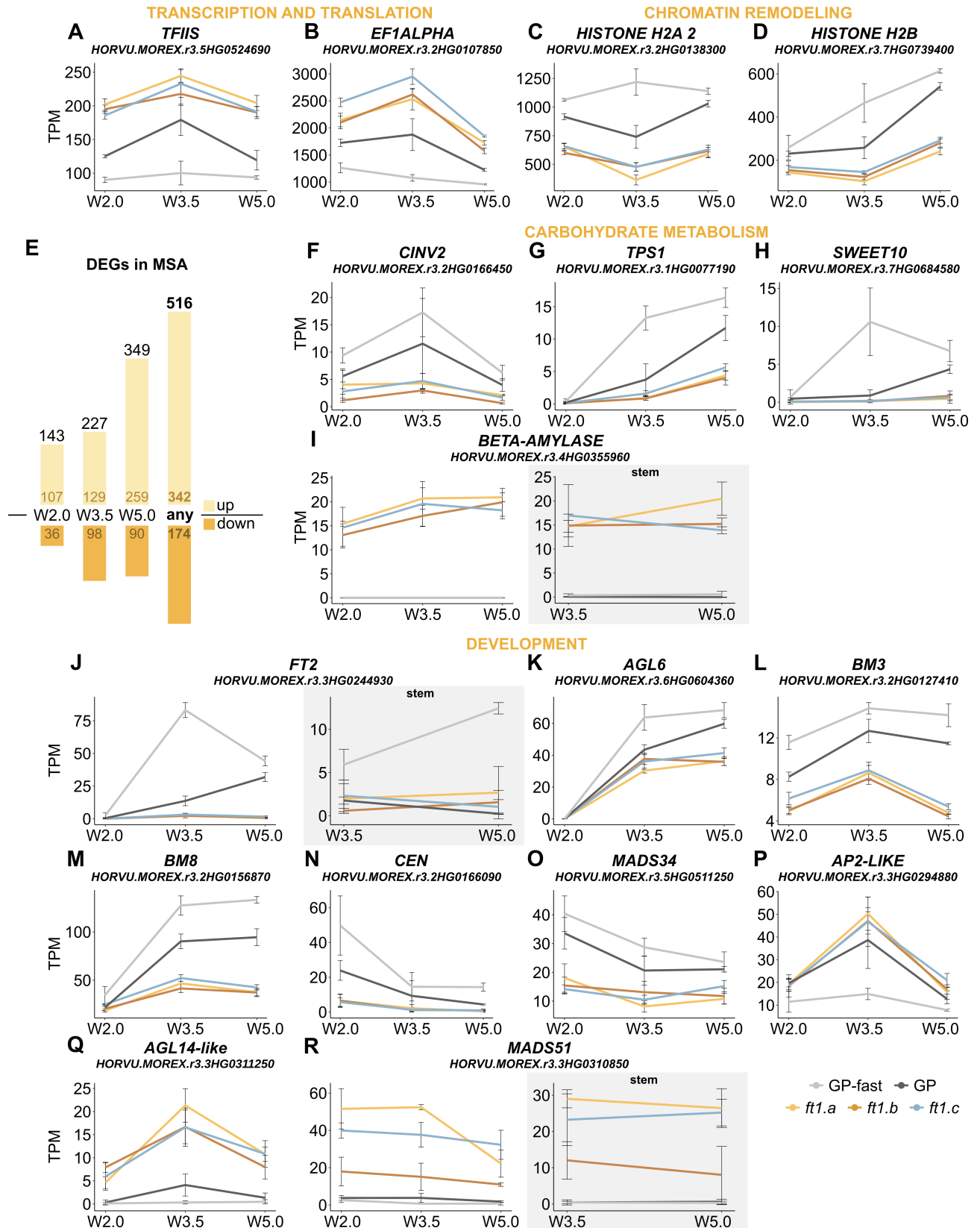


Figure 6. Differentially expressed genes in the MSA. A-D, F-R: Gene expression in GP-fast, GP and *ft1* mutants in the main shoot apex (MSA). Expression patterns of exemplary genes are shown in transcripts per million (TPM) by developmental stage. Shown are genes related to transcription and translation (A-B), chromatin remodeling (C-D), carbohydrate metabolism (F-I), and development (J-R). The expression of *BETA-AMYLASE* (I), *FT2* (J), and *MADS51* (R) are shown also for stem tissue (grey boxes). Each value represents the mean of three independent biological replicates; error bars indicate the standard deviation of the mean. E The number of differentially expressed genes (DEGs). Shown are the overlap of DEGs in *ft1.a* and *ft1.b* compared to GP-fast and *ft1.c* compared to GP. DEGs are either counted separately by developmental stage (W2.0, W3.5, W5.0) or combined as DEGs at any of these stages (“any”). The latter are considered as the core set of 516 DEGs. Numbers are separated into upregulated (light orange) and downregulated (dark orange) genes. The numbers on top equal the total number of genes for each stage.

FLOWERING LOCUS T1 is a pleiotropic regulator of reproductive development, plant architecture, and source-sink relations in barley

A

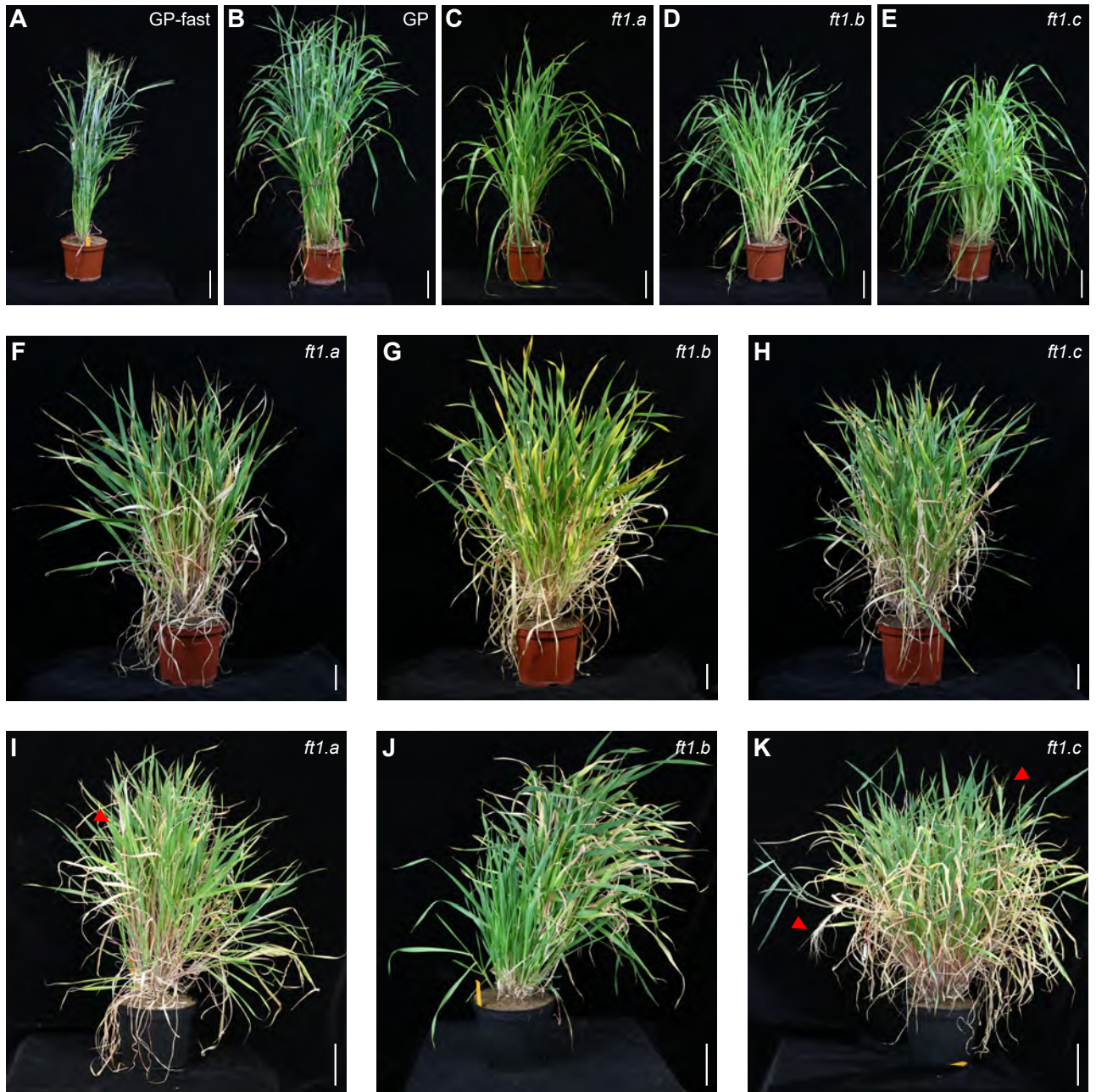
WT	ATGGCCGGGAGGGACAGGGATCCGCTGGTTGTCGGCAGGGTTGTGGGGGACGTGCTGGAC	60
<i>ft1.a</i>	ATGGCCGGGAGGGACAGGGATCCGCTGGTTGTCGGCAGGGTTGTGGGGGACGTGCTGGAC	60
<i>ft1.b</i>	ATGGCCGGGAGGGACAGGGATCCGCTGGTTGTCGGCAGGGTTGTGGGGGACGTGCTGGAC	60
<i>ft1.c</i>	ATGGCCGGGAGGGACAGGGATCCGCTGGTTGTCGGCAGGGTTGTGGGGGACGTGCTGGAC	60
	***** gRNA PAM	
WT	CCCTTCGTCCGAACCACCAACCTCAGGGT GACCTTCGGGAACAGGGCCGTGTC-CAACCGG	119
<i>ft1.a</i>	CCCTTCGTCCGAACCACCAACCTCAGGGT GACCTTCGGGAACAGGGCCGTGTC-CAACCGG	120
<i>ft1.b</i>	CCCTTCGTCCGAACCACCAACCTCAGGGT GACCTTCGGGAACAGGGCCGTGTC-CAACCGG	118
<i>ft1.c</i>	CCCTTCGTCCGAACCACCAACCTCAGG TGA -----	90

WT	CTGCGAGTCAAGCCGTCCATGGTCGCCAGCAGCCAGGGTGGAGGTGGGCGGCAATGA	179
<i>ft1.a</i>	CTGCGAGTCAAGCCGTCCATGGTCGCCAGCAGCCAGGGTGGAGGTGGGCGGCAAT TGA	180
<i>ft1.b</i>	CTGCGAGTCAAGCCGTCCATGGTCGCCAGCAGCCAGGGTGGAGGTGGGCGGCAAT TGA	178
<i>ft1.c</i>	-----	90
WT	GATGAGGACCTTCTACACGCTCGTGATGGTAGACCCAGATGCTCCAAGTCTAGCGACCC	239
<i>ft1.a</i>	-----	180
<i>ft1.b</i>	-----	178
<i>ft1.c</i>	-----	90
WT	CAACCTTAGAGAGTATCTCCACTGGTTGGTGACAGATATCCCGGGTACAACCTGGGGCGTC	299
<i>ft1.a</i>	-----	180
<i>ft1.b</i>	-----	178
<i>ft1.c</i>	-----	90
WT	GTTCGGGCAGGAGGTGATGTGCTACGAGAGCCCTCGTCCAACCATGGGGATCCACCGCTT	359
<i>ft1.a</i>	-----	180
<i>ft1.b</i>	-----	178
<i>ft1.c</i>	-----	90
WT	CGTGCTCGTGCTCTTCCAGCAGCTGGGGCGGCAGACGGTGTACGCCCCGGGTGGCGCCA	419
<i>ft1.a</i>	-----	180
<i>ft1.b</i>	-----	178
<i>ft1.c</i>	-----	90
WT	GAACTTCAACACCAGGGACTTTGCCGAGCTCTACAACCTCGGCCAGCCCGTTGCCGCCGT	479
<i>ft1.a</i>	-----	180
<i>ft1.b</i>	-----	178
<i>ft1.c</i>	-----	90
WT	CTACTTCAACTGCCAGCGCAGGCCGGCTCCGGCGGCAGGAGGATGTACAAT TGA	534
<i>ft1.a</i>	-----	180
<i>ft1.b</i>	-----	178
<i>ft1.c</i>	-----	90

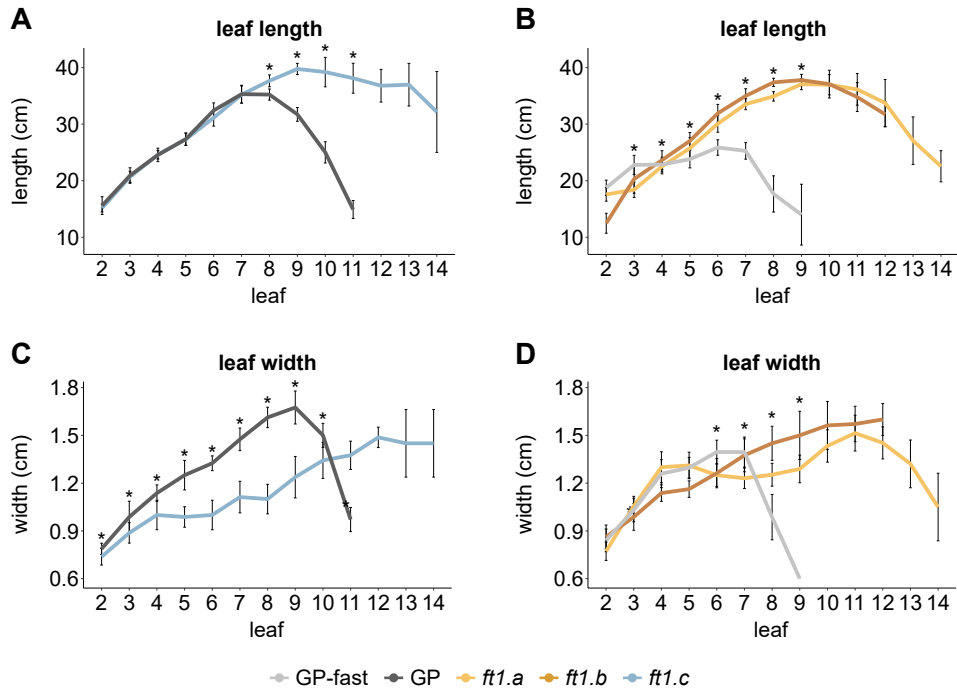
B

WT	MAGRDRDPLVVGRRVVDVLDPFVRTTNLRVTFGNRAVSNGLKPSMVAQQPRVEVGGNE	60
<i>ft1.a</i>	MAGRDRDPLVVGRRVVDVLDPFVRTTNLRVTFGNRAV QLRAQAVHGRPAEEGGGRQ*	59
<i>ft1.b</i>	MAGRDRDPLVVGRRVVDVLDPFVRTTNLRVTFGNRAV TAASSSRPWSPSSRGWRWAMR	60
<i>ft1.c</i>	MAGRDRDPLVVGRRVVDVLDPFVRTTNLR * -----	29
WT	MRTFYTLVMVDPDAPSPDPNLRREYLHWLVTDI PGTTGASFGQEVMCYESPRPTMGIHRF	120
<i>ft1.a</i>	-----	59
<i>ft1.b</i>	* -----	60
<i>ft1.c</i>	-----	29
WT	VLVLFQQLGRQTVYAPGWRQNFNTRDFAELYNLGQPVAAVYFNCQREAGSGGRRMYN*	177
<i>ft1.a</i>	-----	59
<i>ft1.b</i>	-----	60
<i>ft1.c</i>	-----	29

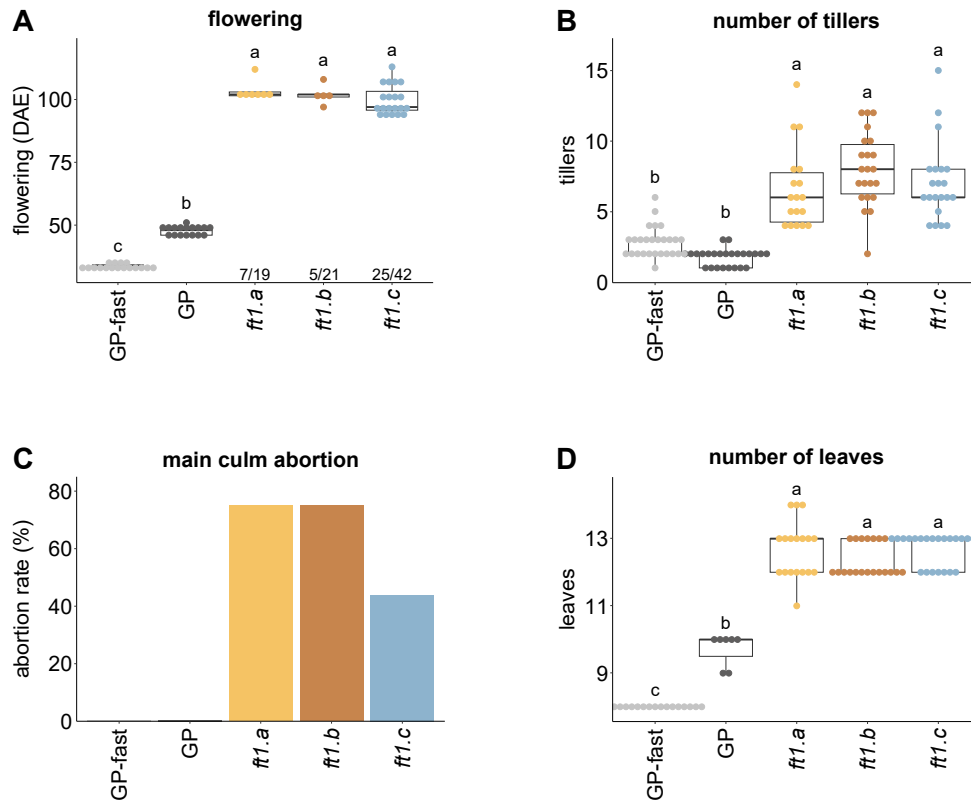
Supplemental Figure S1. Nucleotide and amino acid alignment of FT1. A Nucleotide alignment of *ft1.a*, *ft1.b*, and *ft1.c* to the wild-type (WT) reference sequence of *FT1* (*HORVU.MOREX.r3.7HG0653910*). gRNA and PAM sequences are labeled accordingly and are indicated by grey background in the WT sequence. Single insertions/deletions in mutants are indicated in white on black background. Stop codons are indicated in bold on grey background. **B** Amino acid alignment of the translated sequences from (A). Residues that differ from the WT reference sequence are indicated in bold, stop codons by asterisks. Alignments were performed with CLUSTAL O (1.2.4, Sievers et al., 2011) multiple sequence alignment.



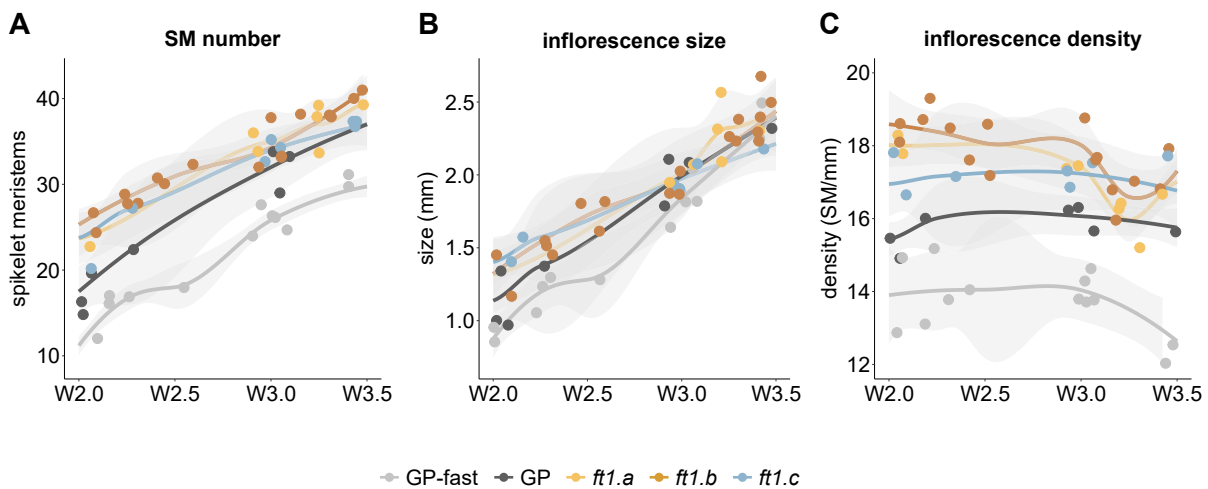
Supplemental Figure S2. Shoot architecture of *ft1* plants. Wild-types GP, GP-fast, and *ft1* mutants were grown under controlled long-day (LD) conditions. Shown are representative images of plants at different ages. **A-E** GP-fast, GP, *ft1.a*, *ft1.b*, and *ft1.c* ten weeks after emergence in 1.5 L pots. **F-H** *ft1.a*, *ft1.b*, and *ft1.c* six months after emergence in 1.5 L pots. **I-K** *ft1.a*, *ft1.b*, and *ft1.c* ten months after emergence in 3 L pots. Senescent non-flowering tillers were removed throughout the experiment. Individual flowering tillers are visible ten months after sowing and are indicated by red arrows. Scale equals 10 cm in all panels.



Supplemental Figure S3. Effect of *FT1* on leaf size. Plants were grown under controlled long-day (LD) conditions in 1.5 L pots, and leaf length and width of fully expanded leaves were measured. **A, C** Leaf length and width of GP plants (dark grey) compared to *ft1.c* (blue). **B, D** Leaf length and width of GP-fast plants (light grey) compared to *ft1.a* and *ft1.b* (yellow and orange). Error bars indicate the standard deviation of the mean; significant differences are indicated by asterisks (* $p \leq 0.05$) comparing *ft1.c* to GP (A, C) or *ft1.a* and *ft1.b* to GP-fast (B, D) with Student's *t*-test, $n = 8$.



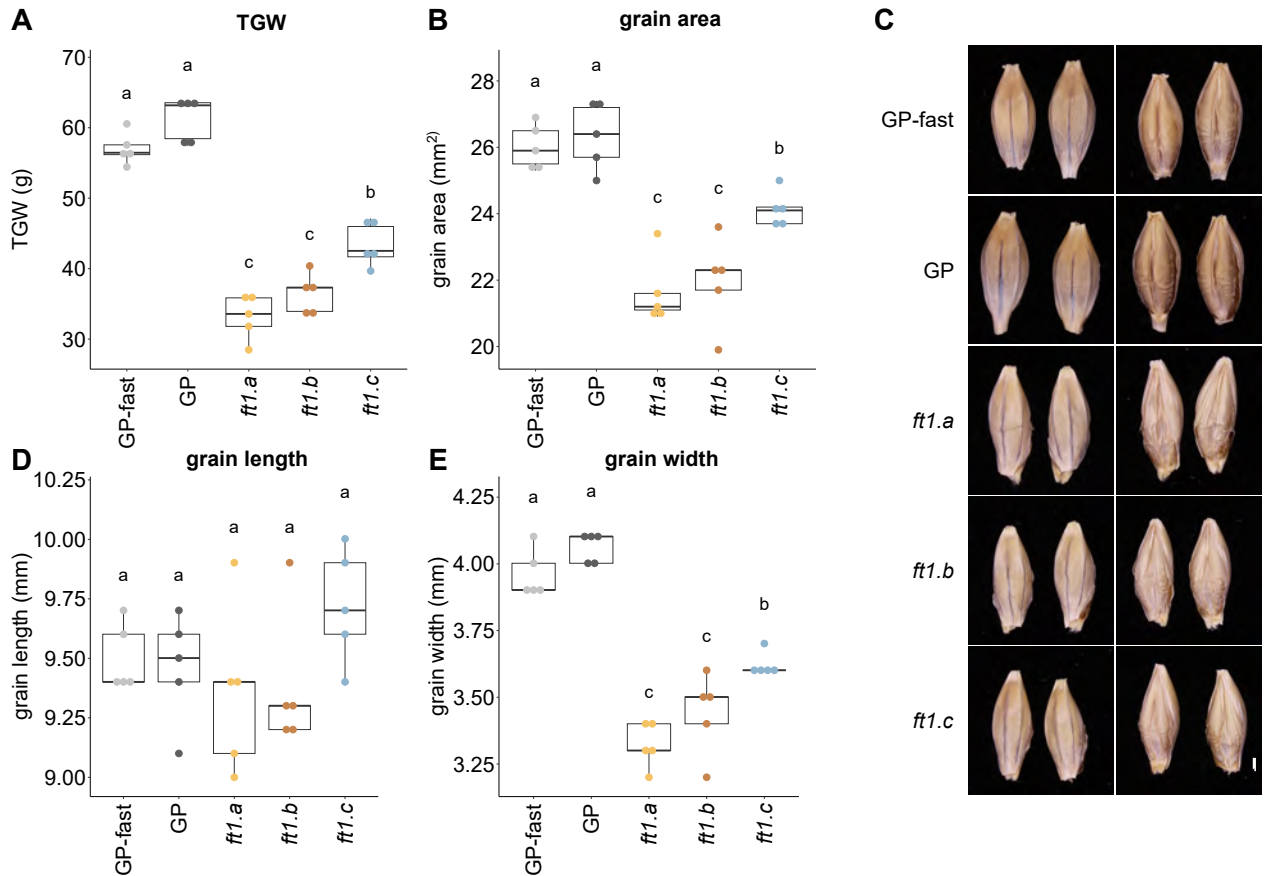
Supplemental Figure S4. Phenotype of *ft1* mutants grown in 75 cm³ soil. Wild-types GP-fast, GP, and *ft1* mutants were grown in 75 cm³ pots under controlled long-day (LD) conditions, and different traits related to the development and plant architecture were scored at heading (A-C) or at the end of stem elongation (D). **A** Flowering was scored in days after emergence (DAE) as tipping of the awns on the main culm of the plants. The numbers below the boxplots indicate the number of plants that did flower on the main culm compared to the total number of plants scored. **B** The number of tillers was scored at flowering. **C** Main culm abortion rate was scored as the percentage of plants that produced a main culm spike emerging from the leaf sheath. **D** The number of leaves was counted at the end of stem elongation on the main culm. Significance levels were determined by one-way ANOVA and subsequent Tukey's test ($p \leq 0.05$, $n = 4-27$).



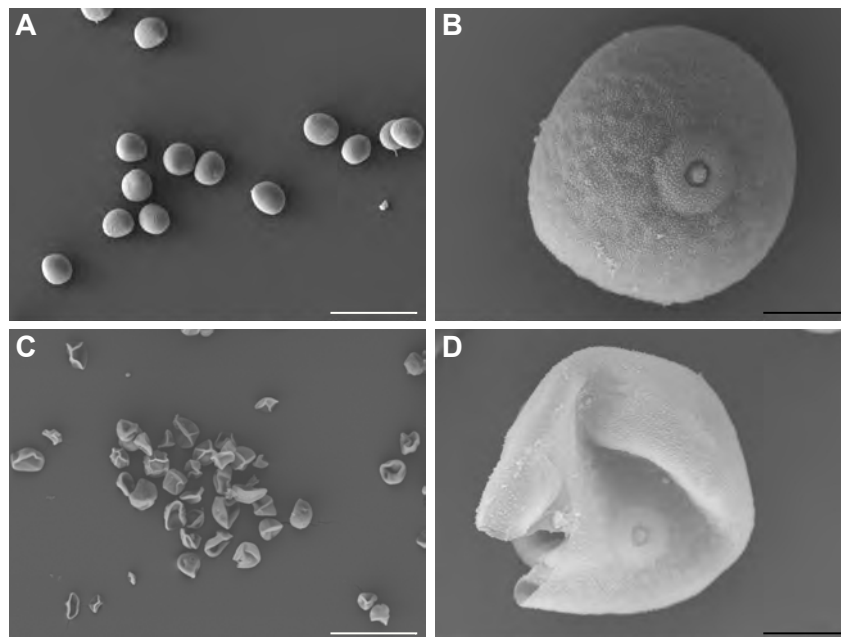
Supplemental Figure S5. Effects of *FT1* on reproductive development. GP, GP-fast, and *ft1* mutants were grown under controlled long-day (LD) conditions in 75 cm³ pots, and 3-4 plants per genotype were dissected per time point to monitor the development of the main shoot apex (MSA). Spikelet meristem (SM) number (**A**), inflorescence size (**B**), and inflorescence density (**C**) of the main culm were scored during early reproductive development (W2.0 to W3.5). The density was calculated by dividing the number of spikelet primordia by inflorescence size (in mm). Each dot represents one plant. Grey areas show the 95% confidence interval of a polynomial regression (Loess smooth line).



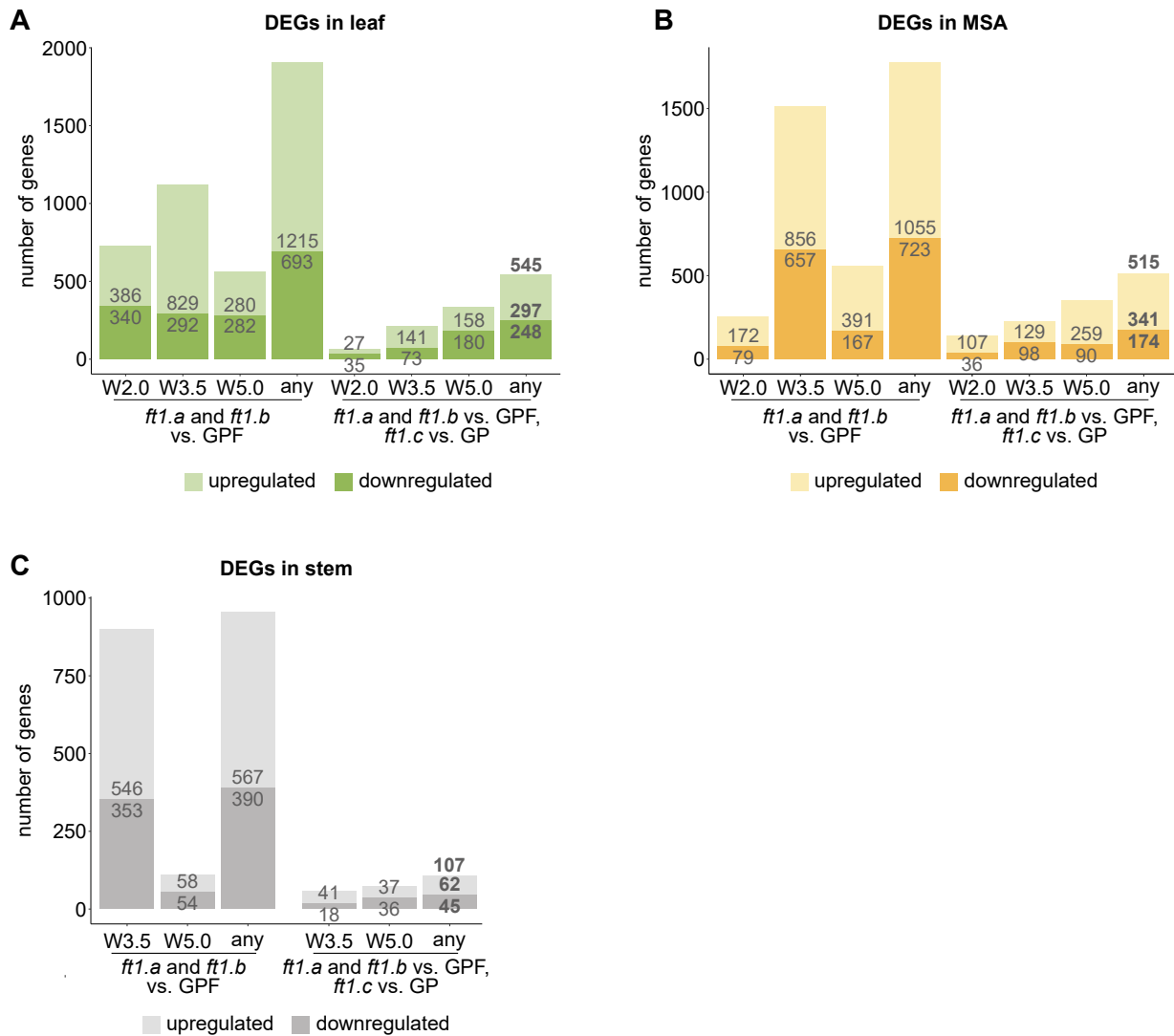
Supplemental Figure S6. Spike phenotypes. Plants were grown under controlled long-day (LD) conditions, and spikes of GP-fast (**A**), *ft1.a* (**B**), *ft1.b* (**C**), and *ft1.c* (**D**) axillary tillers were photographed on the plants. White arrows indicate secondary inflorescences, and the red arrow in (B) indicates an ectopic tiller. Scales equal 1 cm.



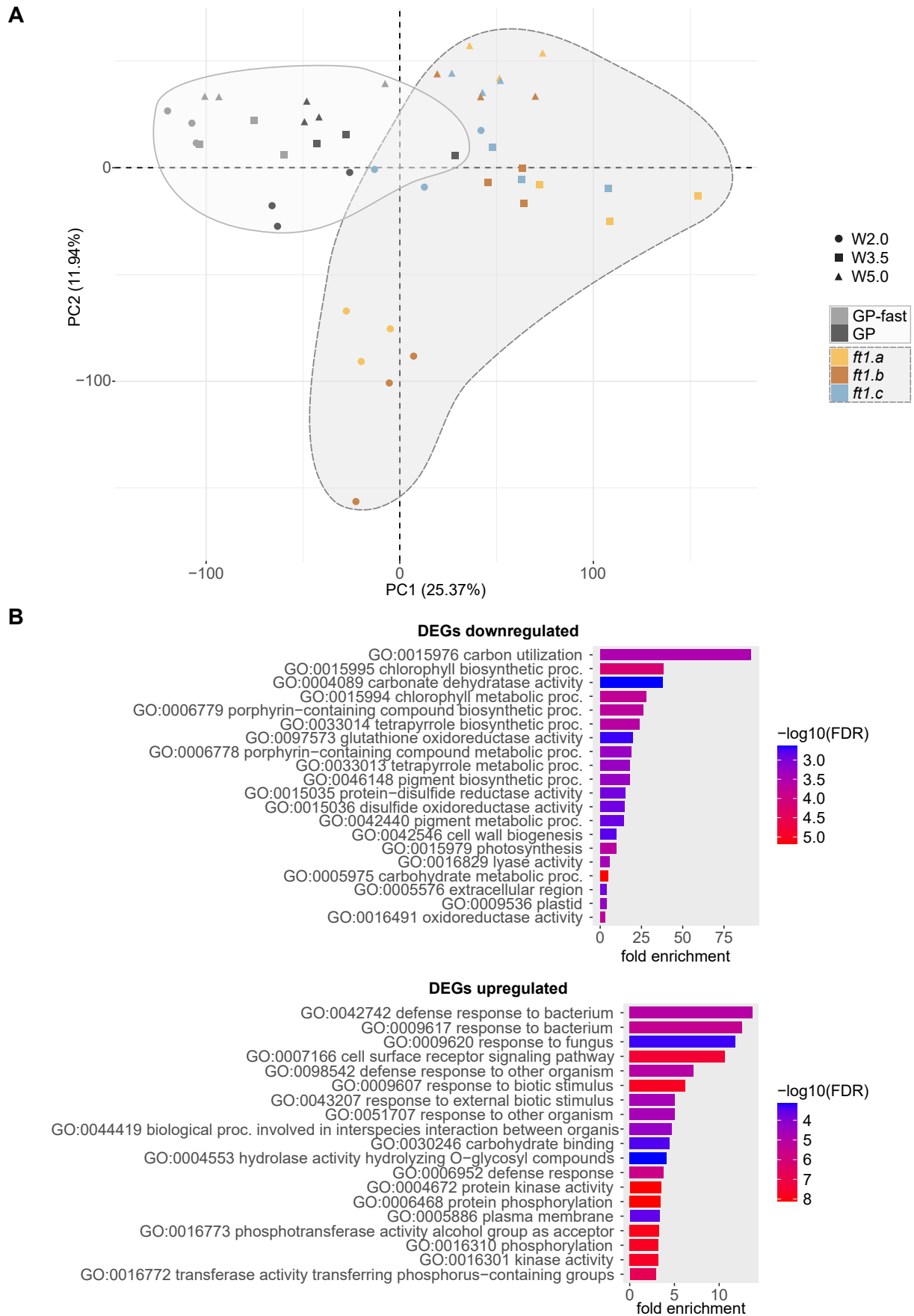
Supplemental Figure S7. MARViN measurements of grains. GP-fast, GP, and *ft1* mutants were grown under controlled long-day (LD) conditions in 75 cm³ pots until maturity, and grains were harvested individually for each plant. Thousand grain weight (TGW) (A), grain area (B), grain length (C), and grain width (D) were measured via MARViN imaging, performed with the palea facing upwards. Individual grain values were averaged for each biological replicate. Measurements were performed with five biological replicates, each containing pooled seeds from three individual plants. Significance levels were determined by one-way ANOVA and subsequent Tukey's test ($p \leq 0.05$, $n = 5$). E Images of randomly chosen grains with the lemma (first two grains on the left) and palea (two grains on the right) side up. Scale equals 2 mm.



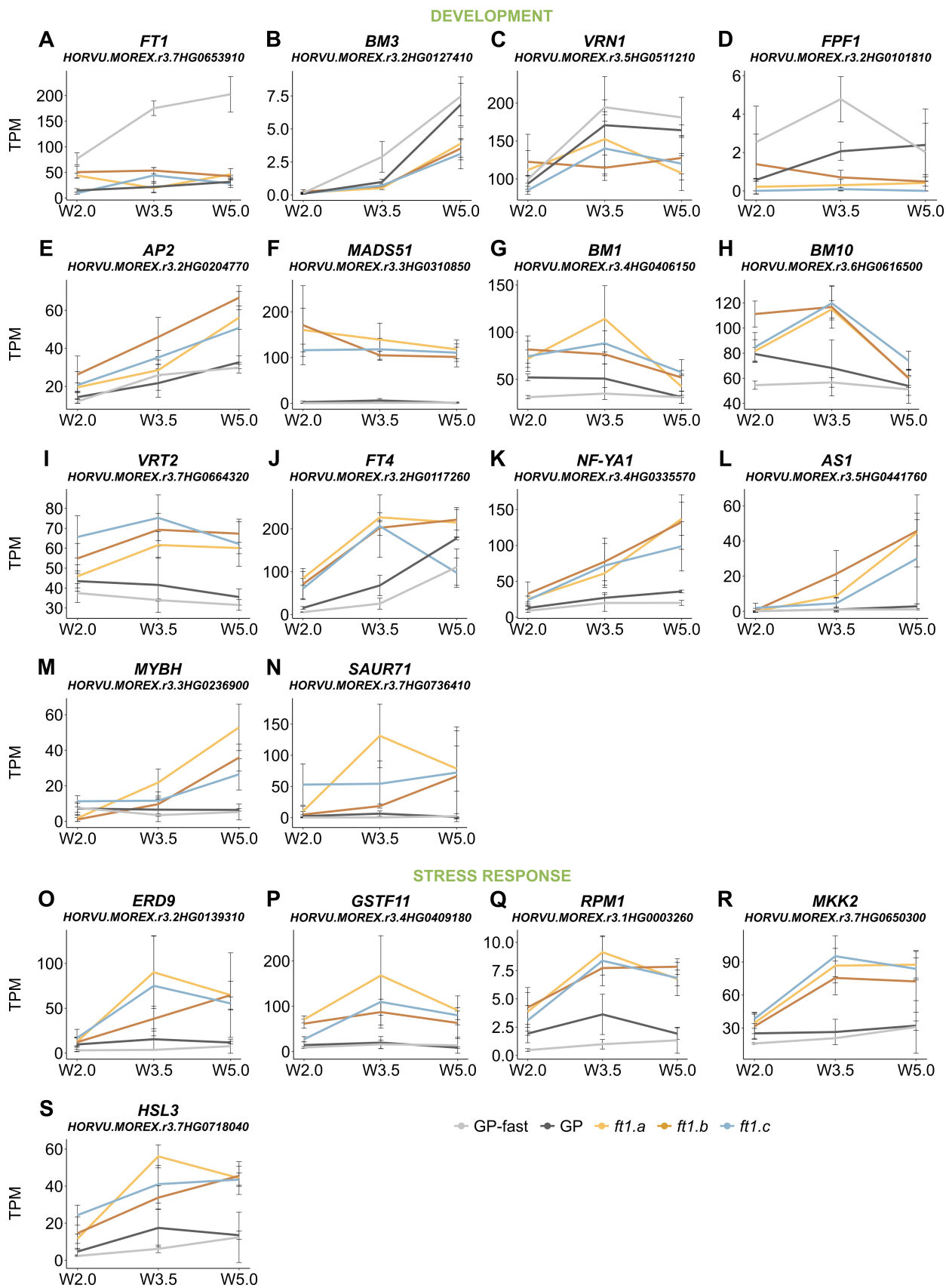
Supplemental Figure S8. SEM imaging of WT and *ft1* pollen. Representative images of pollen harvested from GP-fast (A, B) and *ft1.a* (C, D). Plants were grown under controlled long-day (LD) conditions. White scales equal 100 μ m, black scales 10 μ m.



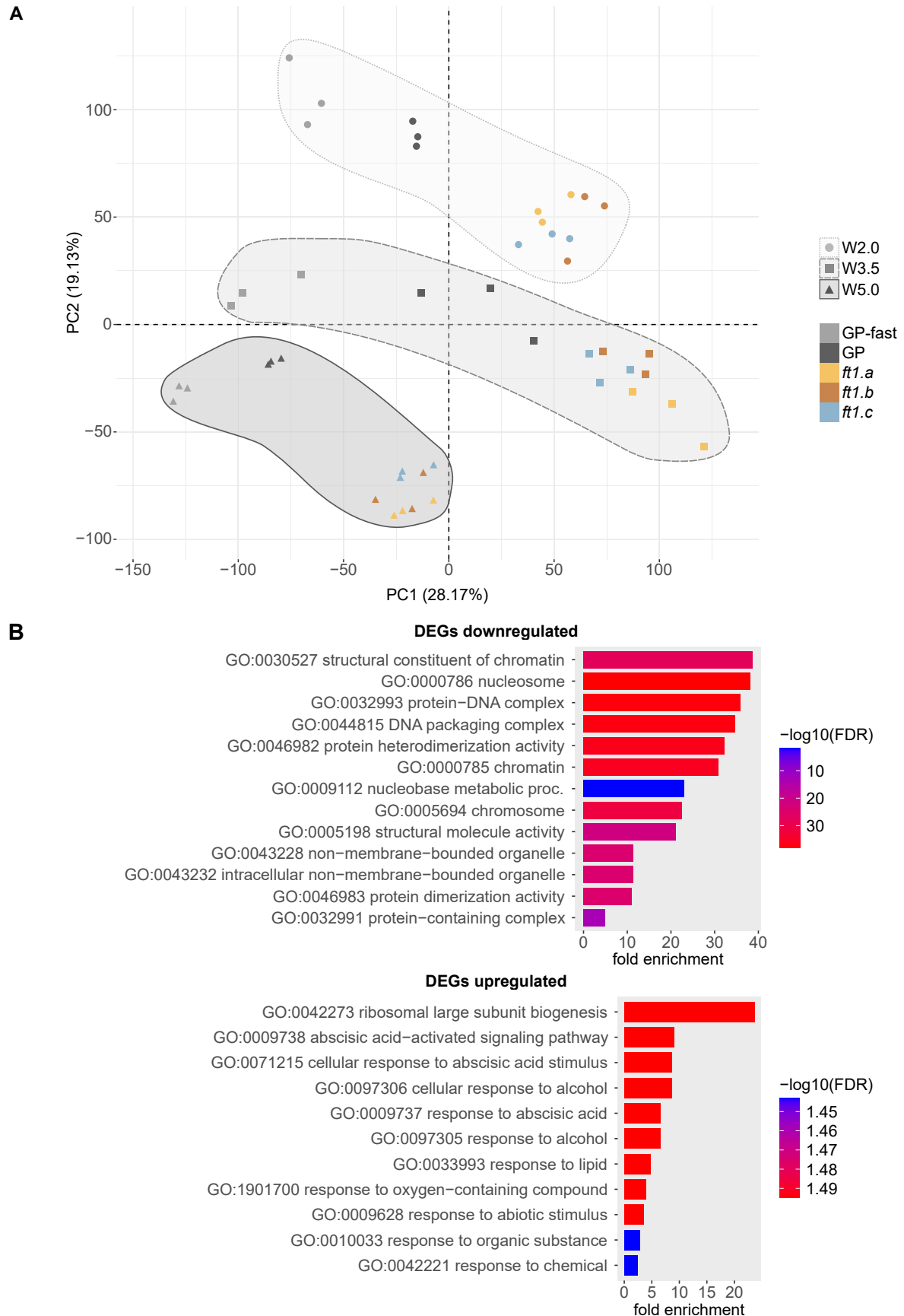
Supplemental Figure S9. Number of DEGs. The number of differentially expressed genes (DEGs) in leaf (A), main shoot apex (MSA) (B), and stem (C). Shown are the overlap of DEGs in *ft1.a* and *ft1.b* compared to GP-fast (bars on the left) and genes that are additionally differentially expressed (DE) in *ft1.c* compared to GP (bars on the right). DEGs are either counted separately by developmental stage (W2.0, W3.5, W5.0) or combined to get the number of genes that are DE at any of these stages (“any”). Genes that are DE in all three comparisons (*ft1.a* vs. GP-fast, *ft1.b* vs. GP-fast, *ft1.c* vs. GP) at any developmental stage are considered as the core set of 545, 516, and 107 DEGs in leaf, MSA and stem, respectively (indicated in bold).



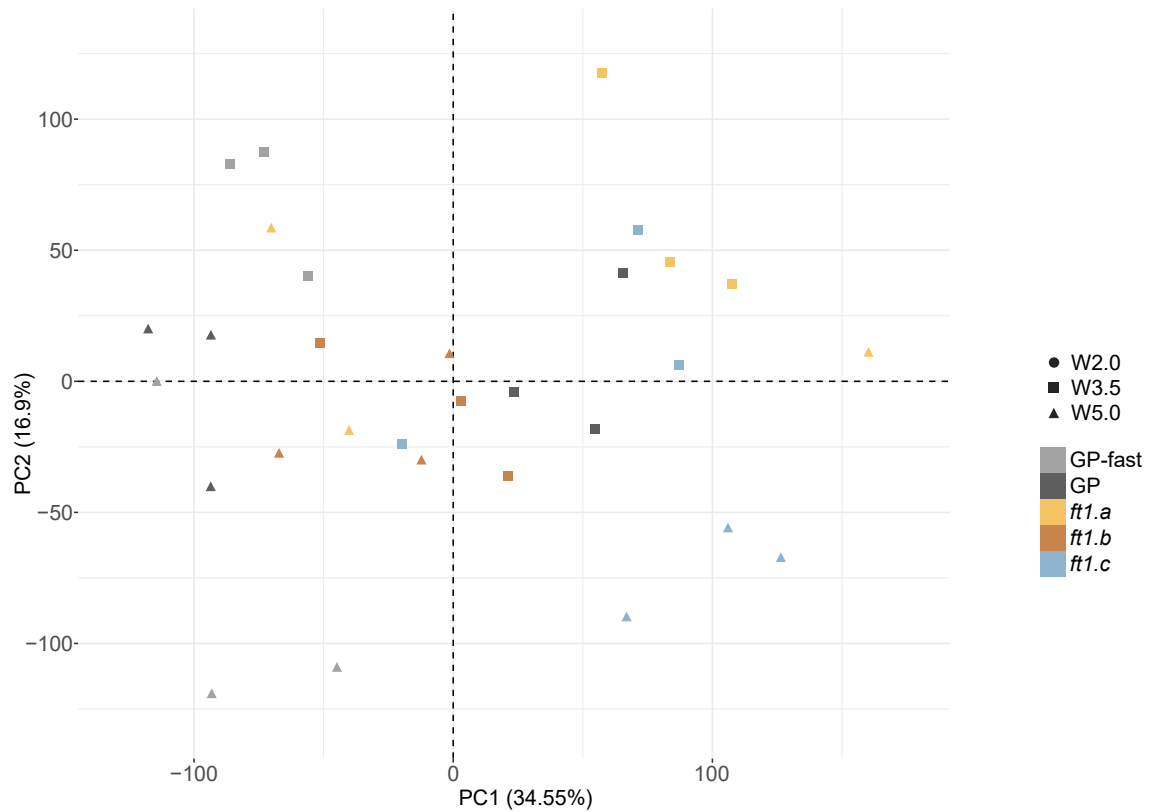
Supplemental Figure S10. PCA and GO term enrichment for leaf samples. **A** Principal component analysis (PCA) of all expressed genes in leaves of GP-fast, GP, and *ft1* mutant plants. Plants were grown under controlled long-day (LD) conditions and sampled at developmental stages W2.0, W3.5, and W5.0. For each genotype and developmental stage, three individual biological replicates were sampled. The triplicate samples are separated by genotype (color) and developmental stage (shape). **B** GO term enrichment on up- and downregulated differentially expressed genes (DEGs) in leaf. The enrichment was performed and plotted with ShinyGO (v0.80) (Ge et al., 2020).



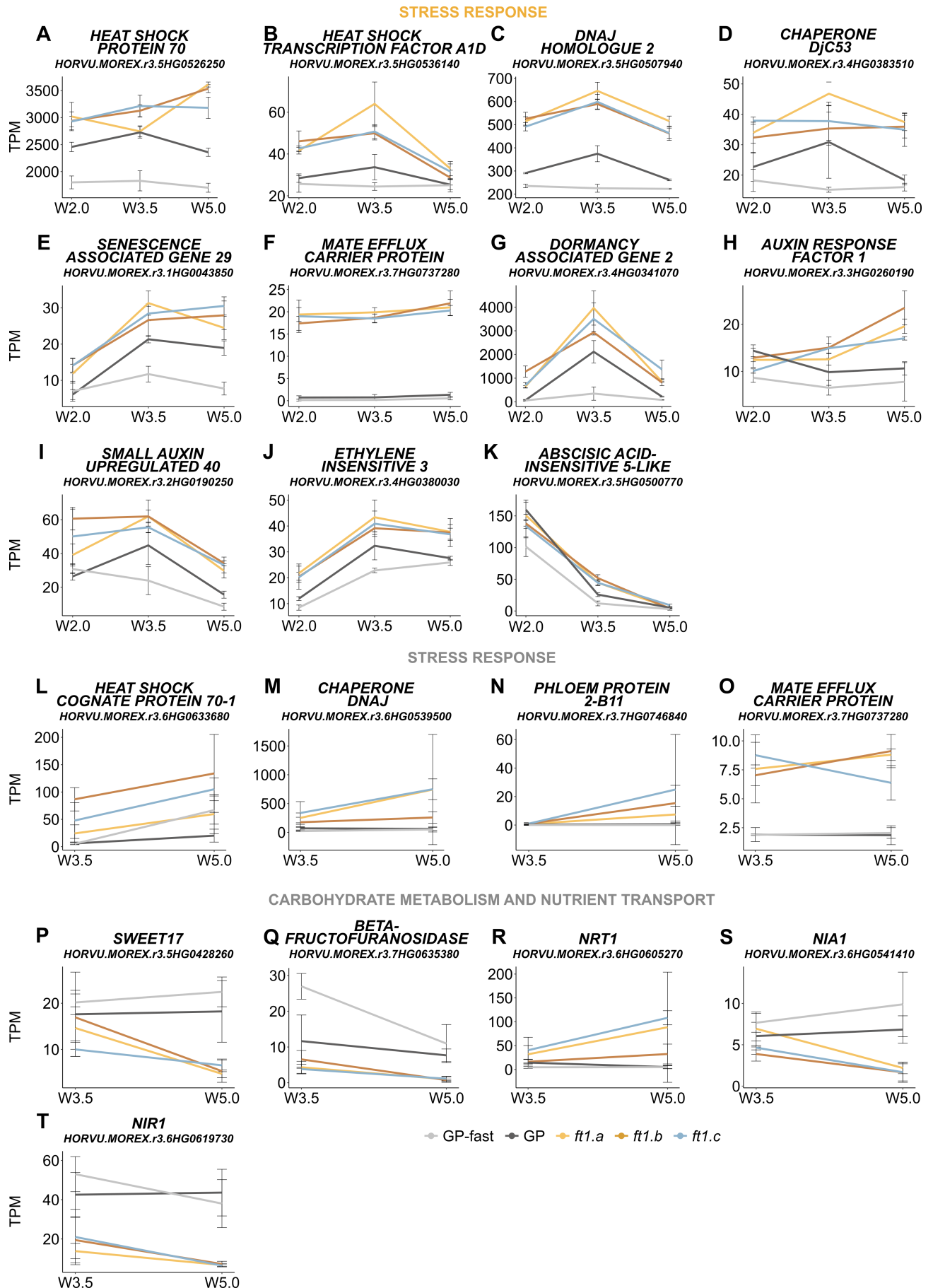
Supplemental Figure S11. DEGs in leaves. Gene expression in GP-fast (light grey), GP (dark grey), *ft1.a* (yellow), *ft1.b* (orange), and *ft1.c* (blue). Expression patterns of exemplary genes are shown in transcripts per million (TPM) by developmental stage. Shown are genes related to development (**A-N**) and stress response (**O-S**). Each value represents the mean of three independent biological replicates; error bars indicate the standard deviation of the mean.



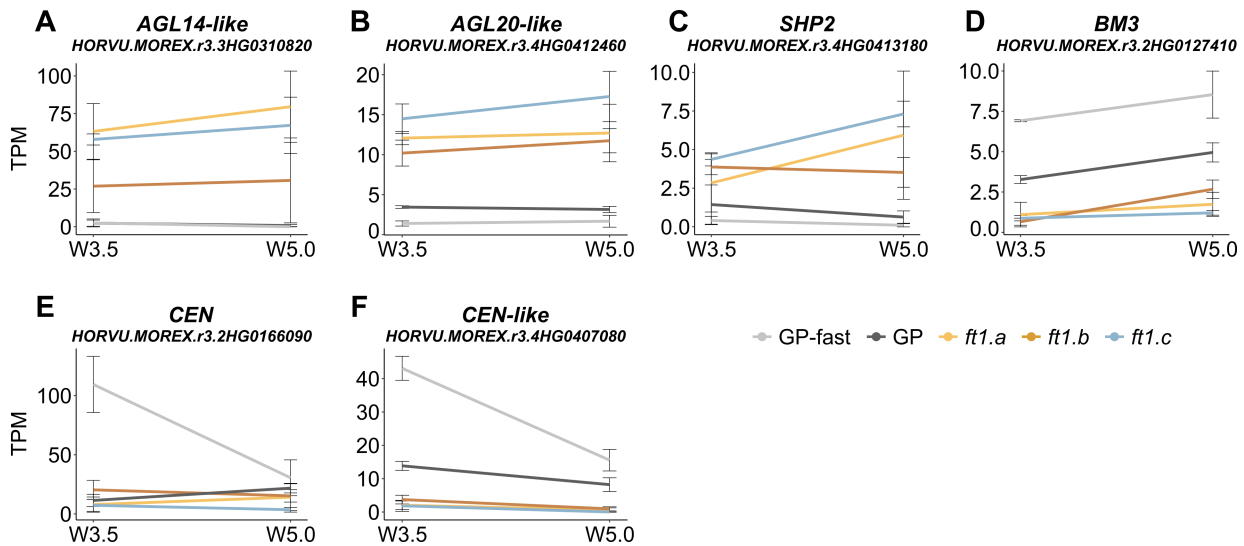
Supplemental Figure S12. PCA and GO term enrichment in the MSA. A Principal component analysis (PCA) of all expressed genes in the main shoot apices (MSAs) of GP-fast, GP, and *ft1* mutant plants. Plants were grown under controlled long-day (LD) conditions and sampled at developmental stages W2.0, W3.5, and W5.0. For each genotype and developmental stage, three individual biological replicates were sampled. The triplicate samples are separated by genotype (color) and developmental stage (shape). **B** GO term enrichment on up- and downregulated differentially expressed genes (DEGs) in the MSA. Enrichment was performed and plotted with ShinyGO (v0.80) (Ge et al., 2020).



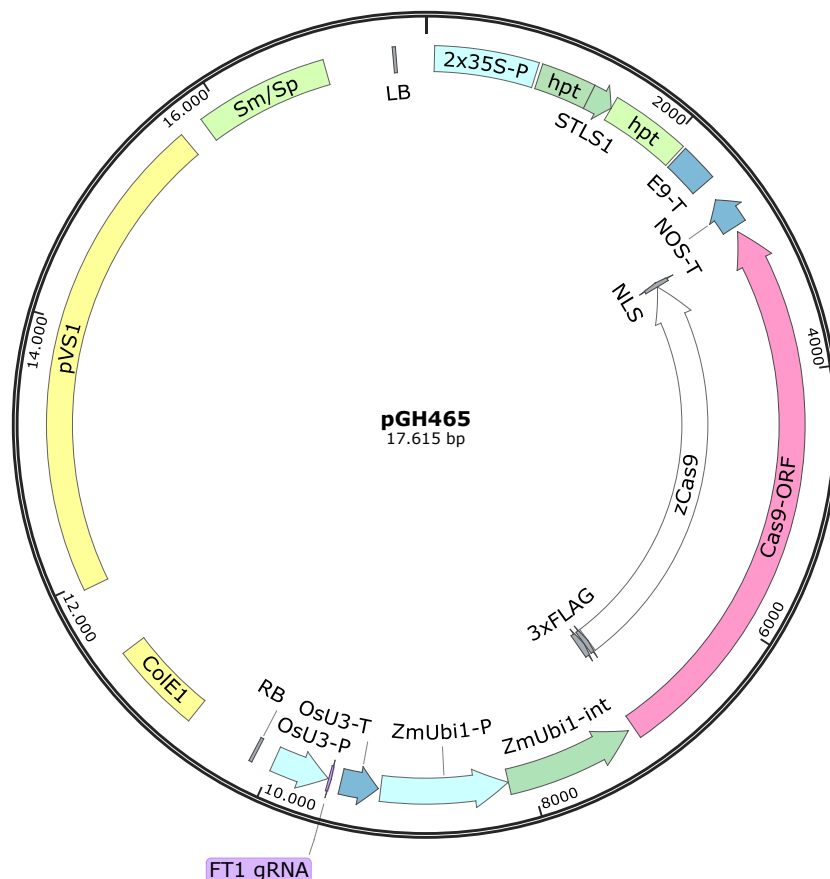
Supplemental Figure S13. PCA in the stem. Principal component analysis (PCA) of all expressed genes in the stem of GP-fast, GP, and *ft1* mutant plants. Plants were grown under controlled long-day (LD) conditions and sampled at developmental stages W3.5 and W5.0. For each genotype and developmental stage, three individual biological replicates were sampled. The triplicate samples are separated by genotype (color) and developmental stage (shape).



Supplemental Figure S14. DEGs related to stress response and nutrient and sugar transport in MSA and stem. Gene expression in GP-fast (light grey), GP (dark grey), *ft1.a* (yellow), *ft1.b* (orange), and *ft1.c* (blue). Expression patterns of exemplary genes are shown in transcripts per million (TPM) by developmental stage. Shown are genes related to stress response in main shoot apices (MSA) (A-K) and stem (L-O), and carbohydrate metabolism and nutrient transport in stem (P-T). Each value represents the mean of three independent biological replicates; error bars indicate the standard deviation of the mean.



Supplemental Figure S15. DEGs related to floral development in the stem. Gene expression in GP-fast (light grey), GP (dark grey), *ft1.a* (yellow), *ft1.b* (orange), and *ft1.c* (blue). Expression patterns of exemplary genes are shown in transcripts per million (TPM) by developmental stage. Each value represents the mean of three independent biological replicates; error bars indicate the standard deviation of the mean.



Supplemental Figure S16. Vector map of transformation construct pGH465. CoIE1: origin of replication, pVS1: origin of replication, Sm/Sp: Streptomycin/Spectinomycin resistance, 2x35S-P: 35S promoter, hpt: Hygromycin resistance, STLS1: Intron, E9-T: E9 terminator, Os-U3-P: *Oryza sativa* U3 promoter, FT1 gRNA, OsU3-T: *Oryza sativa* U3 terminator, ZmUbi1-P: *Zea mays* Ubiquitin 1 promoter, Zm-Ubi1-int: *Zea mays* Ubiquitin 1 intron, Cas9-ORF: Cas9 open reading frame, 3xFLAG: 3x Flag-tag, zCas9: Cas9 coding sequence codon optimized for *Zea mays*, NLS: nuclear localization sequence. The map was generated with SnapGene (GSL Biotech).

Supplemental Table S1. Spikelet meristem number on MSA of parents and *ft1* plants. The maximum spikelet meristem (SM) stage was calculated with the R package *segmented* as the break-point of two separate linear regressions. SM initiation rate equals the slope of the first regression, and the floret meristem (FM) abortion rate is the slope of the second regression. The maximum SM and final FM number were calculated with the linear models provided by *segmented*. Aborted FMs were calculated by subtracting the final FM number from the maximum SM number. All numbers were rounded to one decimal place. The maximum SM stage (Waddington stage) was determined by plotting the development (in Waddington stage) against time (in days after emergence, DAE) and calculating a linear regression from this.

Genotype	Maximum SM stage (DAE)	Maximum SM stage (W-stage)	SM initiation rate (SM/day)	FM abortion rate (FM/day)	Maximum SM number	Final FM number (W10.0)	Number of aborted FM
GP-fast	18.5	4.5	2.9	-3.5	36.8	24.3	12.5
GP	28.8	5.0	2.3	-2.8	47.7	34.4	13.3
<i>ft1.1</i>	53.3	4.5	0.8	-0.9	46.1	43.8	2.3
<i>ft1.b</i>	49.9	4.5	1.0	-1.1	47.3	42.6	4.7
<i>ft1.c</i>	58.2	5.0	0.8	-0.9	47.2	42.6	3.6

Supplemental Table S2. Overview of all leaf samples for RNA Sequencing. “Leaf sampled” describes the leaf sampled for each developmental stage and genotype, counting from the first appearing leaf (leaf 1) up.

Developmental stage	Genotype	Leaf sampled
W2.0	GP-fast	2
	GP	3
	<i>ft1.a</i>	4
	<i>ft1.b</i>	4
	<i>ft1.c</i>	4
W3.5	GP-fast	4
	GP	5
	<i>ft1.a</i>	6
	<i>ft1.b</i>	7
	<i>ft1.c</i>	6
W5.0	GP-fast	5
	GP	7
	<i>ft1.a</i>	9-10
	<i>ft1.b</i>	9-10
	<i>ft1.c</i>	8

Supplemental Table S3. Number of DEGs used for GO Term enrichment in MSA and leaf. “Number of DEGs” refers to the differentially expressed genes (DEGs) in each tissue, divided by up- and downregulation. Due to the conversion from BaRTv2 to MorexV3 identifier, this number was slightly reduced for GO Term enrichment (“Number of DEGs in GO”).

Tissue	Regulation	Number of DEGs	Number of DEGs in GO enrichment
MSA	Up	342	335
	Down	174	167
Leaf	Up	297	283
	Down	248	239

Supplemental Datasets S1 - S8 can be downloaded under the following link:

<http://dx.doi.org/10.25838/d5p-54>

Supplemental Dataset S1. Differentially expressed genes (DEGs) in leaves. Genes were considered as DEGs when they showed significant differences ($FDR \leq 0.01$) in expression in all pairwise comparisons (*ft1.a* vs. GP-fast, *ft1.b* vs. GP-fast, *ft1.c* vs. GP) and a log fold change (\log_2FC) ≥ 1 (upregulated) or ≤ -1 (downregulated) in the comparisons *ft1.a* vs. GP-fast and *ft1.b* vs. GP-fast. Genes were additionally annotated with MorexV3 identifiers (Mascher et al., 2021) and Araport11 (Cheng et al., 2017).

Supplemental Dataset S2. Differentially expressed genes (DEGs) in main shoot apices (MSA). Genes were considered as DEGs when they showed significant differences ($FDR \leq 0.01$) in expression in all pairwise comparisons (*ft1.a* vs. GP-fast, *ft1.b* vs. GP-fast, *ft1.c* vs. GP) and a log fold change (\log_2FC) ≥ 1 (upregulated) or ≤ -1 (downregulated) in the comparisons *ft1.a* vs. GP-fast and *ft1.b* vs. GP-fast. Genes were additionally annotated with MorexV3 identifiers (Mascher et al., 2021) and Araport11 (Cheng et al., 2017).

Supplemental Dataset S3. Differentially expressed genes (DEGs) in stems. Genes were considered as DEGs when they showed significant differences ($FDR \leq 0.05$) in expression in all pairwise comparisons (*ft1.a* vs. GP-fast, *ft1.b* vs. GP-fast, *ft1.c* vs. GP) and a log fold change (\log_2FC) ≥ 1 (upregulated) or ≤ -1 (downregulated) in the comparisons *ft1.a* vs. GP-fast and *ft1.b* vs. GP-fast. Genes were additionally annotated with MorexV3 identifiers (Mascher et al., 2021) and Araport11 (Cheng et al., 2017).

Supplemental Dataset S4. RNA sequencing data in leaves. Log fold changes (\log_2FC) and false discovery rate (FDR) were calculated by pairwise comparisons (*ft1.a* vs. GP-fast, *ft1.b* vs. GP-fast, *ft1.c* vs. GP). Genes were additionally annotated with MorexV3 identifiers (Mascher et al., 2021) and Araport11 (Cheng et al., 2017).

Supplemental Dataset S5. RNA sequencing data in main shoot apices (MSA). Log fold changes (\log_2FC) and false discovery rate (FDR) were calculated by pairwise comparisons (*ft1.a* vs. GP-fast, *ft1.b* vs. GP-fast, *ft1.c* vs. GP). Genes were additionally annotated with MorexV3 identifiers (Mascher et al., 2021) and Araport11 (Cheng et al., 2017).

Supplemental Dataset S6. RNA sequencing data in stems. Log fold changes (\log_2FC) and false discovery rate (FDR) were calculated by pairwise comparisons (*ft1.a* vs. GP-fast, *ft1.b* vs. GP-fast, *ft1.c* vs. GP). Genes were additionally annotated with MorexV3 identifiers (Mascher et al., 2021) and Araport11 (Cheng et al., 2017).

Supplemental Dataset S7. GO term enrichment of differentially expressed genes (DEGs) in leaf. The enrichment was performed with ShinyGO 0.80 (Ge et al., 2020) and only top terms were extracted.

Supplemental Dataset S8. GO term enrichment of differentially expressed genes (DEGs) in main shoot apices (MSA). The enrichment was performed with ShinyGO 0.80 (Ge et al., 2020) and only top terms were extracted.

Acknowledgements

First of all, I would like to express my gratitude to my supervisor Prof. Maria von Korff. You gave me the opportunity to work in your lab and to learn from you on an academic and a personal level, and I am grateful for your continued patience with me and for guiding me through this jungle called science. I would like to thank my second supervisor, Prof. Rüdiger Simon, for your honest input and critique, which made me step up my level.

I want to thank everyone in the von Korff lab for making the last couple of years as enjoyable as they were. In particular, I want to thank Tianyu and Einar for endless discussions about (sometimes) science and (more often) less related topics, for coffee breaks and Mensa dates, for good food and drinks, and for being there almost all the way. I thank Thea for quick and always excellent technical support, discussions about all and everything, for always having a sympathetic ear and for holding the lab together. Thanks to Agatha for spikes of dark humor and always giving the best post-doctoral advice, and to Kumsal for completing the girls' office. I would like to thank my friends that I have met somewhere along the way, be it at school or university or elsewhere, for keeping me sane over the last couple of years and only asking very tentatively and on rare occasions when I'm going to be finished or what I'm planning to do next. Thanks to iGRAD plant and all fellows (especially die coolen kids) for teaching me a lot, for a grim sense of humor, and for good vibes at all events, on whatever continent they might have taken place - but particularly in 40225 Düsseldorf on Monday evenings from 16:30 onwards.

Lastly, I thank my family for believing more in me than I sometimes do myself. Thank you for your continuous support and the knowledge that I will always have you to fall back on. Without this, I would have never even dared to pursue this academic degree.

